



Universiteit Gent  
Faculteit Wetenschappen  
Vakgroep Fysica en Sterrenkunde

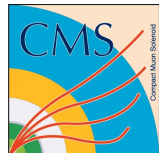
<sup>2</sup> No title yet

<sup>3</sup> No sub-title neither, obviously...

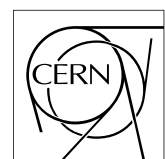
---

<sup>4</sup> Alexis Fagot

5



Thesis to obtain the degree of  
Doctor of Philosophy in Physics  
Academic years 2012-2017





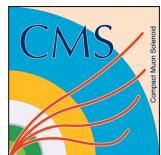


Universiteit Gent  
Faculteit Wetenschappen  
Vakgroep Fysica en Sterrenkunde

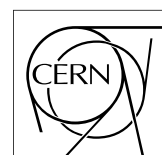
Promotoren: Dr. Michael Tytgat  
Prof. Dr. Dirk Ryckbosch

Universiteit Gent  
Faculteit Wetenschappen  
Vakgroep Fysica en Sterrenkunde  
Proeftuinstraat 86, B-9000 Gent, België  
Tel.: +32 9 264.65.28  
Fax.: +32 9 264.66.97

17



Thesis to obtain the degree of  
Doctor of Philosophy in Physics  
Academic years 2012-2017





## Acknowledgements

<sup>19</sup> Ici on remerciera tous les gens que j'ai pu croiser durant cette aventure et qui m'ont permis de passer  
<sup>20</sup> un bon moment

<sup>21</sup> *Gent, ici la super date de la mort qui tue de la fin d'écriture*  
<sup>22</sup> *Alexis Fagot*



# Table of Contents

24	<b>Acknowledgements</b>	i
25	<b>Nederlandse samenvatting</b>	xvii
26	<b>English summary</b>	xix
27	<b>1 Introduction</b>	1-1
28	1.1 A story of High Energy Physics . . . . .	1-1
29	1.2 Organisation of this study . . . . .	1-1
30	<b>2 Investigating the TeV scale</b>	2-1
31	2.1 The Standard Model of Particle Physics . . . . .	2-1
32	2.2 The Large Hadron Collider and the Compact Muon Solenoid . . . . .	2-1
33	2.3 Muon Phase-II Upgrade . . . . .	2-1
34	<b>3 Amplification processes in gaseous detectors</b>	3-1
35	3.1 Signal formation . . . . .	3-1
36	3.2 Gas transport parameters . . . . .	3-1
37	<b>4 Resistive Plate Chambers</b>	4-1
38	4.1 Principle . . . . .	4-1
39	4.2 Rate capability of Resistive Plate Chambers . . . . .	4-1
40	4.3 High time resolution . . . . .	4-1
41	4.4 Resistive Plate Chambers at CMS . . . . .	4-1
42	4.4.1 Overview . . . . .	4-1
43	4.4.2 The present RPC system . . . . .	4-2
44	4.4.3 Pulse processing of CMS RPCs . . . . .	4-3
45	<b>5 Longevity studies and Consolidation of the present CMS RPC subsystem</b>	5-1
46	5.1 Testing detectors under extreme conditions . . . . .	5-1
47	5.1.1 The Gamma Irradiation Facilities . . . . .	5-3
48	5.1.1.1 GIF . . . . .	5-3
49	5.1.1.2 GIF++ . . . . .	5-5
50	5.2 Preliminary tests at GIF . . . . .	5-7
51	5.2.1 Resistive Plate Chamber test setup . . . . .	5-7
52	5.2.2 Data Acquisition . . . . .	5-9
53	5.2.3 Geometrical acceptance of the setup layout to cosmic muons . . . . .	5-9
54	5.2.3.1 Description of the simulation layout . . . . .	5-10
55	5.2.3.2 Simulation procedure . . . . .	5-12
56	5.2.3.3 Results . . . . .	5-13
57	5.2.4 Photon flux at GIF . . . . .	5-13

---

58	5.2.4.1	Expectations from simulations . . . . .	5-13
59	5.2.4.2	Dose measurements . . . . .	5-18
60	5.2.5	Results and discussions . . . . .	5-19
61	5.3	Longevity tests at GIF++ . . . . .	5-20
62	5.3.1	Description of the Data Acquisition . . . . .	5-23
63	5.3.2	RPC current, environmental and operation parameter monitoring . . . . .	5-24
64	5.3.3	Measurement procedure . . . . .	5-25
65	5.3.4	Longevity studies results . . . . .	5-25
66	<b>6</b>	<b>Investigation on high rate RPCs</b>	<b>6-1</b>
67	6.1	Rate limitations and ageing of RPCs . . . . .	6-1
68	6.1.1	Low resistivity electrodes . . . . .	6-1
69	6.1.2	Low noise front-end electronics . . . . .	6-1
70	6.2	Construction of prototypes . . . . .	6-1
71	6.3	Results and discussions . . . . .	6-1
72	<b>7</b>	<b>Conclusions and outlooks</b>	<b>7-1</b>
73	7.1	Conclusions . . . . .	7-1
74	7.2	Outlooks . . . . .	7-1
75	<b>A</b>	<b>A data acquisition software for CAEN VME TDCs</b>	<b>A-1</b>
76	A.1	GIF++ DAQ file tree . . . . .	A-1
77	A.2	Usage of the DAQ . . . . .	A-2
78	A.3	Description of the readout setup . . . . .	A-3
79	A.4	Data read-out . . . . .	A-3
80	A.4.1	V1190A TDCs . . . . .	A-4
81	A.4.2	DataReader . . . . .	A-6
82	A.4.3	Data quality flag . . . . .	A-10
83	A.5	Communications . . . . .	A-12
84	A.5.1	V1718 USB Bridge . . . . .	A-13
85	A.5.2	Configuration file . . . . .	A-13
86	A.5.3	WebDCS/DAQ intercommunication . . . . .	A-17
87	A.5.4	Example of inter-process communication cycle . . . . .	A-18
88	A.6	Software export . . . . .	A-18
89	<b>B</b>	<b>Details on the offline analysis package</b>	<b>B-1</b>
90	B.1	GIF++ Offline Analysis file tree . . . . .	B-1
91	B.2	Usage of the Offline Analysis . . . . .	B-2
92	B.2.1	Output of the offline tool . . . . .	B-3
93	B.2.1.1	ROOT file . . . . .	B-3
94	B.2.1.2	CSV files . . . . .	B-5
95	B.3	Analysis inputs and information handling . . . . .	B-6
96	B.3.1	Dimensions file and IniFile parser . . . . .	B-6
97	B.3.2	TDC to RPC link file and Mapping . . . . .	B-7
98	B.4	Description of GIF++ setup within the Offline Analysis tool . . . . .	B-9
99	B.4.1	RPC objects . . . . .	B-9
100	B.4.2	Trolley objects . . . . .	B-10
101	B.4.3	Infrastructure object . . . . .	B-11
102	B.5	Handeling of data . . . . .	B-12
103	B.5.1	RPC hits . . . . .	B-13

---

104	B.5.2 Clusters of hits . . . . .	B-14
105	B.6 DAQ data Analysis . . . . .	B-15
106	B.6.1 Determination of the run type . . . . .	B-16
107	B.6.2 Beam time window calculation for efficiency runs . . . . .	B-17
108	B.6.3 Data loop and histogram filling . . . . .	B-18
109	B.6.4 Computation of the final results . . . . .	B-19
110	<b>C Structure of the hybrid simulation software</b>	<b>C-1</b>
111	C.1 Introduction . . . . .	C-1



# List of Figures

112

113	2.1	Absorbed dose in the CMS cavern after an integrated luminosity of 3000 fb. R is the transverse distance from the beamline and Z is the distance along the beamline from the Interaction Point at Z=0. . . . .	2-2
114	2.2	A quadrant of the muon system, showing DTs (yellow), RPCs (light blue), and CSCs (green). The locations of new forward muon detectors for Phase-II are contained within the dashed box and indicated in red for GEM stations (ME0, GE1/1, and GE2/1) and dark blue for improved RPC (iRPC) stations (RE3/1 and RE4/1). . . . .	2-2
115	2.3	RMS of the multiple scattering displacement as a function of muon $p_T$ for the proposed forward muon stations. All of the electromagnetic processes such as bremsstrahlung and magnetic field effect are included in the simulation. . . . .	2-3
116	4.1	Signals from the RPC strips are shaped by the FEE described on Figure 4.1a. Output LVDS signals are then read-out by a TDC module connected to a computer or converted into NIM and sent to scalers. Figure 4.1b describes how these converted signals are put in coincidence with the trigger. . . . .	4-3
117	4.2	Description of the principle of a CFD. A comparison of threshold triggering (left) and constant fraction triggering (right) is shown in Figure 4.2a. Constant fraction triggering is obtained thanks to zero-crossing technique as explained in Figure 4.2b. The signal arriving at the input of the CFD is split into three components. A first one is delayed and connected to the inverting input of a first comparator. A second component is connected to the noninverting input of this first comparator. A third component is connected to the noninverting input of another comparator along with a threshold value connected to the inverting input. Finally, the output of both comparators is fed through an AND gate. . . . .	4-4
118	5.1	(5.1a) Extrapolation from 2016 data of single hit rate per unit area in the barrel region. (5.1b) Extrapolation from 2016 data of single hit rate per unit area in the endcap region. . . . .	5-2
119	5.2	Background Fluka simulation compared to 2016 Data at $L = 10^{34} \text{ cm}^{-2} \cdot \text{s}^{-1}$ in the fourth endcap disk region. A mismatch in between simulation and data can be observed. [To be understood.] . . . . .	5-3
120	5.3	Layout of the test beam zone called X5c GIF at CERN. Photons from the radioactive source produce a sustained high rate of random hits over the whole area. The zone is surrounded by 8 m high and 80 cm thick concrete walls. Access is possible through three entry points. Two access doors for personnel and one large gate for material. A crane allows installation of heavy equipment in the area. . . . .	5-4
121	5.4	$^{137}\text{Cs}$ decays by $\beta^-$ emission to the ground state of $^{137}\text{Ba}$ (BR = 5.64%) and via the 662 keV isomeric level of $^{137}\text{Ba}$ (BR = 94.36%) whose half-life is 2.55 min. . . . .	5-5

149	5.5	Floor plan of the GIF++ facility. When the facility downstream of the GIF++ takes electron beam, a beam pipe is installed along the beam line (z-axis). The irradiator can be displaced laterally (its center moves from $x = 0.65$ m to 2.15 m), to increase the distance to the beam pipe. . . . .	5-5
150	5.6	Simulated unattenuated current of photons in the xz plane (Figure 5.6a) and yz plane (Figure 5.6b) through the source at $x = 0.65$ m and $y = 0$ m. With angular correction filters, the current of 662 keV photons is made uniform in xy planes. . . . .	5-6
151	5.7	Description of the RPC setup. Dimensions are given in mm. A tent containing RPCs is placed at 1720 mm from the source container. The source is situated in the center of the container. RE-4-2-BARC-161 chamber is 160 mm inside the tent. This way, the distance between the source and the chambers plan is 2060 mm. Figure 5.7a provides a side view of the setup in the xz plane while Figure 5.7b shows a top view in the yz plane. . . . .	5-7
152	5.8	RE-4-2-BARC-161 chamber is inside the tent as described in Figure 5.7. In the top right, the two scintillators used as trigger can be seen. This trigger system has an inclination of 10° relative to horizontal and is placed above half-partition B2 of the RPCs. PMT electronics are shielded thanks to lead blocks placed in order to protect them without stopping photons from going through the scintillators and the chamber. . . . .	5-8
153	5.9	Hit distributions over all 3 partitions of RE-4-2-BARC-161 chamber is showed on these plots. Top, middle and bottom figures respectively correspond to partitions A, B, and C. These plots show that some events still occur in other half-partitions than B2, which corresponds to strips 49 to 64, in front of which the trigger is placed, contributing to the inefficiency of detection of cosmic muons. In the case of partitions A and C, the very low amount of data can be interpreted as noise. On the other hand, it is clear that a little portion of muons reach the half-partition B1, corresponding to strips 33 to 48. . . . .	5-9
154	5.10	Results are derived from data taken on half-partition B2 only. On the 18 <sup>th</sup> of June 2014, data has been taken on chamber RE-2-BARC-161 at building 904 (Prevessin Site) with cosmic muons providing us a reference efficiency plateau of $(97.54 \pm 0.15)\%$ represented by a black curve. A similar measurement has been done at GIF on the 21 <sup>st</sup> of July with the same chamber giving a plateau of $(78.52 \pm 0.94)\%$ represented by a red curve. . . . .	5-10
155	5.11	Representation of the layout used for the simulations of the test setup. The RPC is represented as a yellow trapezoid while the two scintillators as blue cuboids looking at the sky. A green plane corresponds to the muon generation plane within the simulation. Figure 5.7a shows a global view of the simulated setup. Figure 5.7b shows a zommed view that allows to see the 2 scintillators as well as the full RPC plane. . . . .	5-11
156	5.12	$\gamma$ flux $F(D)$ is plot using values from table 5.1. As expected, the plot shows similar attenuation behaviours with increasing distance for each absorption factors. . . . .	5-14
157	5.13	Figure 5.13a shows the linear approximation fit done via formulae 5.7 on data from table 5.2. Figure 5.13b shows a comparison of this model with the simulated flux using a and b given in figure 5.13a in formulae 5.4 and the reference value $D_0 = 50\text{cm}$ and the associated flux for each absorption factor $F_0^{ABS}$ from table 5.1 . . . . .	5-16
158	5.14	Dose measurements has been done in a plane corresponding to the tents front side. This plan is 1900 mm away from the source. As explained in the first chapter, a lens-shaped lead filter provides a uniform photon flux in the vertical plan orthogonal to the beam direction. If the second line of measured fluxes is not taken into account because of lower values due to experimental equipments in the way between the source and the tent, the uniformity of the flux is well showed by the results. . . . .	5-18
159			
160			
161			
162			
163			
164			
165			
166			
167			
168			
169			
170			
171			
172			
173			
174			
175			
176			
177			
178			
179			
180			
181			
182			
183			
184			
185			
186			
187			
188			
189			
190			
191			
192			
193			
194			
195			
196			
197			

---

198	5.15 . . . . .	5-19
199	5.16 Evolution of the maximum efficiency for RE2 (5.16a) and RE4 (5.16b) chambers 200 with increasing extrapolated $\gamma$ rate per unit area at working point. Both irradiated 201 (blue) and non irradiated (red) chambers are shown. . . . .	5-21
202	5.17 Evolution of the working point for RE2 (5.17a) and RE4 (5.17b) with increasing 203 extrapolated $\gamma$ rate per unit area at working point. Both irradiated (blue) and non 204 irradiated (red) chambers are shown. . . . .	5-21
205	5.18 Evolution of the maximum efficiency at HL-LHC conditions, i.e. a background hit 206 rate per unit area of 300 Hz/cm <sup>2</sup> , with increasing integrated charge for RE2 (5.18a) 207 and RE4 (5.18b) detectors. Both irradiated (blue) and non irradiated (red) chambers 208 are shown. The integrated charge for non irradiated detectors is recorded during test 209 beam periods and stays small with respect to the charge accumulated in irradiated 210 chambers. . . . .	5-22
211	5.19 Comparison of the efficiency sigmoid before (triangles) and after (circles) irradiation 212 for RE2 (5.19a) and RE4 (5.19b) detectors. Both irradiated (blue) and non irradiated 213 (red) chambers are shown. . . . .	5-22
214	5.20 Evolution of the Bakelite resistivity for RE2 (5.20a) and RE4 (5.20b) detectors. Both 215 irradiated (blue) and non irradiated (red) chambers are shown. . . . .	5-23
216	5.21 Evolution of the noise rate per unit area for the irradiated chamber RE2-2-BARC-9 217 only. . . . .	5-23
218	A.1 (A.1a) View of the front panel of a V1190A TDC module [10]. (A.1b) View of the 219 front panel of a V1718 Bridge module [11]. (A.1c) View of the front panel of a 6U 220 6021 VME crate [12]. . . . .	A-3
221	A.2 Module V1190A <i>Trigger Matching Mode</i> timing diagram [10]. . . . .	A-4
222	A.3 Structure of the ROOT output file generated by the DAQ. The 5 branches ( <code>EventNumber</code> , 223 <code>number_of_hits</code> , <code>Quality_flag</code> , <code>TDC_channel</code> and <code>TDC_TimeStamp</code> ) are visible on 224 the left panel of the ROOT browser. On the right panel is visible the histogram cor- 225 responding to the variable <code>nHits</code> . In this specific example, there were approximately 226 50k events recorded to measure the gamma irradiation rate on the detectors. Each 227 event is stored as a single entry in the <code>TTree</code> . . . . .	A-10
228	A.4 The effect of the quality flag is explained by presenting the content of <code>TBranch</code> 229 <code>number_of_hits</code> of a data file without <code>Quality_flag</code> in Figure A.4a and the con- 230 tent of the same <code>TBranch</code> for data corresponding to a <code>Quality_flag</code> where all TDCs 231 were labelled as <code>GOOD</code> in Figure A.4b taken with similar conditions. It can be noted 232 that the number of entries in Figure A.4b is slightly lower then in Figure A.4a due 233 to the excluded events. . . . .	A-12
234	A.5 Using the same data as previously showed in Figure A.4, the effect of the quality 235 flag is explained by presenting the reconstructed hit multiplicity of a data file with- 236 out <code>Quality_flag</code> in Figure A.5a and the reconstructed content of the same RPC 237 partition for data corresponding to a <code>Quality_flag</code> where all TDCs were labelled as 238 <code>GOOD</code> in Figure A.5b taken with similar conditions. The artificial high content of bin 239 0 is completely suppressed. . . . .	A-12
240	A.6 WebDCS DAQ scan page. On this page, shifters need to choose the type of scan 241 (Rate, Efficiency or Noise Reference scan), the gamma source configuration at the 242 moment of data taking, the beam configuration, and the trigger mode. These in- 243 formation will be stored in the DAQ ROOT output. Are also given the minimal 244 measurement time and waiting time after ramping up of the detectors is over before 245 starting the data acquisition. Then, the list of HV points to scan and the number of 246 triggers for each run of the scan are given in the table underneath. . . . .	A-14

247	B.1	Example of expected hit time distributions in the cases of efficiency (Figure B.1a)	
248		and noise/gamma rate per unit area (Figure B.1b) measurements as extracted from	
249		the raw ROOT files. The unit along the x-axis corresponds to ns. The fact that	
250		"the" muon peak is not well defined in Figure B.1a is due to the contribution of all	
251		the RPCs being tested at the same time that don't necessarily have the same signal	
252		arrival time. Each individual peak can have an offset with the ones of other detectors.	
253		The inconsistancy in the first 100 ns of both time distributions is an artefact of the	
254		TDCs and are systematically rejected during the analysis. . . . .	B-16
255	B.2	The effect of the quality flag is explained by presenting the reconstructed hit multi-	
256		plicity of a data file without <code>Quality_flag</code> . The artificial high content of bin 0 is the	
257		effect of corrupted data. . . . .	B-19

## List of Tables

258

259	5.1	Total photon flux ( $E\gamma \leq 662$ keV) with statistical error predicted considering a	
260		$^{137}\text{Cs}$ activity of 740 GBq at different values of the distance $D$ to the source along	
261		the x-axis of irradiation field [6]. . . . .	5-13
262	5.2	Correction factor $c$ is computed thanks to formulae 5.5 taking as reference $D_0 =$	
263		50 cm and the associated flux $F_0^{ABS}$ for each absorption factor available in table 5.1. . . . .	5-15
264	5.3	The data at $D_0$ in 1997 is taken from [6]. In a second step, using Equations 5.8	
265		and 5.9, the flux at $D$ can be estimated in 1997. Then, taking into account the	
266		attenuation of the source activity, the flux at $D$ can be estimated at the time of the	
267		tests in GIF in 2014. Finally, assuming a sensitivity of the RPC to $\gamma$ $s = 2 \cdot 10^{-3}$ ,	
268		an estimation of the hit rate per unit area is obtained. . . . .	5-17
269	A.1	Inter-process communication cycles in between the webDCS and the DAQ through	
270		file string signals. . . . .	A-19



# List of Acronyms

271

## List of Acronyms

273

274

### A

275

276

277 AFL

Almost Full Level

278

279

### B

280

281

282 BARC

Bhabha Atomic Research Centre

283 BLT

Block Transfer

284 BR

Branching Ratio

285

286

### C

287

289 CAEN

Costruzioni Apparecchiature Elettroniche Nucleari S.p.A.

290 CERN

European Organization for Nuclear Research

291 CFD

Constant Fraction Discriminator

292 CMS

Compact Muon Solenoid

293 CSC

Cathode Strip Chamber

294

295

### D

296

297

298 DAQ

Data Acquisition

299 DCS

Detector Control Software

300 DQM

Data Quality Monitoring

301 DT

Drift Tube

302

303

### F

304

305

306	<b>FEE</b>	Front-End Electronics
307	<b>FEB</b>	Front-End Board
308		
309	<b>G</b>	
310		
311		
312	<b>GE-/-</b>	Find a good description
313	<b>GE1/1</b>	Find a good description
314	<b>GE2/1</b>	Find a good description
315	<b>GEANT</b>	GEometry ANd Tracking - a series of software toolkit platforms developed by CERN
316		
317	<b>GEM</b>	Gas Electron Multiplier
318	<b>GIF</b>	Gamma Irradiation Facility
319	<b>GIF++</b>	new Gamma Irradiation Facility
320		
321	<b>H</b>	
322		
323		
324	<b>HL-LHC</b>	High Luminosity LHC
325	<b>HV</b>	High Voltage
326		
327	<b>I</b>	
328		
329		
330	<b>iRPC</b>	improved RPC
331	<b>IRQ</b>	Interrupt Request
332		
333	<b>L</b>	
334		
335		
336	<b>LHC</b>	Large Hadron Collider
337	<b>LS1</b>	First Long Shutdown
338	<b>LS3</b>	Third Long Shutdown
339	<b>LV</b>	Low Voltage
340	<b>LVDS</b>	Low-Voltage Differential Signaling
341		
342	<b>M</b>	
343		
344		
345	<b>MC</b>	Monte Carlo
346	<b>MCNP</b>	Monte Carlo N-Particle
347	<b>ME-/-</b>	Find good description
348	<b>ME0</b>	Find good description

---

349		
350	<b>N</b>	
351		
352		
353	<b>NIM</b>	Nuclear Instrumentation Module logic signals
354		
355	<b>P</b>	
356		
357		
358	<b>PMT</b>	PhotoMultiplier Tube
359		
360	<b>R</b>	
361		
362		
363	<b>RE-/-</b>	Find a good description
364	<b>RE2/2</b>	Find a good description
365	<b>RE3/1</b>	Find a good description
366	<b>RE3/2</b>	Find a good description
367	<b>RE4/1</b>	Find a good description
368	<b>RE4/2</b>	Find a good description
369	<b>RE4/3</b>	Find a good description
370	<b>RMS</b>	Root Mean Square
371	<b>ROOT</b>	a framework for data processing born at CERN
372	<b>RPC</b>	Resistive Plate Chamber
373		
374	<b>S</b>	
375		
376		
377	<b>SPS</b>	Super Proton Synchrotron
378		
379	<b>T</b>	
380		
381		
382	<b>TDC</b>	Time-to-Digital Converter
383		
384	<b>W</b>	
385		
386		
387	<b>webDCS</b>	Web Detector Control System



389

## Nederlandse samenvatting –Summary in Dutch–

391 Le resume en Neerlandais (j'aurais peut-être de apprendre la langue juste pour ca...).

390



## English summary

<sup>393</sup> Le meme résume mais en Anglais (on commencera par la hein!).



# 1

## Introduction

394

395

<sup>396</sup> **1.1 A story of High Energy Physics**

<sup>397</sup> **1.2 Organisation of this study**



# 2

398

399

## Investigating the TeV scale

### 400 2.1 The Standard Model of Particle Physics

### 401 2.2 The Large Hadron Collider and the Compact Muon Solenoid

### 402 2.3 Muon Phase-II Upgrade

403 After the more than two years lasting First Long Shutdown (LS1), the Large Hadron Collider (LHC)  
404 delivered its very first Run-II proton-proton collisions early 2015. LS1 gave the opportunity to the  
405 LHC and to the its experiments to undergo upgrades. The accelerator is now providing collisions  
406 at center-of-mass energy of 13 TeV and bunch crossing rate of 40 MHz, with a peak luminosity  
407 exceeding its design value. During the first and upcoming second LHC Long Shutdown, the Compact  
408 Muon Solenoid (CMS) detector is also undergoing a number of upgrades to maintain a high system  
409 performance [1].

410 From the LHC Phase-2 or High Luminosity LHC (HL-LHC) period onwards, i.e. past the Third  
411 Long Shutdown (LS3), the performance degradation due to integrated radiation as well as the average  
412 number of inelastic collisions per bunch crossing, or pileup, will rise substantially and become a  
413 major challenge for the LHC experiments, like CMS that are forced to address an upgrade program  
414 for Phase-II [2]. Simulations of the expected distribution of absorbed dose in the CMS detector  
415 under HL-LHC conditions, show in figure 5.14 that detectors placed close to the beamline will have  
416 to withstand high irradiation, the radiation dose being of the order of a few tens of Gy.

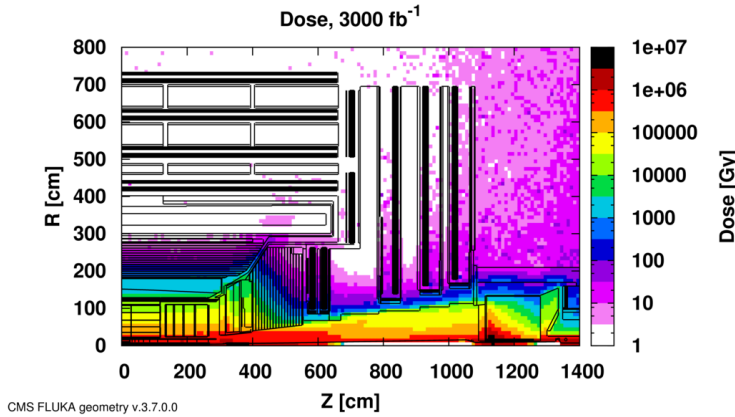


*Figure 2.1: Absorbed dose in the CMS cavern after an integrated luminosity of 3000 fb<sup>-1</sup>. R is the transverse distance from the beamline and Z is the distance along the beamline from the Interaction Point at Z=0.*

417     The measurement of small production cross-section and/or decay branching ratio processes, such  
 418     as the Higgs boson coupling to charge leptons or the  $B_s \rightarrow \mu^+\mu^-$  decay, is of major interest and  
 419     specific upgrades in the forward regions of the detector will be required to maximize the physics  
 420     acceptance on the largest possible solid angle. To ensure proper trigger performance within the  
 421     present coverage, the muon system will be completed with new chambers. In figure 2.2 one can  
 422     see that the existing Cathode Strip Chambers (CSCs) will be completed by Gas Electron Multipliers  
 423     (GEMs) and Resistive Plate Chambers (RPCs) in the pseudo-rapidity region  $1.6 < |\eta| < 2.4$  to  
 424     complete its redundancy as originally scheduled in the CMS Technical Proposal [3].

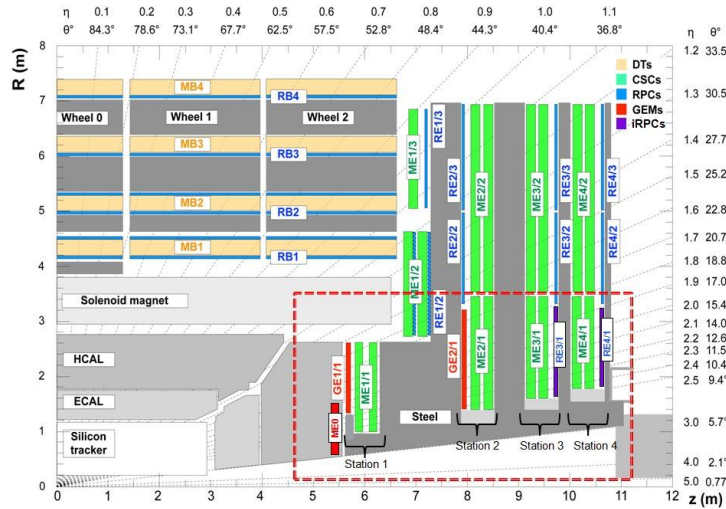


*Figure 2.2: A quadrant of the muon system, showing DTs (yellow), RPCs (light blue), and CSCs (green). The locations of new forward muon detectors for Phase-II are contained within the dashed box and indicated in red for GEM stations (MEO, GE1/1, and GE2/1) and dark blue for improved RPC (iRPC) stations (RE3/1 and RE4/1).*

425     RPCs are used by the CMS first level trigger for their good timing performances. Indeed, a very

good bunch crossing identification can be obtained with the present CMS RPC system, given their fast response of the order of 1 ns. In order to contribute to the precision of muon momentum measurements, muon chambers should have a spatial resolution less or comparable to the contribution of multiple scattering [1]. Most of the plausible physics is covered only considering muons with  $p_T < 100$  GeV thus, in order to match CMS requirements, a spatial resolution of  $\mathcal{O}(\text{few mm})$  the proposed new RPC stations, as shown by the simulation in figure 2.3. According to preliminary designs, RE3/1 and RE4/1 readout pitch will be comprised between 3 and 6 mm and 5  $\eta$ -partitions could be considered.

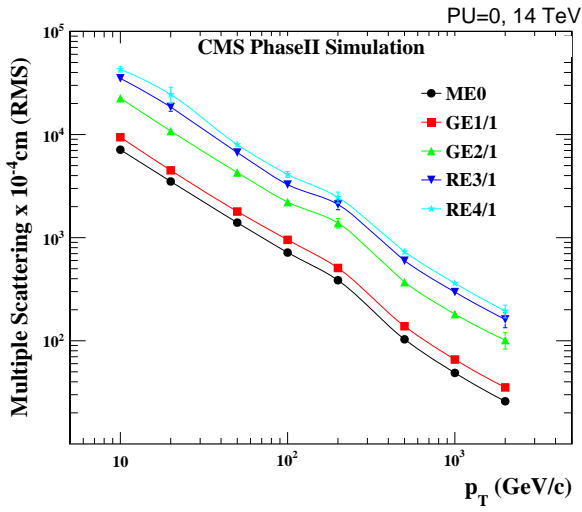


Figure 2.3: RMS of the multiple scattering displacement as a function of muon  $p_T$  for the proposed forward muon stations. All of the electromagnetic processes such as bremsstrahlung and magnetic field effect are included in the simulation.



# 3

434

## Amplification processes in gaseous detectors

436 **3.1 Signal formation**

437 **3.2 Gas transport parameters**



# 4

438

439

## Resistive Plate Chambers

440 **4.1 Principle**

441 **4.2 Rate capability of Resistive Plate Chambers**

442 **4.3 High time resolution**

443 **4.4 Resistive Plate Chambers at CMS**

444 **4.4.1 Overview**

445 The Resistive Plate Chambers (RPC) system, located in both barrel and endcap regions, provides a  
446 fast, independent muon trigger with a looser  $p_T$  threshold over a large portion of the pseudorapidity  
447 range ( $|\eta| < 1.6$ ) [add reconstruction].

448 During High-Luminosity LHC (HL-LHC) operations the expected conditions in terms of back-  
449 ground and pile-up will make the identification and correct  $P_T$  assignment a challenge for the Muon  
450 system. The goal of RPC upgrade is to provide additional hits to the Muon system with precise tim-  
451 ing. All these informations will be elaborated by the trigger system in a global way enhancing the  
452 performance of the trigger in terms of efficiency and rate control. The RPC Upgrade is based on two  
453 projects: an improved Link Board System and the extension of the RPC coverage up to  $|\eta| = 2.4$ .  
454 [FIXME 2.4 or 2.5?]

455 The Link Board system, that will be described in section xxx, is responsible to process, syn-  
456 chronize and zero-suppress the signals coming from the RPC front end boards. The Link Board  
457 components have been produced between 2006 and 2007 and will be subjected to aging and failure  
458 in the long term. The upgraded Link Board system will overcome the aging problems described in  
459 section xxx and will allow for a more precise timing information to the RPC hits from 25 to 1 ns [ref  
460 section xxx].

462 The extension of the RPC system up to  $|\eta| = 2.1$  was already planned in the CMS TDR [ref  
 463 cmstdr] and staged because of budget limitations and expected background rates higher than the rate  
 464 capability of the present CMS RPCs in that region. An extensive R&D program has been done in  
 465 order to develop an improved RPC that fulfills the CMS requirements. Two new RPC layers in the  
 466 innermost ring of stations 3 and 4 will be added with benefits to the neutron-induced background  
 467 reduction and efficiency improvement for both trigger and offline reconstruction.

#### 468 4.4.2 The present RPC system

469 The RPC system is organized in 4 stations called RB1 to RB4 in the barrel region, and RE1 to RE4  
 470 in the endcap region. The innermost barrel stations, RB1 and RB2, are instrumented with 2 layers  
 471 of RPCs facing the innermost (RB1in and RB2in) and outermost (RB1out and RB2out) sides of the  
 472 DT chambers. Every chamber is then divided from the read-out point of view into 2 or 3  $\eta$  partitions  
 473 called “rolls”. The RPC system consist of 480 barrel chambers and 576 endcap chambers. Details  
 474 on the geometry are discussed in the paper [ref to geo paper].

475 The CMS RPC chamber is a double-gap, operated in avalanche mode to ensure reliable operation  
 476 at high rates. Each RPC gap consists of two 2-mm-thick resistive High-Pressure Laminate (HPL)  
 477 plates separated by a 2-mm-thick gas gap. The outer surface of the HPL plates is coated with a thin  
 478 conductive graphite layer, and a voltage is applied. The RPCs are operated with a 3-component,  
 479 non-flammable gas mixture consisting of 95.2% freon ( $C_2H_2F_4$ , known as R134a), 4.5% isobutane  
 480 ( $i-C_4H_{10}$ ), and 0.3% sulphur hexafluoride ( $SF_6$ ) with a relative humidity of 40% - 50%. Readout  
 481 strips are aligned in  $\eta$  between the 2 gas gaps. [\[Add a sentence on FEBs.\]](#)

482 The discriminated signals coming from the Front End boards feed via twisted cables (10 to 20 m  
 483 long) the Link Board System located in UXC on the balconies around the detector. The Link System  
 484 consist of the 1376 Link Boards (LBs) and the 216 Control Boards (CBs), placed in 108 Link Boxes.  
 485 The Link Box is a custom crate (6U high) with 20 slots (for two CBs and eighteen LBs). The Link  
 486 Box contains custom backplane to which the cables from the chambers are connected, as well as the  
 487 cables providing the LBs and CBs power supply and the cables for the RPC FEBs control with use  
 488 of the I2C protocol (trough the CB). The backplane itself contains only connectors (and no any other  
 489 electronic devices).

490 The Link Board has 96 input channels (one channel corresponds to one RPC strip). The input  
 491 signals are the  $\sim 100$  ns binary pulses which are synchronous to the RPC hits, but not to the LHC  
 492 clock (which drives the entire CMS electronics). Thus the first step of the FEB signals processing  
 493 is synchronization, i.e. assignment of the signals to the BXes (25 ns periods). Then the data are  
 494 compressed with a simple zero-suppressing algorithm (the input channels are grouped into 8 bit  
 495 partitions, only the partitions with at least one nonzero bit are selected for each BX). Next, the non-  
 496 empty partitions are time-multiplexed i.e. if there are more than one such partition in a given BX,  
 497 they are sent one-by-one in consecutive BXes. The data from 3 neighbouring LBs are concentrated  
 498 by the middle LB which contains the optical transmitter for sending them to the USC over a fiber at  
 499 1.6 Gbps.

500 The Control Boards provide the communication of the control software with the LBs via the  
 501 FEC/CCU system. The CBs are connected into token rings, each ring consists of 12 CBs of one  
 502 detector tower and a FEC mezzanine board placed on the CCS board located in the VME crate in  
 503 the USC. In total, there are 18 rings in the entire Link System. The CBs also perform automatic  
 504 reloading of the LB's firmware which is needed in order to avoid accumulation of the radiation  
 505 induced SEUs in the LBs firmware.

506 Both LBs and CB are based on the Xilinx Spartan III FPGAs, the CB additionally contains  
 507 radiation-tolerant (FLASH based) FPGA Actel ProAsicPlus.

508 The High Voltage power system is located in USC, not exposed to radiation and easily accessible  
 509 for any reparation. A single HV channel powers 2 RPC chambers both in the barrel and endcap  
 510 regions. The Low Voltage boards are located in UXC on the balconies and provide the voltage to the  
 511 front end electronics.

#### 512 4.4.3 Pulse processing of CMS RPCs

513 Signals induced by cosmic particle in the RPC strips are shaped by standard CMS RPC Front-End  
 514 Electronics (FEE) following the scheme of Figure 4.1. On a first stage, analogic signals are amplified  
 515 and then sent to the Constant Fraction Discriminator (CFD) described in Figure 4.2. At the end of  
 516 the chain, 100 ns long pulses are sent in the LVDS output. These output signal are sent on one side to  
 517 a V1190A Time-to-Digital Converter (TDC) module from CAEN and on the other to an OR module  
 518 to count the number of detected signals. Trigger and hit coïncidences are monitored using scalers.  
 519 The TDC is used to store the data into ROOT files. These files are thus analysed to understand the  
 520 detectors performance.

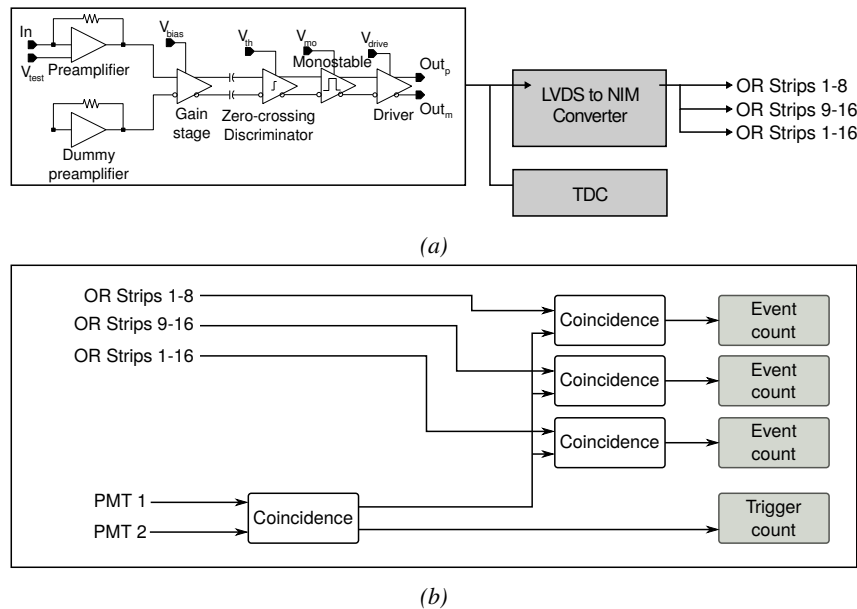
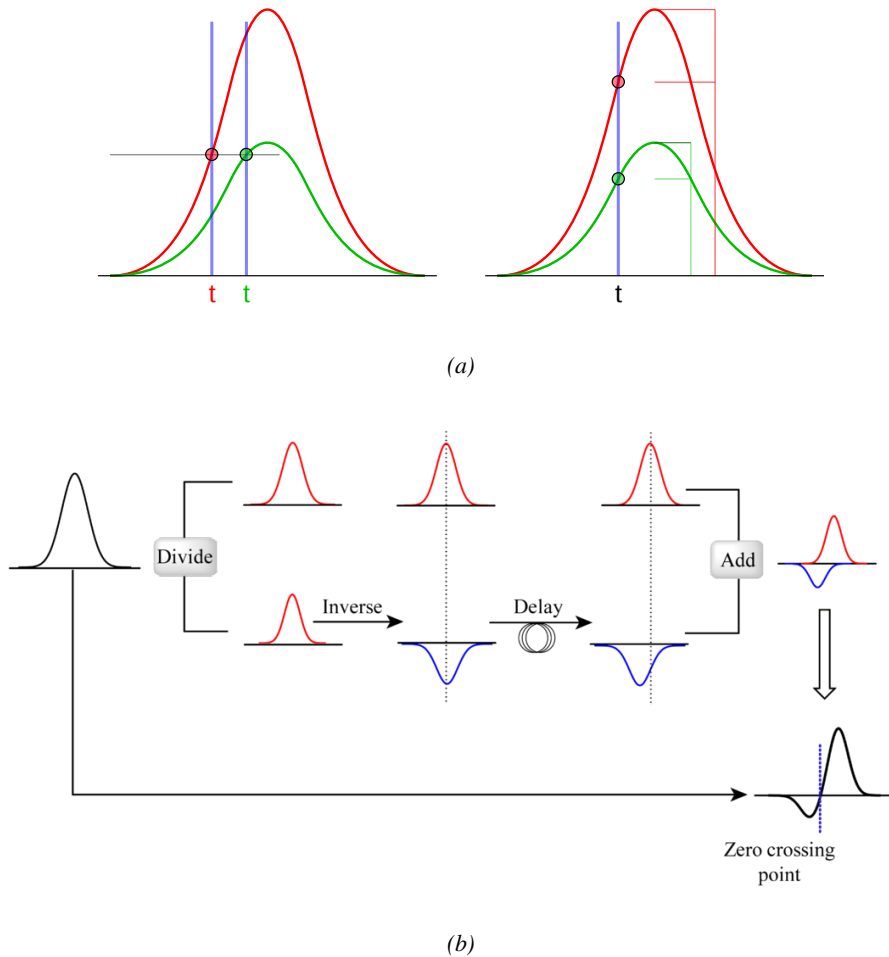


Figure 4.1: Signals from the RPC strips are shaped by the FEE described on Figure 4.1a. Output LVDS signals are then read-out by a TDC module connected to a computer or converted into NIM and sent to scalers. Figure 4.1b describes how these converted signals are put in coincidence with the trigger.



*Figure 4.2: Description of the principle of a CFD. A comparison of threshold triggering (left) and constant fraction triggering (right) is shown in Figure 4.2a. Constant fraction triggering is obtained thanks to zero-crossing technique as explained in Figure 4.2b. The signal arriving at the input of the CFD is split into three components. A first one is delayed and connected to the inverting input of a first comparator. A second component is connected to the noninverting input of this first comparator. A third component is connected to the noninverting input of another comparator along with a threshold value connected to the inverting input. Finally, the output of both comparators is fed through an AND gate.*

# 5

521

522  
523

## Longevity studies and Consolidation of the present CMS RPC subsystem

524

### 5.1 Testing detectors under extreme conditions

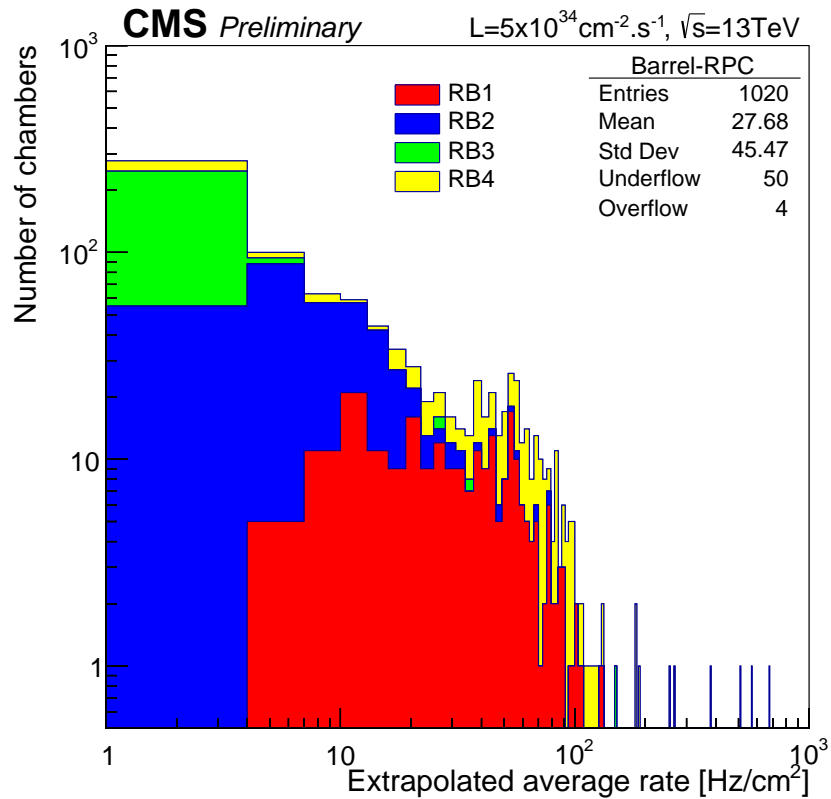
525  
526  
527  
528  
529  
530  
531  
532

The upgrade from LHC to HL-LHC will increase the peak luminosity from  $10^{34} \text{ cm}^{-2} \text{ s}^{-1}$  to reach  $5 \times 10^{34} \text{ cm}^{-2} \text{ s}^{-1}$ , increasing in the same way the total expected background to which the RPC system will be subjected to. Composed of low energy gammas and neutrons from  $p\text{-}p$  collisions, low momentum primary and secondary muons, puch-through hadrons from calorimeters, and particles produced in the interaction of the beams with collimators, the background will mostly affect the regions of CMS that are the closest to the beam line, i.e. the RPC detectors located in the endcaps.

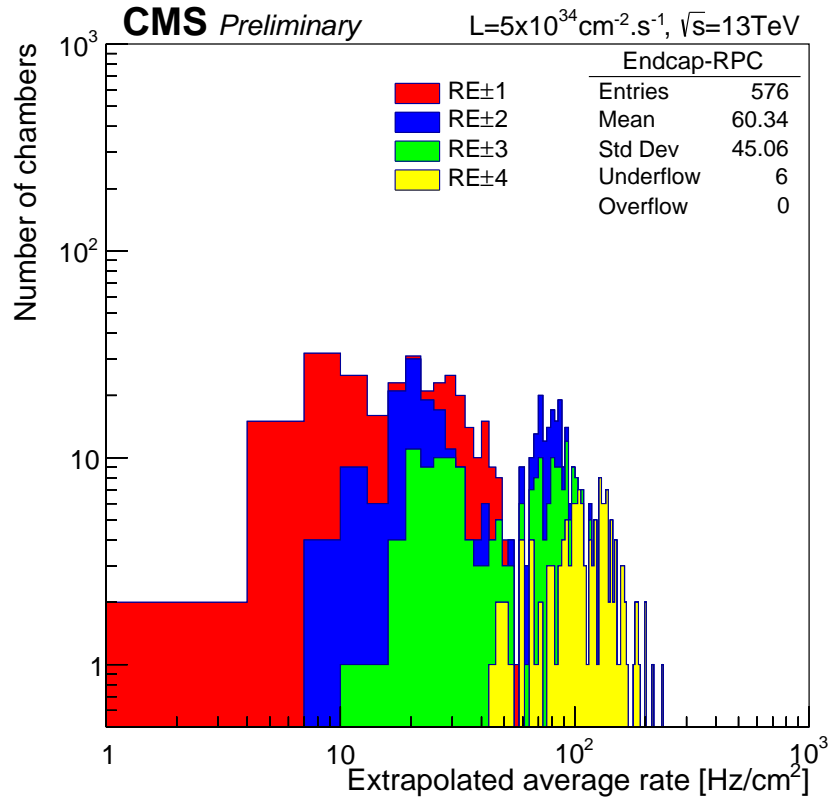
[To update.]

533  
534  
535  
536  
537  
538  
539  
540  
541

The 2016 data allowed to study the values of the background rate in all RPC system. In Figure 5.1, the distribution of the chamber background hit rate per unit area is shown at a luminosity of  $5 \times 10^{34} \text{ cm}^{-2} \cdot \text{s}^{-1}$  linearly extrapolating from data collected in 2016 [ref mentioning the linear dependency of rate vs lumi]. The maximum rate per unit area at HL-LHC conditions is expected to be of the order of  $600 \text{ Hz/cm}^2$  (including a safety factor 3). Nevertheless, Fluka simulations have conducted in order to understand the background at HL-LHC conditions. The comparison to the data has shown, in Figure 5.2, a discrepancy of a factor 2 even though the order of magnitude is consistent. [Understand mismatch.]



(a)



(b)

Figure 5.1: (5.1a) Extrapolation from 2016 data of single hit rate per unit area in the barrel region. (5.1b) Extrapolation from 2016 data of single hit rate per unit area in the endcap region.

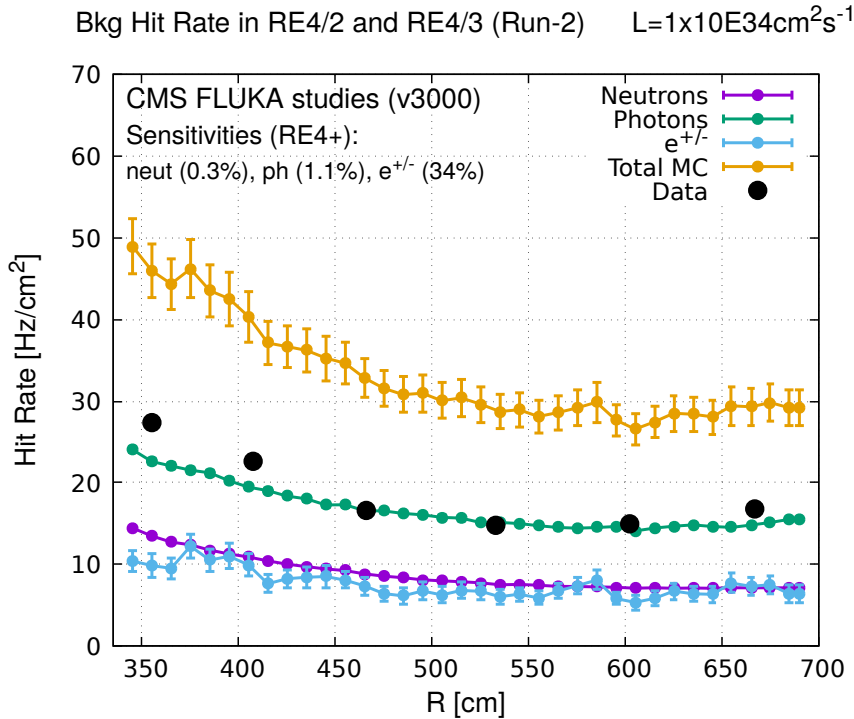


Figure 5.2: Background Fluka simulation compared to 2016 Data at  $L = 10^{34}\text{cm}^{-2}\cdot\text{s}^{-1}$  in the fourth endcap disk region. A mismatch in between simulation and data can be observed. [\[To be understood.\]](#)

542 In the past, extensive long-term tests were carried out at several gamma and neutron facilities  
 543 certifying the detector performance. Both full size and small prototype RPCs have been irradiated  
 544 with photons up to an integrated charge of  $\sim 0.05\text{C}/\text{cm}^2$  and  $\sim 0.4\text{C}/\text{cm}^2$ , respectively [4, 5].  
 545 During Run-I, the RPC system provided stable operation and excellent performance and did not  
 546 show any aging effects for integrated charge of the order of  $0.01\text{C}/\text{cm}^2$ . Projections on currents  
 547 from 2016 Data, has allowed to determine that the total integrated charge, by the end of HL-LHC,  
 548 would be of the order of  $1\text{C}/\text{cm}^2$  (including a safety factor 3). [\[Corresponding figure needed.\]](#)

549

### 550 5.1.1 The Gamma Irradiation Facilities

#### 551 5.1.1.1 GIF

552 Located in the SPS West Area at the downstream end of the X5 test beam, the Gamma Irradiation  
 553 Facility (GIF) was a test area in which particle detectors were exposed to a particle beam in presence  
 554 of an adjustable gamma background [6]. Its goal was to reproduce background conditions these  
 555 detectors would suffer in their operating environment at LHC. GIF layout is shown in Figure 5.3.  
 556 Gamma photons are produced by a strong  $^{137}\text{Cs}$  source installed in the upstream part of the zone  
 557 inside a lead container. The source container includes a collimator, designed to irradiate a  $6 \times 6\text{ m}^2$   
 558 area at 5 m maximum to the source. A thin lens-shaped lead filter helps providing with a uniform  
 559 outcoming flux in a vertical plane, orthogonal to the beam direction. The principal collimator hole  
 560 provides a pyramidal aperture of  $74^\circ \times 74^\circ$  solid angle and provides a photon flux in a pyramidal vol-

ume along the beam axis. The photon rate is controled by further lead filters allowing the maximum rate to be limited and to vary within a range of four orders of magnitude. Particle detectors under test are then placed within the pyramidal volume in front of the source, perpendicularly to the beam line in order to profit from the homogeneous photon flux. Adjusting the background flux of photons can then be done by using the filters and choosing the position of the detectors with respect to the source.

566

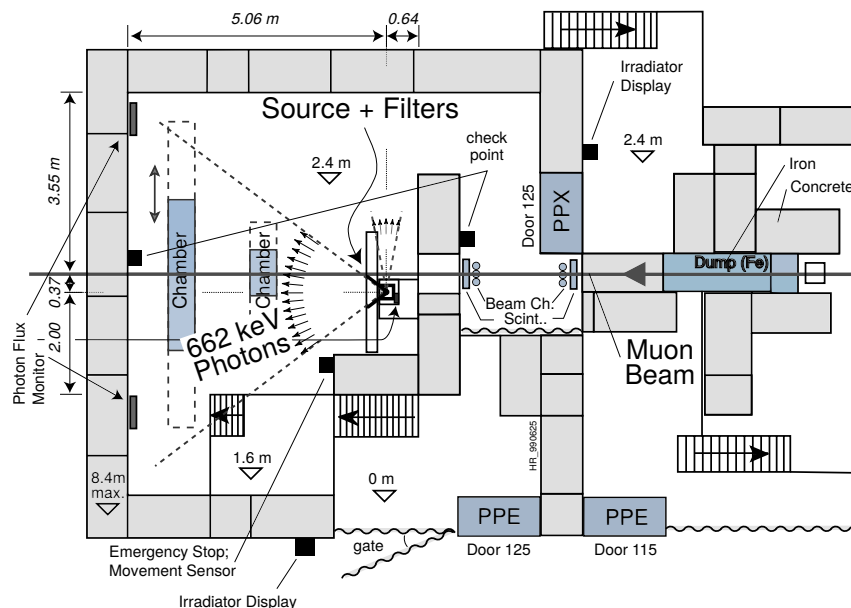


*Figure 5.3: Layout of the test beam zone called X5c GIF at CERN. Photons from the radioactive source produce a sustained high rate of random hits over the whole area. The zone is surrounded by 8 m high and 80 cm thick concrete walls. Access is possible through three entry points. Two access doors for personnel and one large gate for material. A crane allows installation of heavy equipment in the area.*

As described on Figure 5.4, the  $^{137}\text{Cs}$  source emits a 662 keV photon in 85% of the decays. An activity of 740 GBq was measured on the 5<sup>th</sup> March 1997. To estimate the strength of the flux in 2014, it is necessary to consider the nuclear decay through time assiciated to the Cesium source whose half-life is well known ( $t_{1/2} = (30.05 \pm 0.08)$  y). The GIF tests where done in between the 20<sup>th</sup> and the 31<sup>st</sup> of August 2014, i.e. at a time  $t = (17.47 \pm 0.02)$  y resulting in an attenuation of the activity from 740 GBq in 1997 to 494 GBq in 2014.

573

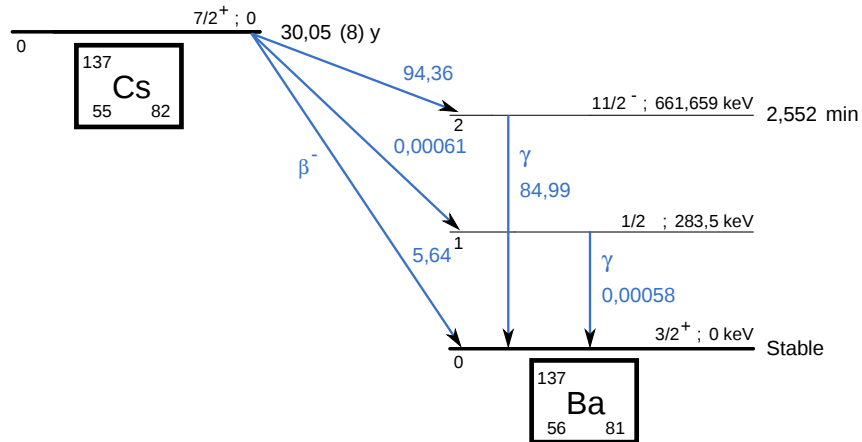


Figure 5.4:  $^{137}\text{Cs}$  decays by  $\beta^-$  emission to the ground state of  $^{137}\text{Ba}$  ( $\text{BR} = 5.64\%$ ) and via the 662 keV isomeric level of  $^{137}\text{Ba}$  ( $\text{BR} = 94.36\%$ ) whose half-life is 2.55 min.

### 5.1.1.2 GIF++

The new Gamma Irradiation Facility (GIF++), located in the SPS North Area at the downstream end of the H4 test beam, has replaced its predecessor during LS1 and has been operational since spring 2015 [7]. Like GIF, GIF++ features a  $^{137}\text{Cs}$  source of 662 keV gamma photons, their fluence being controlled with a set of filters of various attenuation factors. The source provides two separated large irradiation areas for testing several full-size muon detectors with continuous homogeneous irradiation, as presented in Figure 5.5.

581

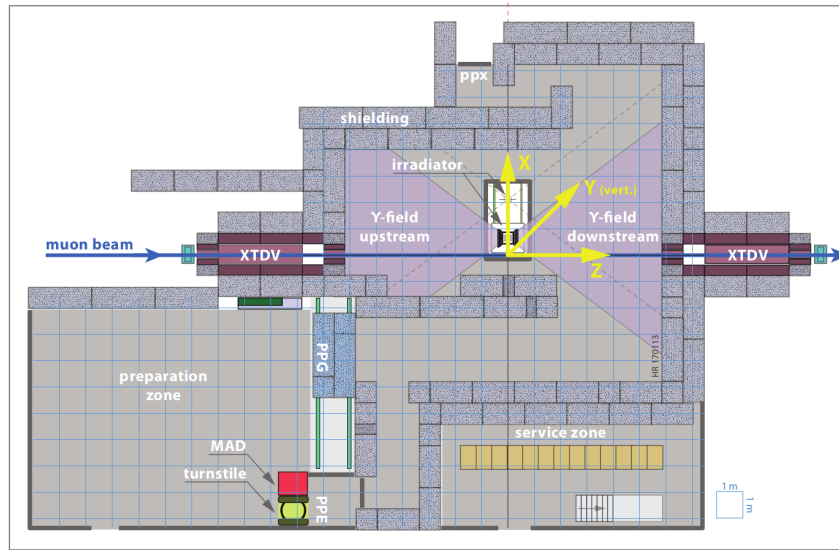
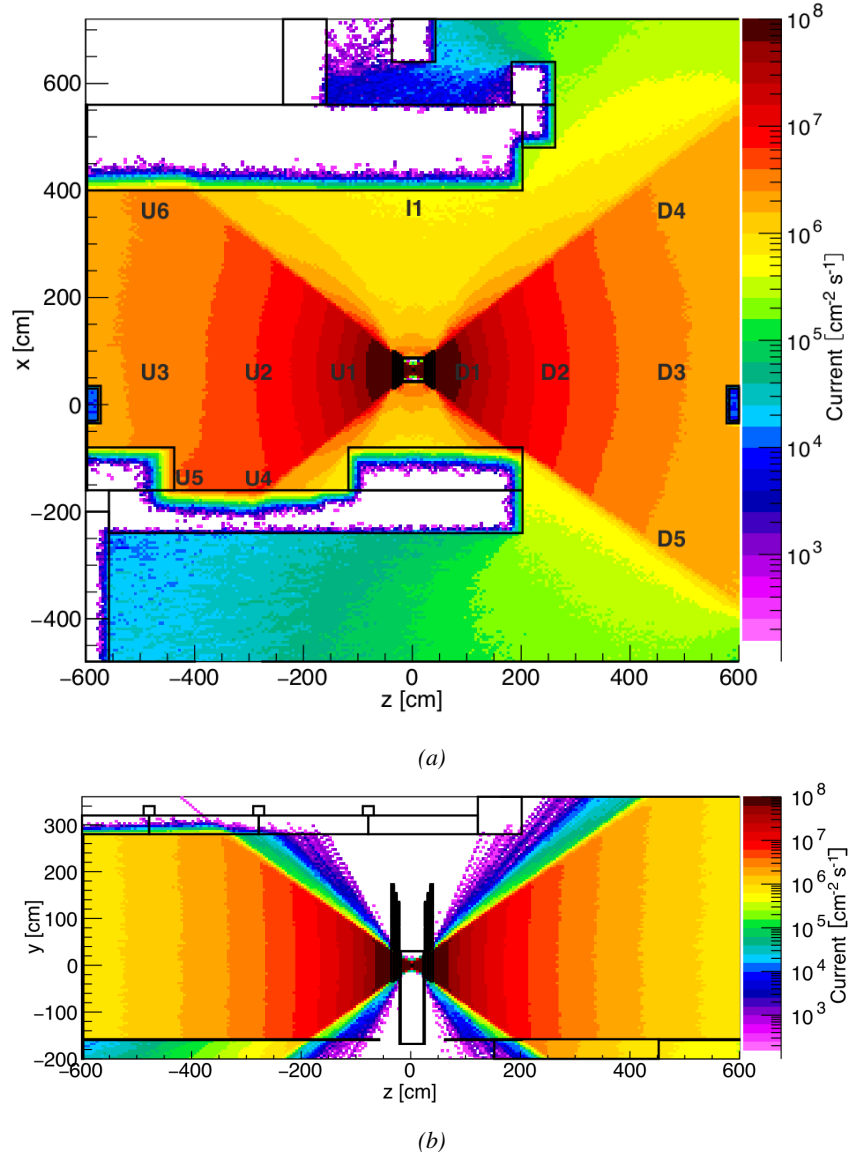


Figure 5.5: Floor plan of the GIF++ facility. When the facility downstream of the GIF++ takes electron beam, a beam pipe is installed along the beam line ( $z$ -axis). The irradiator can be displaced laterally (its center moves from  $x = 0.65$  m to  $2.15$  m), to increase the distance to the beam pipe.

582 The source activity was measured to be about 13.5 TBq in March 2016. The photon flux being  
 583 far greater than HL-LHC expectations, GIF++ provides an excellent facility for accelerated aging  
 584 tests of muon detectors.

585



*Figure 5.6: Simulated unattenuated current of photons in the xz plane (Figure 5.6a) and yz plane (Figure 5.6b) through the source at  $x = 0.65 \text{ m}$  and  $y = 0 \text{ m}$ . With angular correction filters, the current of 662 keV photons is made uniform in xy planes.*

586 The source is situated in the muon beam line with the muon beam being available a few times a  
 587 year. The H4 beam, composed of muons with a momentum of about 150 GeV/c, passes through the  
 588 GIF++ zone and is used to study the performance of the detectors. Its flux is of 104 particles/ $\text{s cm}^2$

589 focused in an area similar to  $10 \times 10 \text{ cm}^2$ . Therefore, with properly adjusted filters, one can imitate  
 590 the HL-LHC background and study the performance of muon detectors with their trigger/readout  
 591 electronics in HL-LHC environment.

592

## 593 5.2 Preliminary tests at GIF

### 594 5.2.1 Resistive Plate Chamber test setup

595 During summer 2014, preliminary tests have been conducted in the GIF area on a newly produced  
 596 RE4/2 chamber labelled RE-4-2-BARC-161. This chamber has been placed into a trolley covered  
 597 with a tent. The position of the RPC inside the tent and of the tent related to the source is described  
 598 in Figure 5.7. To test this CMS RPC, three different absorber settings were used. First of all,  
 599 measurements were done with fully opened source. Then, to complete this preliminary study, the  
 600 gamma flux has been attenuated from a factor 2 and a factor 5. The expected gamma flux at the level  
 601 of our detector will be discussed in subsection ??.

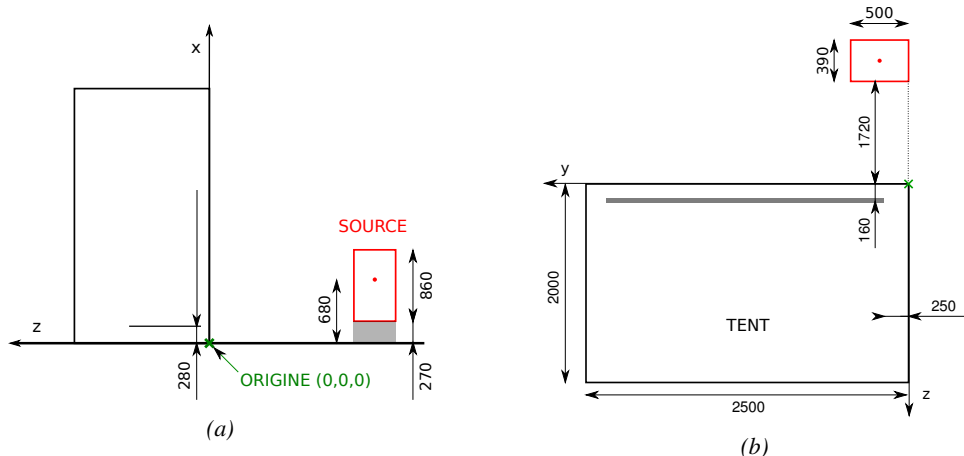
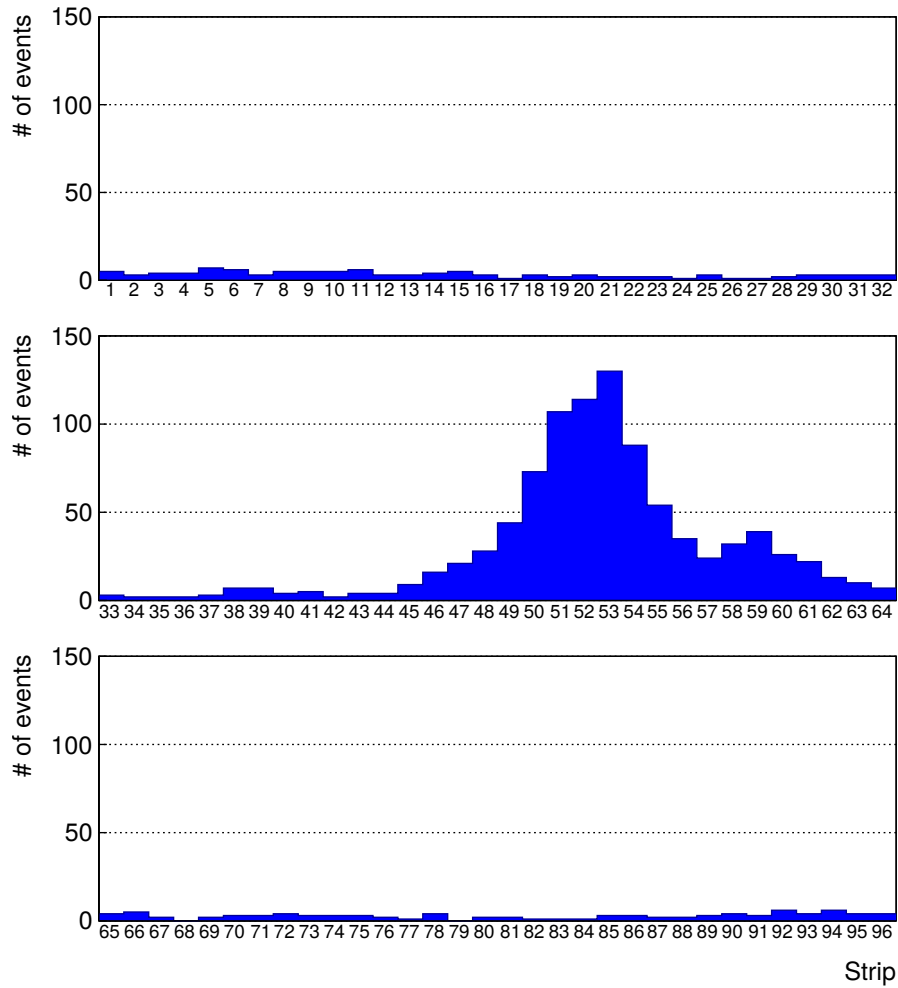


Figure 5.7: Description of the RPC setup. Dimensions are given in mm. A tent containing RPCs is placed at 1720 mm from the source container. The source is situated in the center of the container. RE-4-2-BARC-161 chamber is 160 mm inside the tent. This way, the distance between the source and the chambers plan is 2060 mm. Figure 5.7a provides a side view of the setup in the xz plane while Figure 5.7b shows a top view in the yz plane.



*Figure 5.8: RE-4-2-BARC-161 chamber is inside the tent as described in Figure 5.7. In the top right, the two scintillators used as trigger can be seen. This trigger system has an inclination of 10° relative to horizontal and is placed above half-partition B2 of the RPCs. PMT electronics are shielded thanks to lead blocks placed in order to protect them without stopping photons from going through the scintillators and the chamber.*

602 At the time of the tests, the beam not being operational anymore, a trigger composed of 2  
603 plastic scintillators has been placed in front of the setup with an inclination of 10 deg with respect to  
604 the detector plane in order to look at cosmic muons. Using this particular trigger layout, shown on  
605 Figure 5.8, leads to a cosmic muon hit distribution into the chamber similar to the one in Figure 5.9.  
606 Measured without gamma irradiation, two peaks can be seen on the profil of partition B, centered  
607 on strips 52 and 59. Section ?? will help us understand that these two peaks are due respectively to  
608 forward and backward coming cosmic particles where forward coming particles are first detected by  
609 the scintillators and then the RPC while the backward coming muons are first detected in the RPC.



*Figure 5.9: Hit distributions over all 3 partitions of RE-4-2-BARC-161 chamber is showed on these plots. Top, middle and bottom figures respectively correspond to partitions A, B, and C. These plots show that some events still occur in other half-partitions than B2, which corresponds to strips 49 to 64, in front of which the trigger is placed, contributing to the inefficiency of detection of cosmic muons. In the case of partitions A and C, the very low amount of data can be interpreted as noise. On the other hand, it is clear that a little portion of muons reach the half-partition B1, corresponding to strips 33 to 48.*

### 5.2.2 Data Acquisition

### 5.2.3 Geometrical acceptance of the setup layout to cosmic muons

In order to profit from a constant gamma irradiation, the detectors inside of the GIF bunker need to be placed in a plane orthogonal to the beam line. The muon beam that used to be available was meant to test the performance of detectors under test. This beam not being active anymore, another solution to test detector performance had to be used. Thus, it has been decided to use cosmic muons detected through a telescope composed of two scintillators. Lead blocks were used as shielding to

617 protect the photomultipliers from gammas as can be seen from Figure 5.8.

618 An inclination has been given to the cosmic telescope to maximize the muon flux. A good com-  
 619 promise had to be found between good enough muon flux and narrow enough hit distribution to  
 620 be sure to contain all the events into only one half partitions as required from the limited available  
 621 readout hardware. Nevertheless, a consequence of the misplaced trigger, that can be seen as a loss  
 622 of events in half-partition B1 in Figure 5.9, is an inefficiency. Nevertheless, the inefficiency of ap-  
 623 proximately 20 % highlighted in Figure 5.10 by comparing the performance of chamber BARC-161  
 624 in 904 and at GIF without irradiation seems too important to be explained only by the geometri-  
 625 cal acceptance of the setup itself. Simulations have been conducted to show how the setup brings  
 626 inefficiency.

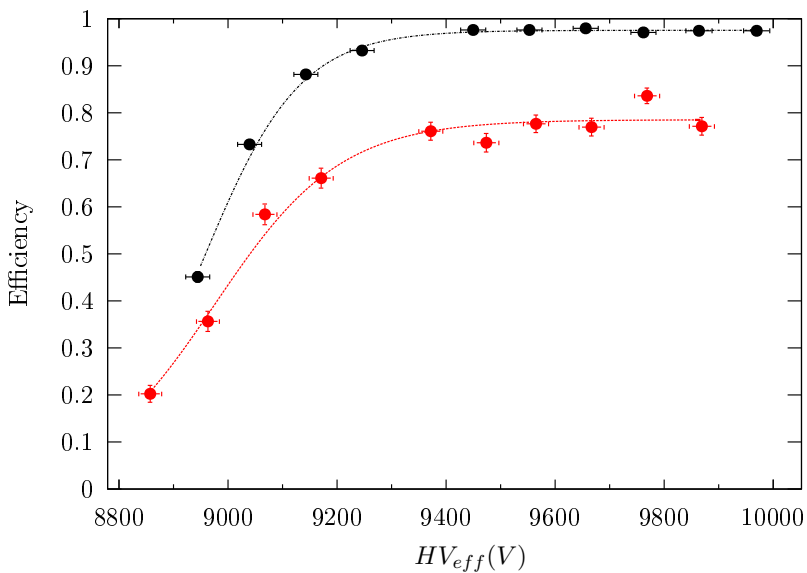
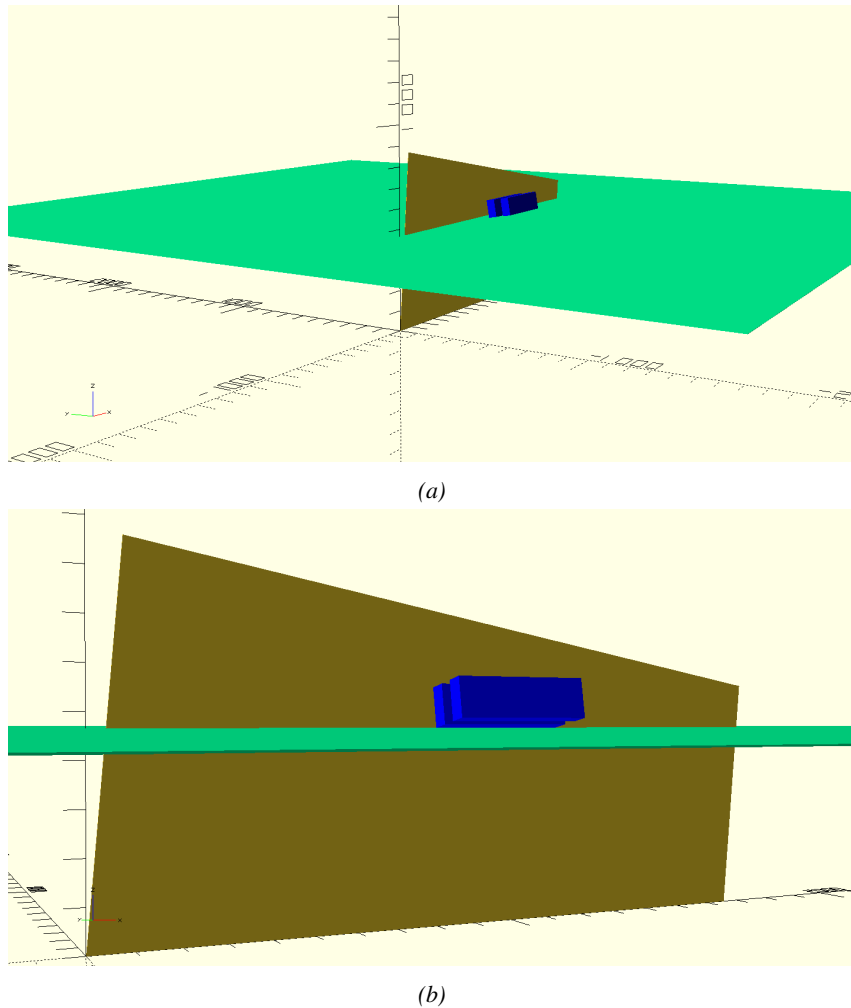


Figure 5.10: Results are derived from data taken on half-partition B2 only. On the 18<sup>th</sup> of June 2014, data has been taken on chamber RE-2-BARC-161 at building 904 (Prevessin Site) with cosmic muons providing us a reference efficiency plateau of  $(97.54 \pm 0.15)\%$  represented by a black curve. A similar measurement has been done at GIF on the 21<sup>st</sup> of July with the same chamber giving a plateau of  $(78.52 \pm 0.94)\%$  represented by a red curve.

### 627 5.2.3.1 Description of the simulation layout

628 The layout of GIF setup has been reproduced and incorporated into a Monte Carlo (MC) simulation  
 629 to study the influence of the disposition of the telescope on the final distribution measured by the  
 630 RPC. A 3D view of the simulated layout is given into Figure 5.11. Muons are generated randomly  
 631 in a horizontal plane located at a height corresponding to the lowest point of the PMTs. This way,  
 632 the needed size of the plane in order to simulate events happening at very big azimuthal angles (i.e.  
 633  $\theta \approx \pi$ ) can be kept relatively small. The muon flux is designed to follow the usual  $\cos^2\theta$  distribution  
 634 for cosmic particle. The goal of the simulation is to look at muons that pass through the muon  
 635 telescope composed of the two scintillators and define their distribution onto the RPC plane. During  
 636 the reconstruction, the RPC plane is then divided into its strips and each muon track is assigned to a  
 637 strip.



*Figure 5.11: Representation of the layout used for the simulations of the test setup. The RPC is represented as a yellow trapezoid while the two scintillators as blue cuboids looking at the sky. A green plane corresponds to the muon generation plane within the simulation. Figure 5.7a shows a global view of the simulated setup. Figure 5.7b shows a zoomed view that allows to see the 2 scintillators as well as the full RPC plane.*

638 In order to further refine the quality of the simulation and understand deeper the results the  
 639 dependance of the distribution has been studied for a range of telescope inclinations. Moreover,  
 640 the threshold applied on the PMT signals has been included into the simulation in the form of a  
 641 cut. In the approximation of uniform scintillators, it has been considered that the threshold can be  
 642 understood as the minimum distance particles need to travel through the scintillating material to give  
 643 a strong enough signal. Particles that travel a distance smaller than the set "threshold" are thus not  
 644 detected by the telescope and cannot trigger the data taking. Finally, the FEE threshold also has  
 645 been considered in a similar way. The mean momentum of horizontal cosmic rays is higher than  
 646 those of vertical ones but the stopping power of matter for momenta ranging from 1 GeV to 1 TeV  
 647 stays comparable. It is then possible to assume that the mean number of primary  $e^-/ion$  pairs per  
 648 unit length will stay similar and thus, depending on the applied discriminator threshold, muons with

649 the shortest path through the gas volume will deposit less charge and induce a smaller signal on the  
 650 pick-up strips that could eventually not be detected. These two thresholds also restrain the overall  
 651 geometrical acceptance of the system.

652 **5.2.3.2 Simulation procedure**

653 The simulation software has been designed using C++ and the output data is saved into ROOT  
 654 histograms. Simulations start for a threshold  $T_{scint}$  varying in a range from 0 to 45 mm in steps  
 655 of 5 mm, where  $T_{scint} = 0$  mm corresponds to the case where there isn't any threshold apply on  
 656 the input signal while  $T_{scint} = 45$  mm, which is the scintillator thickness, is the case where muons  
 657 cannot arrive orthogonally onto the scintillator surface. For a given  $T_{scint}$ , a set of RPC thresholds  
 658 are considered. The RPC threshold,  $T_{RPC}$  varies from 2 mm, the thickness of the gas volume, to  
 659 3 mm in steps of 0.25 mm. For each  $(T_{scint}; T_{RPC})$  pair,  $N_\mu = 10^8$  muons are randomly generated  
 660 inside the muon plane described in the previous paragraph with an azimuthal angle  $\theta$  chosen to follow  
 661 a  $\cos^2\theta$  distribution.

662 Planes are associated to each surface of the scintillators. Knowing muon position into the muon  
 663 plane and its direction allows us, by assuming that muons travel in a straight line, to compute the  
 664 intersection of the muon track with these planes. Applying conditions to the limits of the surfaces  
 665 of the scintillator faces then gives us an answer to whether or not the muon passed through the  
 666 scintillators. In the case the muon has indeed passed through the telescope, the path through each  
 667 scintillator is computed and muons whose path was shorter than  $T_{scint}$  are rejected and are thus  
 668 considered as having not interacted with the setup.

669 On the contrary, if the muon is labeled as good, its position within the RPC plane is computed  
 670 and the corresponding strip, determined by geometrical tests in the case the distance through the  
 671 gas volume was enough not to be rejected because of  $T_{RPC}$ , gets a hit and several histograms  
 672 are filled in order to keep track of the generation point on the muon plane, the intersection points  
 673 of the reconstructed muons within the telescope, or on the RPC plane, the path traveled through  
 674 each individual scintillator or the gas volume, as well as other histograms. Moreover, muons fill  
 675 different histograms whether they are forward or backward coming muons. They are discriminated  
 676 according to their direction components. When a muon is generated, an  $(x, y, z)$  position is assigned  
 677 into the muon plane as well as a  $(\theta; \phi)$  pair that gives us the direction it's coming from. This way,  
 678 muons satisfying the condition  $0 \leq \phi < \pi$  are designated as backward coming muons while muons  
 679 satisfying  $\pi \leq \phi < 2\pi$  as forward coming muons.

680 This simulation is then repeated for different telescope inclinations ranging in between 4 and  $20^\circ$   
 681 and varying in steps of  $2^\circ$ . Due to this inclination and to the vertical position of the detector under  
 682 test, the muon distribution reconstructed in the detector plane is asymmetrical. The choice as been  
 683 made to chose a skew distribution formula to fit the data built as the multiplication of gaussian and  
 684 sigmoidal curves together. A typical gaussian formula is given as 5.1 and has three free parameters  
 685 as  $A_g$ , its amplitude,  $\bar{x}$ , its mean value and  $\sigma$ , its root mean square. Sigmoidal curves as given by  
 686 formula 5.2 are functions converging to 0 and  $A_s$  as  $x$  diverges. The inflection point is given as  $x_i$   
 687 and  $\lambda$  is proportional to the slope at  $x = x_i$ . In the limit where  $\lambda \rightarrow \infty$ , the sigmoid becomes a  
 688 step function.

$$g(x) = A_g e^{-\frac{(x-\bar{x})^2}{2\sigma^2}} \quad (5.1)$$

$$s(x) = \frac{A_s}{1 + e^{-\lambda(x-x_i)}} \quad (5.2)$$

Finally, a possible representation of a skew distribution is given by formula 5.3 and is the product of 5.1 and 5.2. Naturally, here  $A_{sk} = A_g \times A_s$  and represents the theoretical maximum in the limit where the skew tends to a gaussian function.

$$sk(x) = g(x) \times s(x) = A_{sk} \frac{e^{\frac{-(x-\bar{x})^2}{2\sigma^2}}}{1 + e^{-\lambda(x-x_i)}} \quad (5.3)$$

### 5.2.3.3 Results

#### Influence of $T_{scint}$ on the muon distribution

#### Influence of $T_{RPC}$ on the muon distribution

#### Influence of the telescope inclination on the muon distribution

#### Comparison to data taken at GIF without irradiation

### 5.2.4 Photon flux at GIF

#### 5.2.4.1 Expectations from simulations

In order to understand and evaluate the  $\gamma$  flux in the GIF area, simulations had been conducted in 1999 and published by S. Agosteo et al [6]. Table 5.1 presented in this article gives us the  $\gamma$  flux for different distances  $D$  to the source. This simulation was done using GEANT and a Monte Carlo N-Particle (MCNP) transport code, and the flux  $F$  is given in number of  $\gamma$  per unit area and unit time along with the estimated error from these packages expressed in %.

Nominal ABS	Photon flux $F$ [ $s^{-1}cm^{-2}$ ]			
	at $D = 50$ cm	at $D = 155$ cm	at $D = 300$ cm	at $D = 400$ cm
1	$0.12 \cdot 10^8 \pm 0.2\%$	$0.14 \cdot 10^7 \pm 0.5\%$	$0.45 \cdot 10^6 \pm 0.5\%$	$0.28 \cdot 10^6 \pm 0.5\%$
2	$0.68 \cdot 10^7 \pm 0.3\%$	$0.80 \cdot 10^6 \pm 0.8\%$	$0.25 \cdot 10^6 \pm 0.8\%$	$0.16 \cdot 10^6 \pm 0.6\%$
5	$0.31 \cdot 10^7 \pm 0.4\%$	$0.36 \cdot 10^6 \pm 1.2\%$	$0.11 \cdot 10^6 \pm 1.2\%$	$0.70 \cdot 10^5 \pm 0.9\%$

Table 5.1: Total photon flux ( $E\gamma \leq 662$  keV) with statistical error predicted considering a  $^{137}Cs$  activity of 740 GBq at different values of the distance  $D$  to the source along the  $x$ -axis of irradiation field [6].

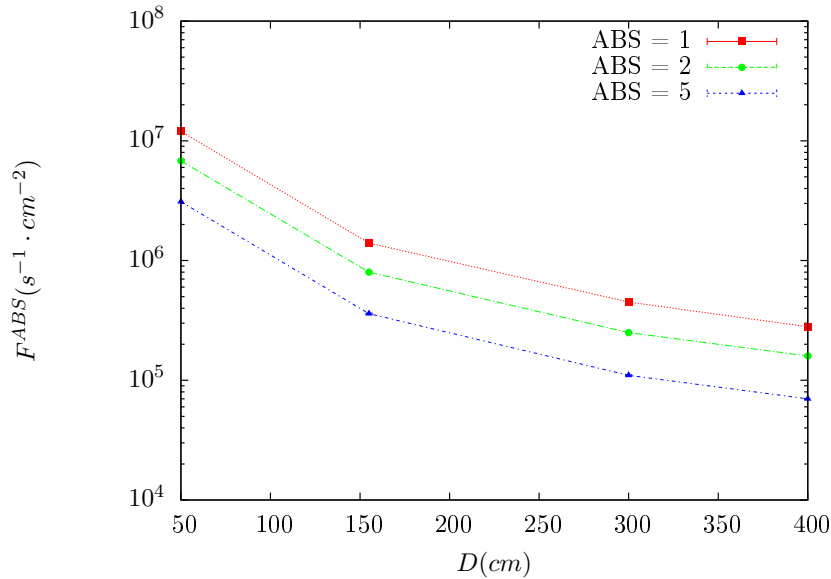


Figure 5.12:  $\gamma$  flux  $F(D)$  is plot using values from table 5.1. As expected, the plot shows similar attenuation behaviours with increasing distance for each absorption factors.

The simulation doesn't directly provide us with an estimated flux at the level of our RPC. First of all, it is needed to extract the value of the flux from the available data contained in the original paper and then to estimate the flux in 2014 at the time the experimentation took place. Figure 5.12 that contains the data from Table 5.1. In the case of a pointlike source emitting isotropic and homogeneous gamma radiations, the gamma flux  $F$  at a distance  $D$  to the source with respect to a reference point situated at  $D_0$  where a known flux  $F_0$  is measured will be expressed like in Equation 5.4, assuming that the flux decreases as  $1/D^2$ , where  $c$  is a fitting factor.

$$F^{ABS} = F_0^{ABS} \times \left( \frac{cD_0}{D} \right)^2 \quad (5.4)$$

By rewriting Equation 5.4, it comes that :

$$c = \frac{D}{D_0} \sqrt{\frac{F^{ABS}}{F_0^{ABS}}} \quad (5.5)$$

$$\Delta c = \frac{c}{2} \left( \frac{\Delta F^{ABS}}{F^{ABS}} + \frac{\Delta F_0^{ABS}}{F_0^{ABS}} \right) \quad (5.6)$$

Finally, using Equation 5.5 and the data in Table 5.1 with  $D_0 = 50$  cm as reference point, we can build Table 5.2. It is interesting to note that  $c$  for each value of  $D$  doesn't depend on the absorption factor.

Nominal ABS	Correction factor $c$		
	at $D = 155$ cm	at $D = 300$ cm	at $D = 400$ cm
1	$1.059 \pm 0.70\%$	$1.162 \pm 0.70\%$	$1.222 \pm 0.70\%$
2	$1.063 \pm 1.10\%$	$1.150 \pm 1.10\%$	$1.227 \pm 0.90\%$
5	$1.056 \pm 1.60\%$	$1.130 \pm 1.60\%$	$1.202 \pm 1.30\%$

Table 5.2: Correction factor  $c$  is computed thanks to formulae 5.5 taking as reference  $D_0 = 50$  cm and the associated flux  $F_0^{ABS}$  for each absorption factor available in table 5.1.

715 For the range of  $D/D_0$  values available, it is possible to use a simple linear fit to get the evolution  
 716 of  $c$ . The linear fit will then use only 2 free parameters,  $a$  and  $b$ , as written in Equation 5.7. This gives  
 717 us the results showed in Figure 5.13. Figure 5.13b confirms that using only a linear fit to extract  $c$  is  
 718 enough as the evolution of the rate that can be obtained superimposes well on the simulation points.

$$c \left( \frac{D}{D_0} \right) = a \frac{D}{D_0} + b \quad (5.7)$$

$$F^{ABS} = F_0^{ABS} \left( a + \frac{bD_0}{D} \right)^2 \quad (5.8)$$

$$\Delta F^{ABS} = F^{ABS} \left[ \frac{\Delta F_0^{ABS}}{F_0^{ABS}} + 2 \frac{\Delta a + \Delta b \frac{D_0}{D}}{a + \frac{bD_0}{D}} \right] \quad (5.9)$$

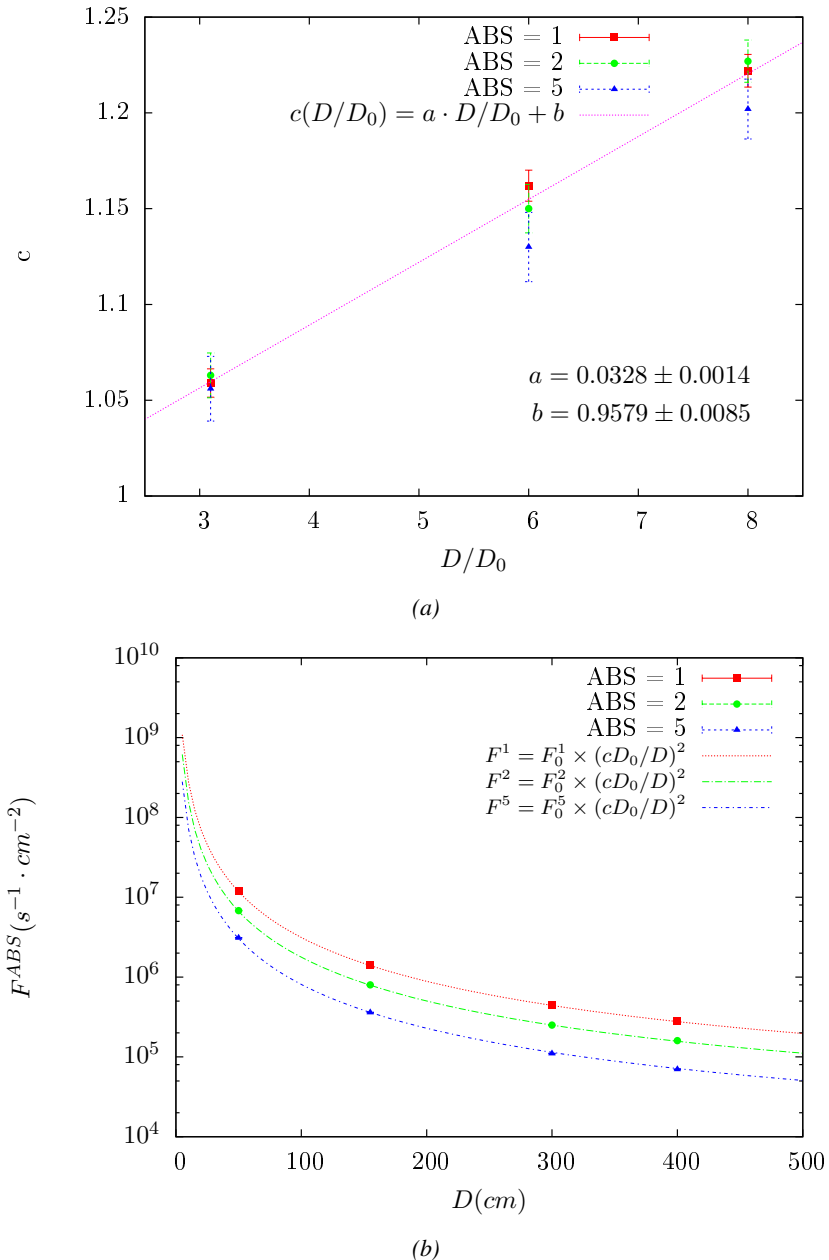


Figure 5.13: Figure 5.13a shows the linear approximation fit done via formulae 5.7 on data from table 5.2. Figure 5.13b shows a comparison of this model with the simulated flux using  $a$  and  $b$  given in figure 5.13a in formulae 5.4 and the reference value  $D_0 = 50\text{cm}$  and the associated flux for each absorption factor  $F_0^{ABS}$  from table 5.1

In the case of the 2014 GIF tests, the RPC plane is located at a distance  $D = 206\text{ cm}$  to the source. Moreover, to estimate the strength of the flux in 2014, it is necessary to consider the nuclear decay through time associated to the Cesium source whose half-life is well known ( $t_{1/2} = (30.05 \pm 0.08)\text{ y}$ ). The very first source activity measurement has been done on the 5<sup>th</sup> of March 1997 while the GIF

723 tests where done in between the 20<sup>th</sup> and the 31<sup>st</sup> of August 2014, i.e. at a time  $t = (17.47 \pm 0.02)$  y  
 724 resulting in an attenuation of the activity from 740 GBq in 1997 to 494 GBq in 2014. All the needed  
 725 information to extrapolate the flux through our detector in 2014 has now been assembled, leading  
 726 to the Table 5.3. It is interesting to note that for a common RPC sensitivity to  $\gamma$  of  $2 \cdot 10^{-3}$ , the  
 727 order of magnitude of the estimated hit rate per unit area is of the order of the kHz for the fully  
 728 opened source. Moreover, taking profit of the two working absorbers, it will be possible to scan  
 729 background rates at 0 Hz,  $\sim 300$  Hz as well as  $\sim 600$  Hz. Without source, a good estimate of the  
 730 intrinsic performance will be available. Then at 300 Hz, the goal will be to show that the detectors  
 731 fulfill the performance certification of CMS RPCs. Then a first idea of the performance of the  
 732 detectors at higher background will be provided with absorption factors 2 ( $\sim 600$  Hz) and 1 (no  
 733 absorption). *[Here I will also put a reference to the plot showing the estimated background rate at  
 734 the level of RE3/1 in the case of HL-LHC but this one being in another chapter, I will do it later.]*

Nominal ABS	Photon flux $F$ [ $s^{-1}cm^{-2}$ ]			Hit rate/unit area [ $Hz cm^{-2}$ ] at $D^{2014} = 206$ cm
	at $D_0^{1997} = 50$ cm	at $D_0^{1997} = 206$ cm	at $D^{2014} = 206$ cm	
1	$0.12 \cdot 10^8 \pm 0.2\%$	$0.84 \cdot 10^6 \pm 0.3\%$	$0.56 \cdot 10^6 \pm 0.3\%$	$1129 \pm 32$
2	$0.68 \cdot 10^7 \pm 0.3\%$	$0.48 \cdot 10^6 \pm 0.3\%$	$0.32 \cdot 10^6 \pm 0.3\%$	$640 \pm 19$
5	$0.31 \cdot 10^7 \pm 0.4\%$	$0.22 \cdot 10^6 \pm 0.3\%$	$0.15 \cdot 10^6 \pm 0.3\%$	$292 \pm 9$

Table 5.3: The data at  $D_0$  in 1997 is taken from [6]. In a second step, using Equations 5.8 and 5.9, the flux at  $D$  can be estimated in 1997. Then, taking into account the attenuation of the source activity, the flux at  $D$  can be estimated at the time of the tests in GIF in 2014. Finally, assuming a sensitivity of the RPC to  $\gamma$   $s = 2 \cdot 10^{-3}$ , an estimation of the hit rate per unit area is obtained.

<sup>735</sup> **5.2.4.2 Dose measurements**

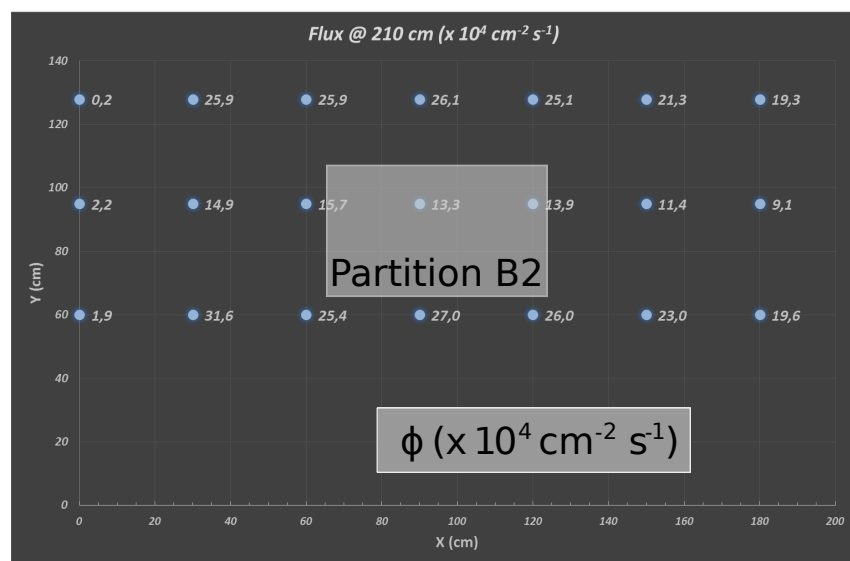


Figure 5.14: Dose measurements has been done in a plane corresponding to the tents front side. This plan is 1900 mm away from the source. As explained in the first chapter, a lens-shaped lead filter provides a uniform photon flux in the vertical plan orthogonal to the beam direction. If the second line of measured fluxes is not taken into account because of lower values due to experimental equipments in the way between the source and the tent, the uniformity of the flux is well showed by the results.

<sup>736</sup> **5.2.5 Results and discussions**

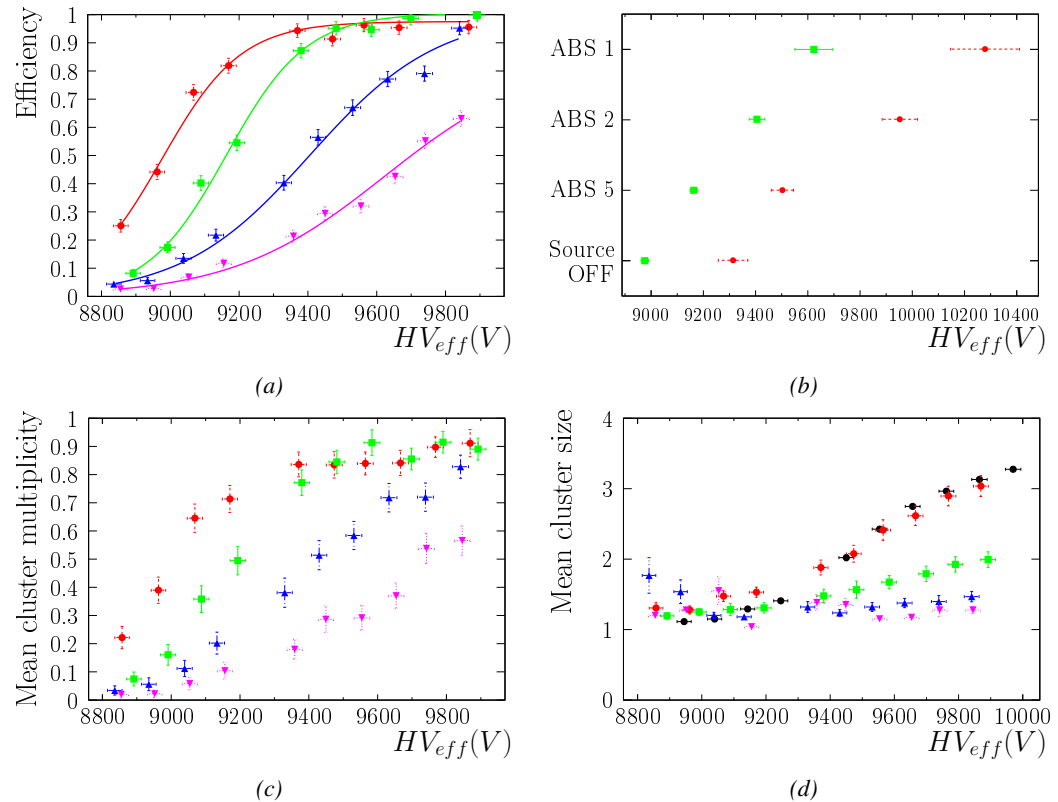


Figure 5.15

### <sup>737</sup> 5.3 Longevity tests at GIF++

<sup>738</sup> Longevity studies imply a monitoring of the performance of the detectors probed using a high inten-  
<sup>739</sup> sity muon beam in a irradiated environment by periodically measuring their rate capability, the dark  
<sup>740</sup> current running through them and the bulk resistivity of the Bakelite composing their electrodes.  
<sup>741</sup> GIF++, with its very intense  $^{137}\text{Cs}$  source, provides the perfect environment to perform such kind  
<sup>742</sup> of tests. Assuming a maximum acceleration factor of 3, it is expected to accumulate the equivalent  
<sup>743</sup> charge in 1.7 years.

<sup>744</sup> As the maximum background is found in the endcap, the choice naturally was made to focus the  
<sup>745</sup> GIF++ longevity studies on endcap chambers. Most of the RPC system was installed in 2007. Nev-  
<sup>746</sup> ertheless, the large chambers in the fourth endcap (RE4/2 and RE4/3) have been installed during  
<sup>747</sup> LS1 in 2014. The Bakelite of these two different productions having different properties, four spare  
<sup>748</sup> chambers of the present system were selected, two RE2,3/2 spares and two RE4/2 spares. Having  
<sup>749</sup> two chambers of each type allows to always keep one of them non irradiated as reference, the per-  
<sup>750</sup> formance evolution of the irradiated chamber being then compared through time to the performance  
<sup>751</sup> of the non irradiated one.

<sup>752</sup> The performance of the detectors under different level of irradiation is measured periodically dur-  
<sup>753</sup> ing dedicated test beam periods using the H4 muon beam. In between these test beam periods, the  
<sup>754</sup> two RE2,3/2 and RE4/2 chambers selected for this study are irradiated by the  $^{137}\text{Cs}$  source in order  
<sup>755</sup> to accumulate charge and the gamma background is monitored, as well as the currents. The two  
<sup>756</sup> remaining chambers are kept non-irradiated as reference detectors. Due to the limited gas flow in  
<sup>757</sup> GIF++, the RE4 chamber remained non-irradiated until end of November 2016 where a new mass  
<sup>758</sup> flow controller has been installed allowing for bigger volumes of gas to flow in the system.

<sup>759</sup> Figures 5.16 and 5.17 give us for different test beam periods, and thus for increasing integrated  
<sup>760</sup> charge through time, a comparison of the maximum efficiency, obtained using a sigmoid-like func-  
<sup>761</sup> tion, and of the working point of both irradiated and non irradiated chambers [8]. No aging is yet to  
<sup>762</sup> see from this data, the shifts in  $\gamma$  rate per unit area in between irradiated and non irradiated detec-  
<sup>763</sup> tors and RE2 and RE4 types being easily explained by a difference of sensitivity due to the various  
<sup>764</sup> Bakelite resistivities of the HPL electrodes used for the electrode production.

<sup>765</sup> Collecting performance data at each test beam period allows us to extrapolate the maximum effi-  
<sup>766</sup> ciency for a background hit rate of  $300\text{ Hz}/\text{cm}^2$  corresponding to the expected HL-LHC conditions.  
<sup>767</sup> Aging effects could emerge from a loss of efficiency with increasing integrated charge over time,  
<sup>768</sup> thus Figure 5.18 helps us understand such degradation of the performance of irradiated detectors in  
<sup>769</sup> comparison with non irradiated ones. The final answer for an eventual loss of efficiency is given in  
<sup>770</sup> Figure 5.19 by comparing for both irradiated and non irradiated detectors the efficiency sigmoids  
<sup>771</sup> before and after the longevity study. Moreover, to complete the performance information, the Bake-  
<sup>772</sup> lite resistivity is regularly measured thanks to  $Ag$  scans (Figure 5.20) and the noise rate is monitored  
<sup>773</sup> weekly during irradiation periods (Figure 5.21). At the end of 2016, no signs of aging were observed  
<sup>774</sup> and further investigation is needed to get closer to the final integrated charge requirements proposed  
<sup>775</sup> for the longevity study of the present CMS RPC sub-system.

<sup>776</sup>

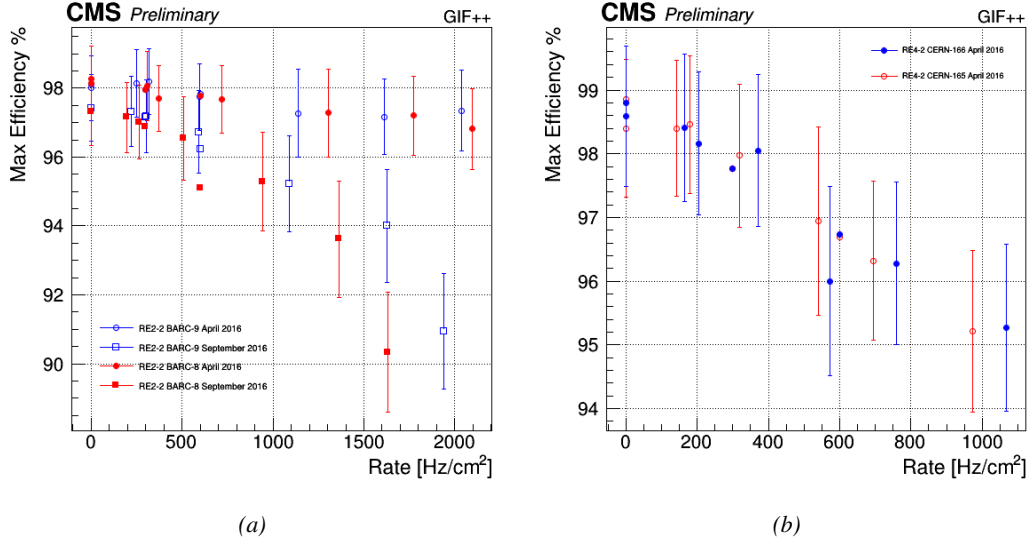


Figure 5.16: Evolution of the maximum efficiency for RE2 (5.16a) and RE4 (5.16b) chambers with increasing extrapolated  $\gamma$  rate per unit area at working point. Both irradiated (blue) and non irradiated (red) chambers are shown.

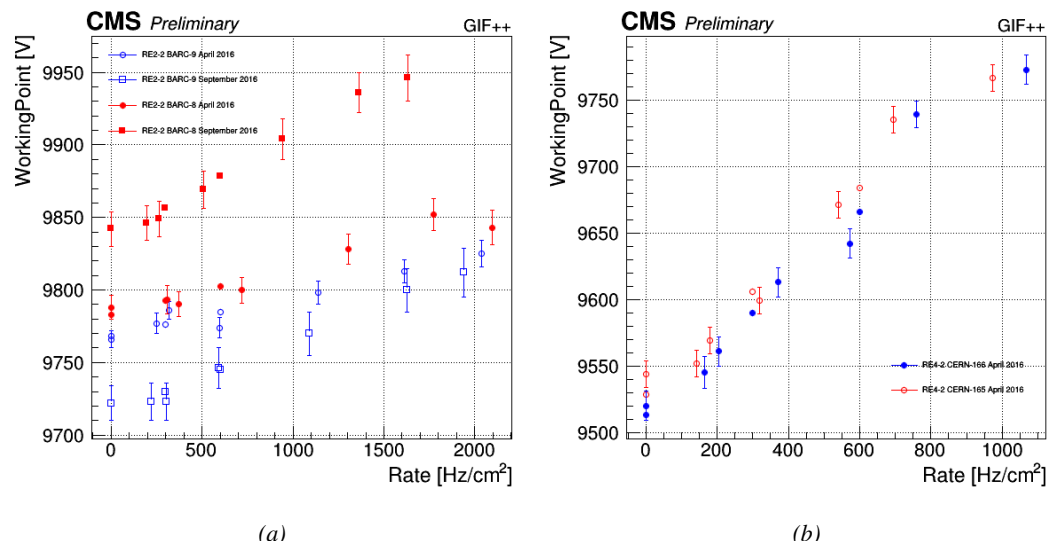


Figure 5.17: Evolution of the working point for RE2 (5.17a) and RE4 (5.17b) with increasing extrapolated  $\gamma$  rate per unit area at working point. Both irradiated (blue) and non irradiated (red) chambers are shown.

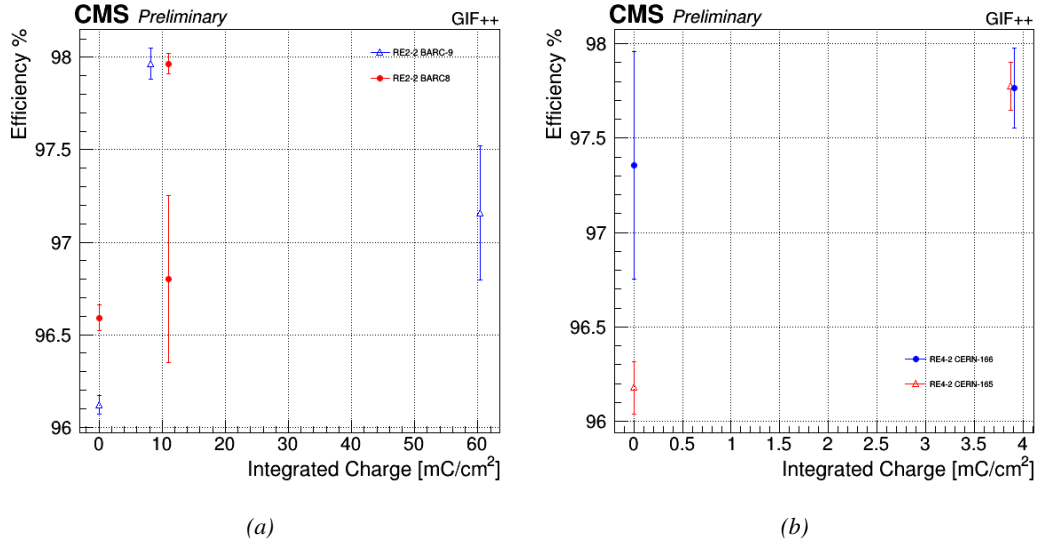


Figure 5.18: Evolution of the maximum efficiency at HL-LHC conditions, i.e. a background hit rate per unit area of  $300 \text{ Hz}/\text{cm}^2$ , with increasing integrated charge for RE2 (5.18a) and RE4 (5.18b) detectors. Both irradiated (blue) and non irradiated (red) chambers are shown. The integrated charge for non irradiated detectors is recorded during test beam periods and stays small with respect to the charge accumulated in irradiated chambers.

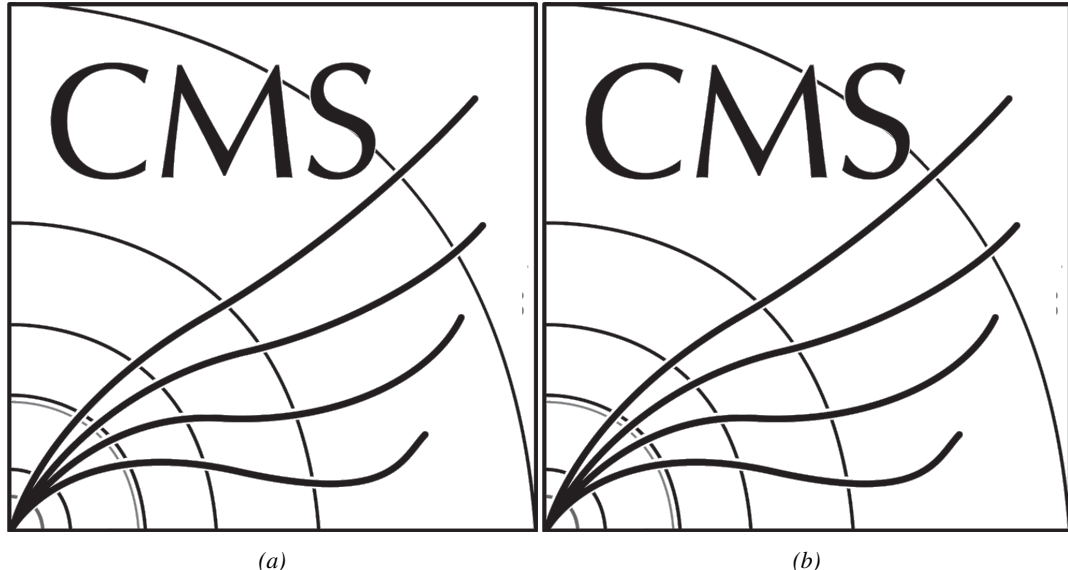


Figure 5.19: Comparison of the efficiency sigmoid before (triangles) and after (circles) irradiation for RE2 (5.19a) and RE4 (5.19b) detectors. Both irradiated (blue) and non irradiated (red) chambers are shown.

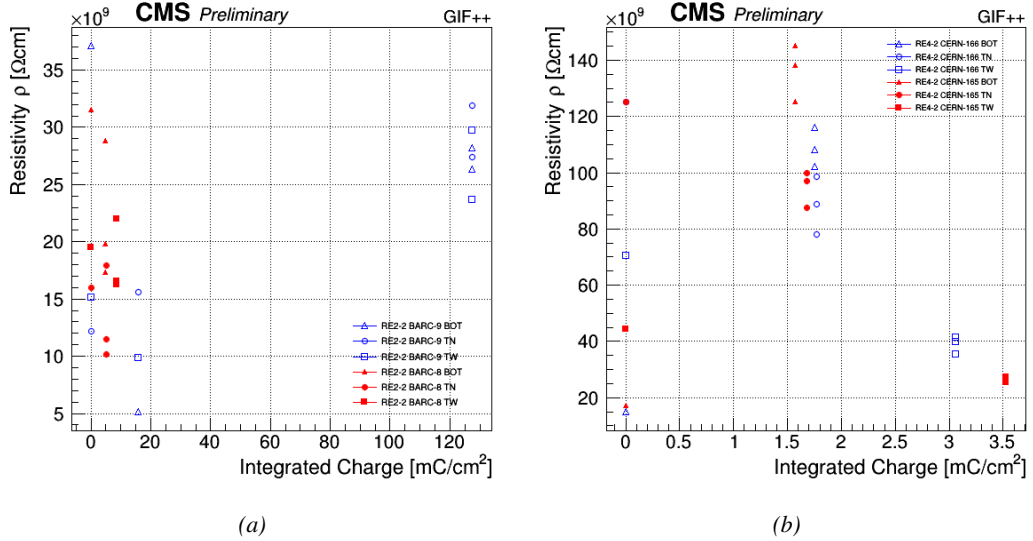


Figure 5.20: Evolution of the Bakelite resistivity for RE2 (5.20a) and RE4 (5.20b) detectors. Both irradiated (blue) and non-irradiated (red) chambers are shown.

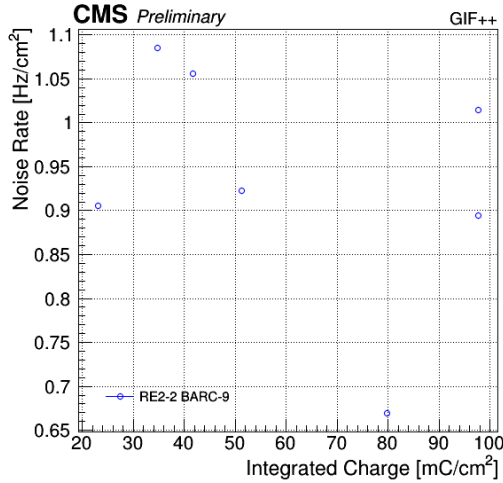


Figure 5.21: Evolution of the noise rate per unit area for the irradiated chamber RE2-2-BARC-9 only.

### 5.3.1 Description of the Data Acquisition

For the longevity studies, four spare chambers of the present system are used. Two spare RPCs of the RE2,3 stations as well as two spare RPCs from the new RE4 stations have been mounted in a Trolley. Six RE4 gaps are also placed in the trolley. The trolley is placed inside the GIFT++ in the upstream region of the bunker, taking the cesium source as a reference. The trolley is oriented for the detection surface of the chambers to be orthogonal to the beam line. The system can be moved along the orthogonal plane in order to have the beam in all  $\eta$ -partitions. For the aging the trolley is

784 moved outside the beam line and is placed in a distance of 5.2 m to the source, which irradiates the  
 785 bunker using an attenuation filter of 2.2 which corresponds to a fluence of  $10^7 \text{ gamma/cm}^2$ .

786 During GIF++ operation, the data collected can be divided into different categories as several  
 787 parameters are monitored in addition to the usual RPC performance data. On one hand, to know  
 788 the performance of a chamber, it is need to measure its efficiency and to know the background  
 789 conditions in which it is operated. To do this, the hit signals from the chamber are recorded and  
 790 stored in a ROOT file via a Data Acquisition (DAQ) software. On the other hand, it is also very  
 791 important to monitor parameters such as environmental pressure and temperature, gas temperature  
 792 and humidity, RPC HV, LV, and currents, or even source and beam status. This is done through the  
 793 GIF++ web Detector Control Software (DCS) that stores this information in a database.

794 Two different types of tests are conducted on RPCs via the DAQ. Indeed, the performance of the  
 795 detectors is measured periodically during dedicated test beam periods using the H4 muon beam. In  
 796 between these test beam periods, when the beam is not available, the chambers are irradiated by the  
 797  $^{137}\text{Cs}$  in order to accumulate deposited charge and the gamma background is measured.

798 RPCs under test are connected through LVDS cables to V1190A Time-to-Digital Converter  
 799 (TDC) modules manufactured by CAEN. These modules, located in the rack area outside of the  
 800 bunker, get the logic signals sent by the chambers and save them into their buffers. Due to the  
 801 limited size of the buffers, the collected data is regularly erased and replaced. A trigger signal is  
 802 needed for the TDC modules to send the useful data to the DAQ computer via a V1718 CAEN USB  
 803 communication module.

804 In the case of performance test, the trigger signal used for data acquisition is generated by the  
 805 coincidence of three scintillators. A first one is placed upstream outside of the bunker, a second one  
 806 is placed downstream outside of the bunker, while a third one is placed in front of the trolley, close by  
 807 the chambers. Every time a trigger is sent to the TDCs, i.e. every time a muon is detected, knowing  
 808 the time delay in between the trigger and the RPC signals, signals located in the right time window  
 809 are extracted from the buffers and saved for later analysis. Signals are taken in a time window of  
 810 400 ns centered on the muon peak (here we could show a time spectrum). On the other hand, in the  
 811 case of background rate measurement, the trigger signal needs to be "random" not to measure muons  
 812 but to look at gamma background. A trigger pulse is continuously generated at a rate of 300 Hz using  
 813 a dual timer. To integrate an as great as possible time, all signals contained within a time window of  
 814 10us prior to the random trigger signal are extracted form the buffers and saved for further analysis  
 815 (here another time spectrum to illustrate could be useful, maybe even place both spectrum together  
 816 as a single Figure).

817 The signals sent to the TDCs correspond to hit collections in the RPCs. When a particle hits  
 818 a RPC, it induce a signal in the pickup strips of the RPC readout. If this signal is higher than the  
 819 detection threshold, a LVDS signal is sent to the TDCs. The data is then organised into 4 branches  
 820 keeping track of the event number, the hit multiplicity for the whole setup, and the time and channel  
 821 profile of the hits in the TDCs.

### 822 **5.3.2 RPC current, environmental and operation parameter monitoring**

823 In order to take into account the variation of pressure and temperature between different data taking  
 824 periods the applied voltage is corrected following the relationship :

$$825 \quad HV_{eff} = HV_{app} \times \left( 0.2 + 0.8 \cdot \frac{P_0}{P} \times \frac{T}{T_0} \right) \quad (5.10)$$

825 where  $T_0$  (=293 K) and  $P_0$  (=990 mbar) are the reference values.

826 **5.3.3 Measurement procedure**

827 Insert a short description of the online tools (DAQ, DCS, DQM).

828 Insert a short description of the offline tools : tracking and efficiency algorithm.

829 Identify long term aging effects we are monitoring the rates per strip.

830 **5.3.4 Longevity studies results**



# 6

831

832

## Investigation on high rate RPCs

833 **6.1 Rate limitations and ageing of RPCs**

834 **6.1.1 Low resistivity electrodes**

835 **6.1.2 Low noise front-end electronics**

836 **6.2 Construction of prototypes**

837 **6.3 Results and discussions**



# 7

838

839

## Conclusions and outlooks

<sup>840</sup> **7.1 Conclusions**

<sup>841</sup> **7.2 Outlooks**



## References

- 843 [1] CERN. Geneva. LHC Experiments Committee. *The CMS muon project : Technical Design*  
844 *Report*. Tech. rep. CERN-LHCC-97-032. CMS Collaboration, 1997.
- 845 [2] CERN. Geneva. LHC Experiments Committee. *Technical Proposal for the Phase-II Upgrade*  
846 *of the CMS Detector*. Tech. rep. CERN-LHCC-2015-010. CMS Collaboration, 2015.
- 847 [3] CERN. Geneva. LHC Experiments Committee. *CMS, the Compact Muon Solenoid : technical*  
848 *proposal*. Tech. rep. CERN-LHCC-94-38. CMS Collaboration, 1994.
- 849 [4] M. Abbrescia et al. “Study of long-term performance of CMS RPC under irradiation at the  
850 CERN GIF”. In: *NIMA* 533 (2004), pp. 102–106.
- 851 [5] H.C. Kim et al. “Quantitative aging study with intense irradiation tests for the CMS forward  
852 RPCs”. In: *NIMA* 602 (2009), pp. 771–774.
- 853 [6] S. Agosteo et al. “A facility for the test of large-area muon chambers at high rates”. In: *NIMA*  
854 452 (2000), pp. 94–104.
- 855 [7] PoS, ed. *CERN GIF ++ : A new irradiation facility to test large-area particle detectors for*  
856 *the high-luminosity LHC program*. Vol. TIPP2014. 2014, pp. 102–109.
- 857 [8] M. Abbrescia et al. “Cosmic ray tests of double-gap resistive plate chambers for the CMS  
858 experiment”. In: *NIMA* 550 (2005), pp. 116–126.
- 859 [9] A. Fagot. *GIF++ DAQ v4.0*. 2017. URL: [https://github.com/afagot/GIF\\_DAQ](https://github.com/afagot/GIF_DAQ).
- 860 [10] CAEN. *Mod. V1190-VX1190 A/B, 128/64 Ch Multihit TDC*. 14th ed. 2016.
- 861 [11] CAEN. *Mod. V1718 VME USB Bridge*. 9th ed. 2009.
- 862 [12] W-Ie-Ne-R. *VME 6021-23 VXI*. 5th ed. 2016.
- 863 [13] Wikipedia. *INI file*. 2017. URL: [https://en.wikipedia.org/wiki/INI\\_file](https://en.wikipedia.org/wiki/INI_file).
- 864 [14] S. Carrillo A. Fagot. *GIF++ Offline Analysis v6*. 2017. URL: [https://github.com/afagot/GIF\\_OfflineAnalysis](https://github.com/afagot/GIF_OfflineAnalysis).



# A

866

867

868

## A data acquisition software for CAEN VME TDCs

869 Certifying detectors in the perspective of HL-LHC required to develop tools for the GIF++ ex-  
870 periment. Among them was the C++ Data Acquisition (DAQ) software that allows to make the com-  
871 munications in between a computer and TDC modules in order to retrieve the RPC data [9]. In this  
872 appendix, details about this software, as of how the software was written, how it functions and how  
873 it can be exported to another similar setup, will be given.

### 874 A.1 GIF++ DAQ file tree

875 GIF++ DAQ source code is fully available on github at [https://github.com/afagot/GIF\\_](https://github.com/afagot/GIF_DAQ)  
876 DAQ. The software requires 3 non-optional dependencies:

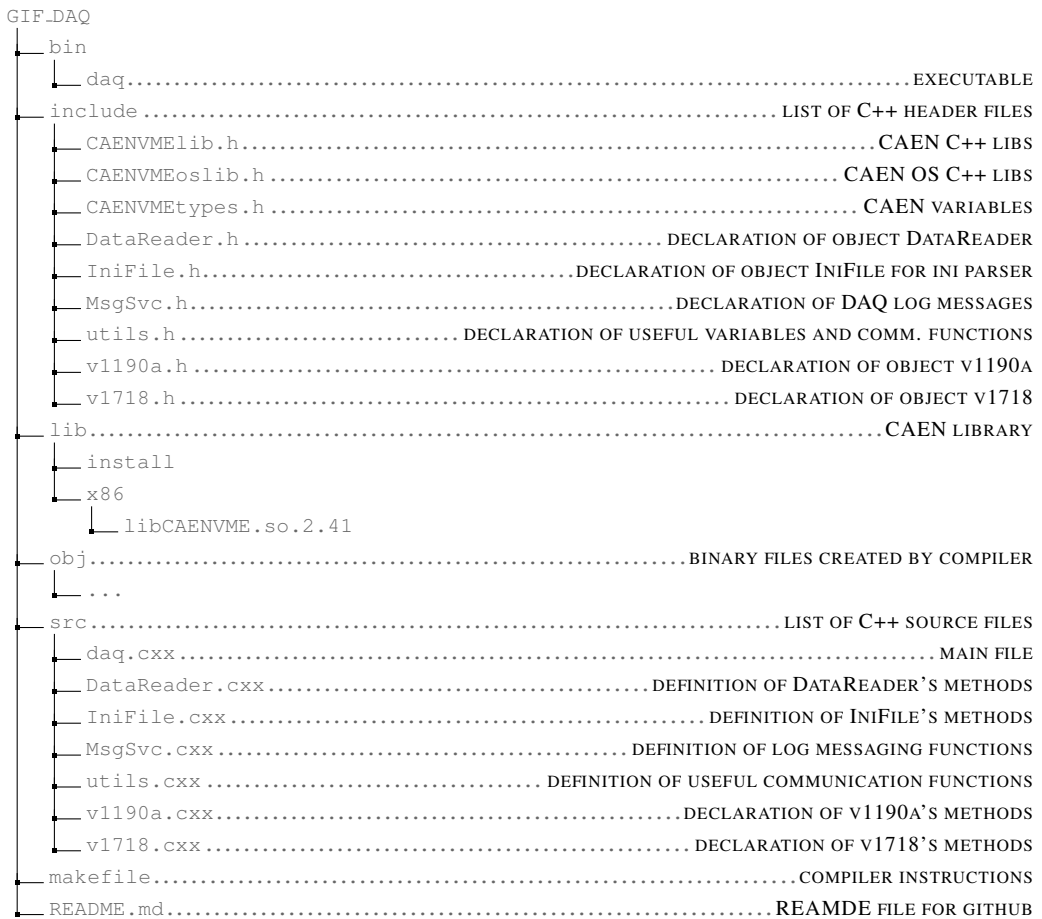
- 877 • CAEN USB Driver, to mount the VME hardware,  
878 • CAEN VME Library, to communicate with the VME hardware, and  
879 • ROOT, to organize the collected data into a TTree.

880 The CAEN VME library will not be packaged by distributions and will need to be installed man-  
881 ually. To compile the GIF++ DAQ project via a terminal, from the DAQ folder use the command:

882  
883 make

884 The source code tree is provided below along with comments to give an overview of the files' con-  
885 tent. The different objects created for this project (`v1718`, `v1190a`, `IniFile` & `DataReader`) will be  
886 described in details in the following sections.

887



## 888 A.2 Usage of the DAQ

889 GIF++ DAQ, as used in GIF++, is not a standalone software. Indeed, the system being more complexe,  
 890 the DAQ only is a sub-layer of the software architecture developped to control and monitor  
 891 the RPCs that are placed into the bunker for performance study in an irradiated environment. The top  
 892 layer of GIF++ is a Web Detector Control System (webDCS) application. The DAQ is only called  
 893 by the webDCS when data needs to be acquired. The webDCS operates the DAQ through command  
 894 line. To start the DAQ, the webDCS calls:

895

```
896     bin/daq /path/to/the/log/file/in/the/output/data/folder
```

897 where `/path/to/the/log/file/in/the/output/data/folder` is the only argument required. This  
 898 log file is important for the webDCS as this file contains all the content of the communication of the  
 899 webDCS and the different systems monitored by the webDCS. Its content is constantly displayed  
 900 during data taking for the users to be able to follow the operations. The communication messages  
 901 are normally sent to the webDCS log file via the functions declared in file `MsgSvc.h`, typically  
 902 `MSG_INFO(string message)`.

903

### 904 A.3 Description of the readout setup

905 The CMS RPC setup at GIF++ counts 5 V1190A Time-to-Digital Converter (TDC) manufactured  
 906 by CAEN [10]. V1190A are VME units accepting 128 independent Multi-Hit/Multi-Event TDC  
 907 channels whose signals are treated by 4 100 ps high performance TDC chips developed by CERN  
 908 / ECP-MIC Division. The communication between the computer and the TDCs to transfer data is  
 909 done via a V1718 VME master module also manufactured by CAEN and operated from a USB  
 910 port [11]. These VME modules are all hosted into a 6U VME 6021 powered crate manufactured by  
 911 W-Ie-Ne-R than can accommodate up to 21 VME bus cards [12]. These 3 components of the DAQ  
 912 setup are shown in Figure A.1.

913

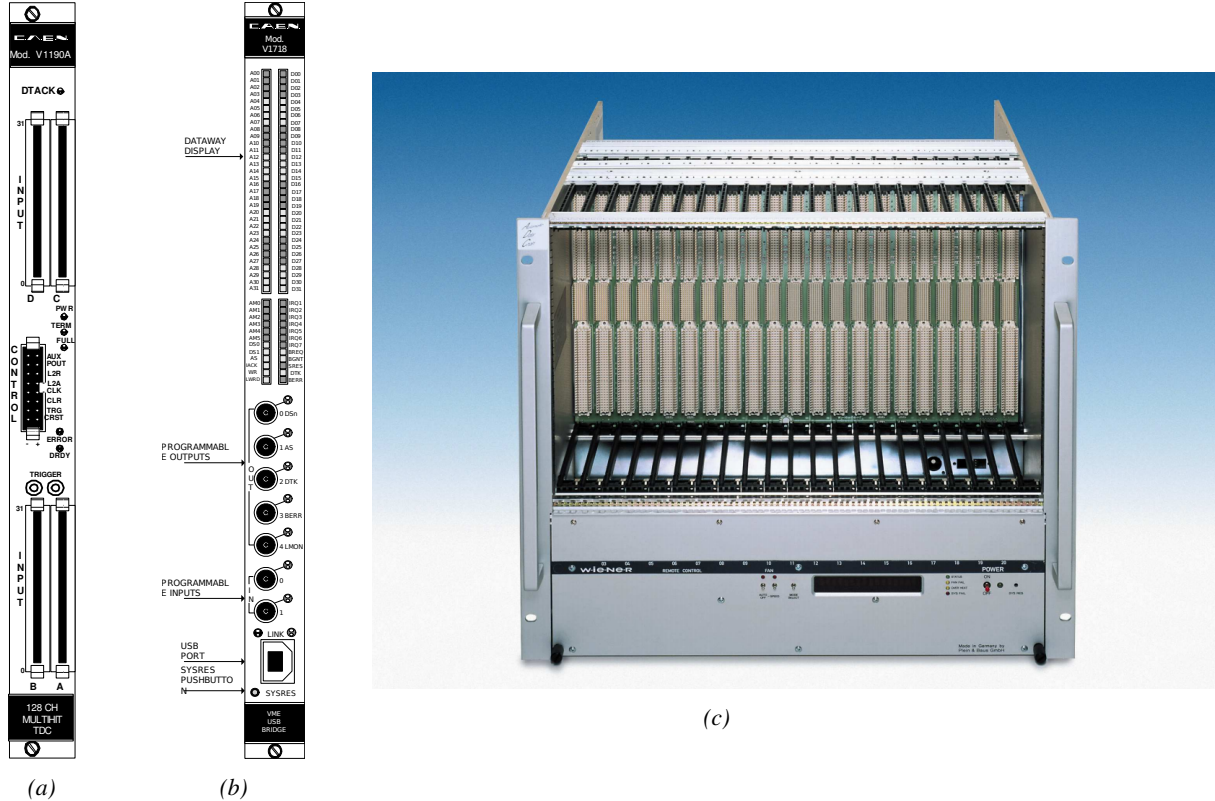


Figure A.1: (A.1a) View of the front panel of a V1190A TDC module [10]. (A.1b) View of the front panel of a V1718 Bridge module [11]. (A.1c) View of the front panel of a 6U 6021 VME crate [12].

914

### A.4 Data read-out

915 To efficiently perform a data readout algorithm, C++ objects to handle the VME modules (TDCs  
 916 and VME bridge) have been created along with objects to store data and read the configuration file

917 that comes as an input of the DAQ software.

918

### 919 A.4.1 V1190A TDCs

920 The DAQ used at GIF takes profit of the *Trigger Matching Mode* offered by V1190A modules.  
 921 This setting is enabled through the method `v1190a::SetTrigMatching (int ntdcs)` where `ntdcs`  
 922 is the total number of TDCs in the setup this setting needs to be enabled for (Source Code A.1). A  
 923 trigger matching is performed in between a trigger time tag, a trigger signal sent into the TRIGGER  
 924 input of the TDC visible on Figure A.1a, and the channel time measurements, signals recorded from  
 925 the detectors under test in our case. Control over this data acquisition mode, explained through  
 926 Figure A.2, is offered via 4 programmable parameters:

- 927 • **match window:** the matching between a trigger and a hit is done within a programmable time  
 928 window. This is set via the method

929 `void v1190a::SetTrigWindowWidth(Uint windowHeight, int ntdcs)`

- 930 • **window offset:** temporal distance between the trigger tag and the start of the trigger matching  
 931 window. This is set via the method

932 `void v1190a::SetTrigWindowWidth(Uint windowHeight, int ntdcs)`

- 933 • **extra search margin:** an extended time window is used to ensure that all matching hits are  
 934 found. This is set via the method

935 `void v1190a::SetTrigSearchMargin(Uint searchMargin, int ntdcs)`

- 936 • **reject margin:** older hits are automatically rejected to prevent buffer overflows and to speed  
 937 up the search time. This is set via the method

938 `void v1190a::SetTrigRejectionMargin(Uint rejectMargin, int ntdcs)`

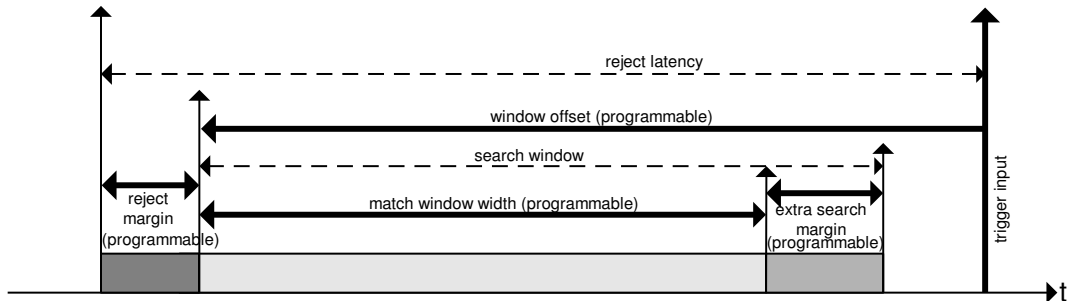


Figure A.2: Module V1190A Trigger Matching Mode timing diagram [10].

939 Each of these 4 parameters are given in number of clocks, 1 clock being 25 ns long. It is easy to  
 940 understand at this level that there are 3 possible functioning settings:

- 941 • **1:** the match window is entirely contained after the trigger signal,

- 942 • **2:** the match window overlaps the trigger signal, or

- 943 • **3:** the match window is entirely contained before the trigger signal as displayed on Figure A.2.

944 In both the first and second cases, the sum of the window width and of the offset can be set to  
945 a maximum of 40 clocks, which corresponds to 1  $\mu$ s. Evidently, the offset can be negative, allowing  
946 for a longer match window, with the constraint of having the window ending at most 1  $\mu$ s after the  
947 trigger signal. In the third case, the maximum negative offset allowed is of 2048 clocks (12 bit) cor-  
948 responding to 51.2  $\mu$ s, the match window being strictly smaller than the offset. In the case of GIF++,  
949 the choice has been made to use this last setting by delaying the trigger signal. During the studies  
950 performed in GIF++, both the efficiency of the RPCs, probed using a muon beam, and the noise or  
951 gamma background rate are monitored. The extra search and reject margins are left unused.  
952 To probe the efficiency of RPC detectors, the trigger time tag is provided by the coïncidence of  
953 scintillators when a bunch of muons passes through GIF++ area is used to trigger the data acquisi-  
954 tion. For this measurement, it is useful to reduce the match window width only to contain the muon  
955 information. Indeed, the delay in between a trigger signal and the detection of the corresponding  
956 muon in the RPC being very contant (typically a few tens of ns due to jitter and cable length), the  
957 muon signals are very localised in time. Thus, due to a delay of approximalety 325 ns in between  
958 the muons and the trigger, the settings where chosen to have a window width of 24 clocks (600 ns)  
959 centered on the muon peak thanks to a negative offset of 29 clocks (725 ns).  
960 On the otherhand, monitoring the rates don't require for the DAQ to look at a specific time window.  
961 It is important to integrate enough time to have a robust measurement of the rate as the number of  
962 hits per time unit. The triggerring signal is provided by a pulse generator at a frequency of 300 Hz  
963 to ensure that the data taking occurs in a random way, with respect to beam physics, to probe only  
964 the irradiation spectrum on the detectors. The match window is set to 400 clocks (10  $\mu$ s) and the  
965 negative offset to 401 clocks as it needs to exceed the value of the match window.

```

966
class v1190a
{
private :
    long           Handle;
    vector<Data32>   Address;
    CVDataWidth     DataWidth;
    CVAddressModifier AddressModifier;

public:
    v1190a(long handle, IniFile *inifile, int ntdcs);
    ~v1190a();
    Data16 write_op_reg(Data32 address, int code, string error);
    Data16 read_op_reg(Data32 address, string error);
    void Reset(int ntdcs);
    void Clear(int ntdcs);
    void TestWR(Data16 value,int ntdcs);
    void CheckTDCStatus(int ntdcs);
    void CheckCommunication(int ntdcs);
    void SetTDCTestMode(Data16 mode,int ntdcs);
    void SetTrigMatching(int ntdcs);
    void SetTrigTimeSubtraction(Data16 mode,int ntdcs);
    void SetTrigWindowWidth(Uint windowHeight,int ntdcs);
    void SetTrigWindowOffset(Uint windowOffset,int ntdcs);
    void SetTrigSearchMargin(Uint searchMargin,int ntdcs);
    void SetTrigRejectionMargin(Uint rejectMargin,int ntdcs);
    void GetTrigConfiguration(int ntdcs);
    void SetTrigConfiguration(IniFile *inifile,int ntdcs);
    void SetTDCDetectionMode(Data16 mode,int ntdcs);
    void SetTDCResolution(Data16 lsb,int ntdcs);
    void SetTDCDeadTime(Data16 time,int ntdcs);
    void SetTDCHeadTrailer(Data16 mode,int ntdcs);
    void SetTDCEventSize(Data16 size,int ntdcs);
    void SwitchChannels(IniFile *inifile,int ntdcs);
    void SetIRQ(Data32 level, Data32 count,int ntdcs);
    void SetBlockTransferMode(Data16 mode,int ntdcs);
    void Set(IniFile *inifile,int ntdcs);
    void CheckStatus(CVErrorCodes status) const;
    int ReadBlockD32(Uint tdc, const Data16 address,
                     Data32 *data, const Uint words, bool ignore_berr);
    Uint Read(RAWData *DataList,int ntdcs);
};

967

```

968       *Source Code A.1: Description of C++ object v1190a.*

969       The v1190a object, defined in the DAQ software as in Source Code A.1, offers the possibility to  
 970       concatenate all TDCs in the readout setup into a single object containing a list of hardware addresses  
 971       (addresses to access the TDCs' buffer through the VME crate) and each constructor and method acts  
 972       on the list of TDCs.  
 973

#### 974       A.4.2 DataReader

975       Enabled thanks to v1190a::SetBlockTransferMode(Data16 mode, int ntdcs), the data transfer  
 976       is done via Block Transfer (BLT). Using BLT allows to tranfer a fixed number of events called a  
 977       *block*. This is used together with an Almost Full Level (AFL) of the TDCs' output buffers, defined

978 through `v1190a::SetIRQ(Data32 level, Data32 count, int ntdcs)`. This AFL gives the maximum amount of 32735 words (16 bits, corresponding to the depth of a TDC output buffer) that can  
 979 written in a buffer before an Interrupt Request (IRQ) is generated and seen by the VME Bridge,  
 980 stopping the data acquisition to transfer the content of each TDC buffers before resuming. For each  
 981 trigger, 6 words or more are written into the TDC buffer:

- 983     • a **global header** providing information of the event number since the beginning of the data  
       acquisition,
- 985     • a **TDC header**,
- 986     • the **TDC data** (*if any*), 1 for each hit recorded during the event, providing the channel and the  
       time stamp associated to the hit,
- 988     • a **TDC error** providing error flags,
- 989     • a **TDC trailer**,
- 990     • a **global trigger time tag** that provides the absolute trigger time relatively to the last reset,  
       and
- 992     • a **global trailer** providing the total word count in the event.

993     As previously described in Section 4.4.3, CMS RPC FEEs provide us with 100 ns long LVDS  
 994 output signals that are injected into the TDCs' input. Any avalanche signal that gives a signal above  
 995 the FEEs threshold is thus recorded by the TDCs as a hit within the match window. Each hit is  
 996 assigned to a specific TDC channel with a time stamp, with a precision of 100 ps. The reference  
 997 time,  $t_0 = 0$ , is provided by the beginning of the match window. Thus for each trigger, coming from  
 998 a scintillator coïncidence or the pulse generator, a list of hits is stored into the TDCs' buffers and  
 999 will then be transferred into a ROOT Tree.

1000     When the BLT is used, it is easy to understand that the maximum number of words that have  
 1001 been set as ALF will not be a finite number of events or, at least, the number of events that would  
 1002 be recorded into the TDC buffers will not be a multiple of the block size. In the last BLT cycle to  
 1003 tranfer data, the number of events to transfer will most probably be lower than the block size. In that  
 1004 case, the TDC can add fillers at the end of the block but this option requires to send more data to the  
 1005 computer and is thus a little slower. Another solution is to finish the transfer after the last event by  
 1006 sending a bus error that states that the BLT reached the last event in the pile. This method has been  
 1007 chosen in GIF++.

1009     Due to irradiation, an event in GIF++ can count up to 300 words per TDC. A limit of 4096 words  
 1010 (12 bits) has been set to generate IRQ which represent from 14 to almost 700 events depending on  
 1011 the average of hits collected per event. Then the block size has been set to 100 events with enabled  
 1012 bus errors. When an AFL is reached for one of the TDCs, the VME bridge stops the acquisition by  
 1013 sending a BUSY signal.

1015

1016     The data is then transferred one TDC at a time into a structure called `RAWData` (Source Code A.2).

```
1017
1018 struct RAWData{
1019     vector<int>           *EventList;
1020     vector<int>           *NHitsList;
1021     vector<int>           *QFlagList;
1022     vector<vector<int>>   *Channellist;
1023     vector<vector<float>>  *TimeStampList;
1024 };
1025
```

1019                 *Source Code A.2: Description of data holding C++ structure `RAWData`.*

1020     In order to organize the data transfer and the data storage, an object called `DataReader` was  
1021     created (Source Code A.3). On one hand, it has `v1718` and `v1190a` objects as private members for  
1022     communication purposes, such as VME modules settings via the configuration file `*iniFile` or data  
1023     read-out through `v1190a::Read()` and on the other hand, it contains the structure `RAWData` that allows  
1024     to organise the data in vectors reproducing the tree structure of a ROOT file.

```
1025
1026 class DataReader
1027 {
1028     private:
1029         bool      StopFlag;
1030         IniFile *iniFile;
1031         Data32  MaxTriggers;
1032         v1718   *VME;
1033         int       nTDCs;
1034         v1190a  *TDCs;
1035         RAWData TDCData;

1036     public:
1037         DataReader();
1038         virtual ~DataReader();
1039         void      SetIniFile(string inifilename);
1040         void      SetMaxTriggers();
1041         Data32  GetMaxTriggers();
1042         void      SetVME();
1043         void      SetTDC();
1044         int       GetQFlag(Uint it);
1045         void      Init(string inifilename);
1046         void      FlushBuffer();
1047         void      Update();
1048         string  GetFileName();
1049         void      WriteRunRegistry(string filename);
1050         void      Run();
1051 };

1052
```

1027                 *Source Code A.3: Description of C++ object `DataReader`.*

1028     Each event is transferred from `TDCData` and saved into branches of a ROOT `TTree` as 3 integers  
1029     that represent the event ID (`EventCount`), the number of hits read from the TDCs (`nHits`), and the  
1030     quality flag that provides information for any problem in the data transfer (`qflag`), and 2 lists of  
1031     `nHits` elements containing the fired TDC channels (`TDCCh`) and their respective time stamps (`TDCTS`),  
1032     as presented in Source Code A.4. The ROOT file file is named using information contained into  
1033     the configuration file, presented in section A.5.2. The needed information is extracted using method  
1034     `DataReader::GetFileName()` and allow to build the output filename format `ScanXXXXXX_HVX_DAQ.root`

1035 where ScanXXXXXX is a 6 digit number representing the scan number into GIFT++ database and HVX  
 1036 the HV step within the scan that can be more than a single digit. An example of ROOT data file is  
 1037 provided with Figure A.3.

```
1038
RAWData TDCData;
TFile *outputFile = new TFile(outputFileName.c_str(),"recreate");
TTree *RAWDataTree = new TTree("RAWData","RAWData");

int EventCount = -9;
int nHits = -8;
int qflag = -7;
vector<int> TDCCh;
vector<float> TDCTS;

RAWDataTree->Branch("EventNumber",&EventCount, "EventNumber/I");
RAWDataTree->Branch("number_of_hits",&nHits,"number_of_hits/I");
RAWDataTree->Branch("Quality_flag",&qflag,"Quality_flag/I");
RAWDataTree->Branch("TDC_channel",&TDCCh);
RAWDataTree->Branch("TDC_TimeStamp",&TDCTS);

1039
//...
//Here read the TDC data using v1190a::Read() and place it into
//TDCData for as long as you didn't collect the requested amount
//of data.
//...

for(Uint i=0; i<TDCData.EventList->size(); i++){
    EventCount = TDCData.EventList->at(i);
    nHits = TDCData.NHitsList->at(i);
    qflag = TDCData.QFlagList->at(i);
    TDCCh = TDCData.ChannelList->at(i);
    TDCTS = TDCData.TimeStampList->at(i);
    RAWDataTree->Fill();
}
```

1040 *Source Code A.4: Highlight of the data transfer and organisation within DataReader::Run() after the data has been collected into TDCData.*

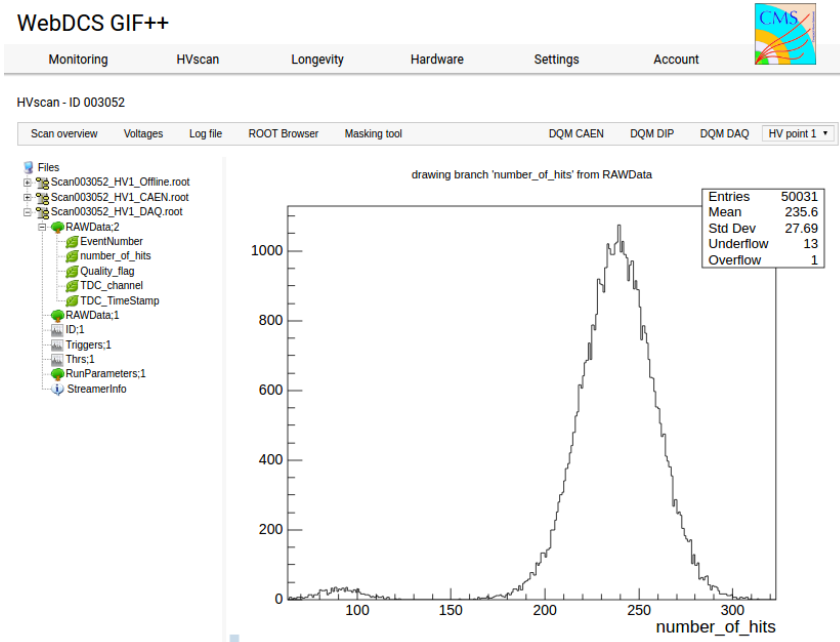


*Figure A.3: Structure of the ROOT output file generated by the DAQ. The 5 branches (EventNumber, number\_of\_hits, Quality\_flag, TDC\_channel and TDC\_TimeStamp) are visible on the left panel of the ROOT browser. On the right panel is visible the histogram corresponding to the variable nHits. In this specific example, there were approximately 50k events recorded to measure the gamma irradiation rate on the detectors. Each event is stored as a single entry in the TTree.*

#### 1041    A.4.3 Data quality flag

1042    Among the parameters that are recorded for each event, the quality flag, defined in Source Code A.5,  
 1043    is determined on the fly by checking the data recorded by every single TDC. From method `v1190a::Read()`,  
 1044    it can be understood that the content of each TDC buffer is readout one TDC at a time. Entries are  
 1045    created in the data list for the first TDC and then, when the second buffer is readout, events corre-  
 1046    sponding to entries that have already been created to store data for the previous TDC are added to  
 1047    the existing list element. On the contrary, when an event entry has not been yet created in the data  
 1048    list, a new entry is created.

```
1049
 1050   typedef enum _QualityFlag {
 1051     GOOD      = 1,
 1052     CORRUPTED = 0
 1053   } QualityFlag;
```

1051    *Source Code A.5: Definition of the quality flag `enum`.*

1052    It is possible that each TDC buffer contains a different number of events. In cases where the first  
 1053    element in the buffer list is an event for corresponds to a new entry, the difference in between the  
 1054    entry from the buffer and the last entry in the data list is recorded and checked. If it is greater than 1,  
 1055    what should never be the case, the quality flag is set to CORRUPTED for this TDC and an empty entry  
 1056    is created in the place of the missing ones. Missing entries are believe to be the result of a bad hold

1057 on the TDC buffers at the moment of the readout. Indeed, the software hold is effective only on 1  
 1058 TDC at a time and no solution as been found yet to completely block the writting in the buffers when  
 1059 an IRQ is received.

1060 At the end of each BLT cycle, the ID of the last entry stored for each TDC buffer is not recorded.  
 1061 When starting the next cycle, if the first entry in the pile corresponds to an event already existing  
 1062 in the list, the readout will start from this list element and will not be able to check the difference  
 1063 in between this entry's ID and the one of the last entry that was recorded for this TDC buffer in  
 1064 the previous cycle. In the case events were missing, the flag stays at its initial value of 0, which is  
 1065 similar to CORRUPTED and it is assumed that then this TDC will not contribute to `number_of_hits`,  
 1066 `TDC_channel` or `TDC_TimeStamp`.

1067 Finally, since there will be 1 `RAWData` entry per TDC for each event (meaning `nTDCs` entries,  
 1068 referring to `DataReader` private attribute), the individual flags of each TDC will be added together.  
 1069 The final format is an integer composed `nTDCs` digits where each digit is the flag of a specific TDC.  
 1070 This is constructed using powers of 10 like follows:

```
1071 TDC 0: QFlag = 100 × _QualityFlag
1072 TDC 1: QFlag = 101 × _QualityFlag
1073 ...
1074 TDC N: QFlag = 10N × _QualityFlag
```

1075 and the final flag to be with N digits:

```
1076 QFlag = n....3210
```

1077 each digit being 1 or 0. Below is given an example with a 4 TDCs setup.

1078 If all TDCs were good : `QFlag = 1111`,

1079 but if TDC 2 was corrupted : `QFlag = 1011`.

1080 When data taking is over and the data contained in the dynamical `RAWData` structure is transferred  
 1081 to the ROOT file, all the 0s are changed into 2s by calling the method `DataReader::GetQFlag()`.  
 1082 This will help translating the flag without knowing the number of TDCs beforehand. Indeed, a flag  
 1083 111 could be due to a 3 TDC setup with 3 good individual TDC flags or to a more than 3 TDC setup  
 1084 with TDCs those ID is greater than 2 being CORRUPTED, thus giving a 0.

1085 The quality flag has been introduced quite late, in October 2017 only, to the list of GIFT++ DAQ  
 1086 parameters to be recorded into the output ROOT file. Before this addition, the missing data, corrupting  
 1087 the quality for the offline analysis, was contributing to artificially fill data with lower multiplicity.  
 1088 Looking at `TBranch number_of_hits` provides an information about the data of the full GIFT++  
 1089 setup. When a TDC is not able to transfer data for a specific event, the effect is a reduction of the  
 1090 total number of hits recorded in the full setup, this is what can be seen from Figure A.4. After offline  
 1091 reconstruction detector by detector, the effect of missing events can be seen in the artificially filled  
 1092 bin at multiplicity 0 shown in Figure A.5. Nonetheless, for data with high irradiation levels, as it is  
 1093 the case for Figure A.5a, discarding the fake multiplicity 0 data can be done easily during the offline  
 1094 analysis. At lower radiation, the missing events contribution becomes more problematic the multi-  
 1095 plicity distribution overlaps the multiplicity 0 and that in the same time the proportion of missing

1096 events decreases. Attempts to fit the distribution with a Poisson or skew distribution function were  
 1097 not conclusive.

1098

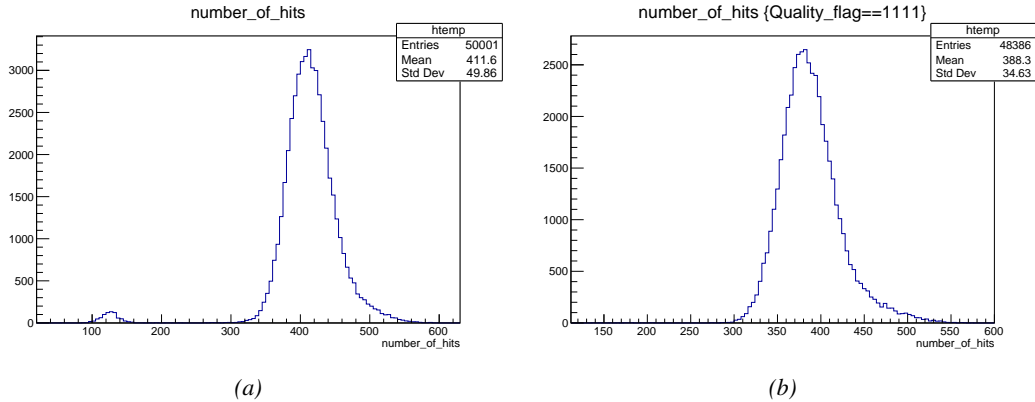


Figure A.4: The effect of the quality flag is explained by presenting the content of TBranch `number_of_hits` of a data file without `Quality_flag` in Figure A.4a and the content of the same TBranch for data corresponding to a `Quality_flag` where all TDCs were labelled as `GOOD` in Figure A.4b taken with similar conditions. It can be noted that the number of entries in Figure A.4b is slightly lower than in Figure A.4a due to the excluded events.

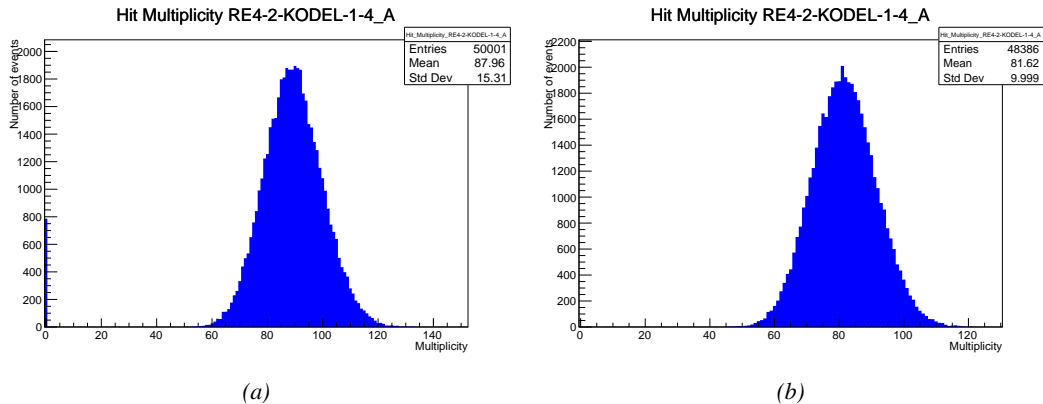


Figure A.5: Using the same data as previously showed in Figure A.4, the effect of the quality flag is explained by presenting the reconstructed hit multiplicity of a data file without `Quality_flag` in Figure A.5a and the reconstructed content of the same RPC partition for data corresponding to a `Quality_flag` where all TDCs were labelled as `GOOD` in Figure A.5b taken with similar conditions. The artificial high content of bin 0 is completely suppressed.

## 1099 A.5 Communications

1100 To ensure data readout and dialog in between the machine and the TDCs or in between the webDCS  
 1101 and the DAQ, different communication solutions were used. First of all, it is important to have a  
 1102 module to allow the communication in between the TDCs and the computer from which the DAQ

1103 operates. When this communication is effective, shifters using the webDCS to control data taking  
 1104 can thus send instructions to the DAQ.

1105

### 1106 A.5.1 V1718 USB Bridge

1107 In the previous section, the data transfer has been discussed. The importance of the `v1718` object  
 1108 (Source Code A.6), used as private member of `DataReader`, was not explicated. VME master  
 1109 modules are used for communication purposes as they host the USB port that connects the pow-  
 1110 ered crate buffer to the computer where the DAQ is installed. From the source code point of view,  
 1111 this object is used to control the communication status, by reading the returned error codes with  
 1112 `v1718::CheckStatus()`, or to check for IRQs coming from the TDCs through `v1718::CheckIRQ()`.  
 1113 Finally, to ensure that triggers are blocked at the hardware level, a NIM pulse is sent out of one of the  
 1114 5 programmable outputs (`v1718::SendBUSY()`) to the VETO of the coincidence module where the  
 1115 trigger signals originate from. As long as this signal is ON, no trigger can reach the TDCs anymore.

1116

```
class v1718{
private:
    int             Handle;
    Data32          Data;           // Data
    CVIRQLevels    Level;         // Interrupt level
    CVAddressModifier AM;          // Addressing Mode
    CVDataWidth     DataSize;      // Data Format
    Data32          BaseAddress;   // Base Address

public:
    v1718(IniFile *inifile);
    ~v1718();
    long            GetHandle(void) const;
    int             SetData(Data16 data);
    Data16          GetData(void);
    int             SetLevel(CVIRQLevels level);
    CVIRQLevels    GetLevel(void);
    int             SetAM(CVAddressModifier am);
    CVAddressModifier GetAM(void);
    int             SetDatasize(CVDataWidth datasize);
    CVDataWidth     GetDataSize(void);
    int             SetBaseAddress(Data16 baseaddress);
    Data16          GetBaseAddress(void);
    void            CheckStatus(CVErrorCodes status) const;
    void            CheckIRQ();
    void            SetPulsers();
    void            SendBUSY(BusyLevel level);
};
```

1118

*Source Code A.6: Description of C++ object v1718.*

### 1119 A.5.2 Configuration file

1120 The DAQ software takes as input a configuration file written using INI standard [13]. This file is  
 1121 partly filled with the information provided by the shifters when starting data acquisition using the  
 1122 webDCS, as shown by Figure A.6. This information is written in section [`General`] and will later  
 1123 be stored in the ROOT file that contains the DAQ data as can be seen from Figure A.3. Indeed,

1124 another `TTree` called `RunParameters` as well as the 2 histograms `ID`, containing the scan number,  
 1125 start and stop time stamps, and `Triggers`, containing the number of triggers requested by the shifter,  
 1126 are available in the data files. Moreover, `ScanID` and `HV` are then used to construct the file name  
 1127 thanks to the method `DataReader::GetFileName()`.

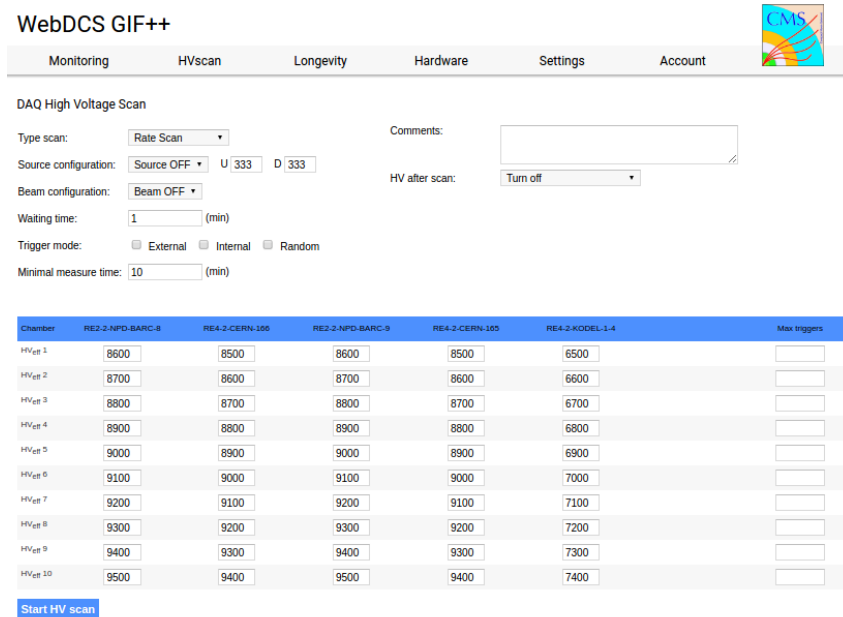


Figure A.6: WebDCS DAQ scan page. On this page, shifters need to choose the type of scan (Rate, Efficiency or Noise Reference scan), the gamma source configuration at the moment of data taking, the beam configuration, and the trigger mode. These information will be stored in the DAQ ROOT output. Are also given the minimal measurement time and waiting time after ramping up of the detectors is over before starting the data acquisition. Then, the list of HV points to scan and the number of triggers for each run of the scan are given in the table underneath.

1128 The rest of the information is written beforehand in the configuration file template, as explicated  
 1129 in Source Code A.7, and contains the hardware addresses to the different VME modules in the  
 1130 setup as well as settings for the TDCs. As the TDC settings available in the configuration file are not  
 1131 supposed to be modified, an improvement would be to remove them from the configuration file and  
 1132 to hardcode them inside of the DAQ code itself or to place them into a different INI file that would  
 1133 host only the TDC settings to lower the probability for a bad manipulation of the configuration file  
 1134 that can be modified from one of webDCS' menus.

1135

```
[General]
TdcS=4
ScanID=$scanid
HV=$HV
RunType=$runtype
MaxTriggers=$maxtriggers
Beam=$beam
[VMEInterface]
Type=V1718
BaseAddress=0xFF0000
Name=VmeInterface
[TDC0]
Type=V1190A
BaseAddress=0x00000000
Name=Tdc0
StatusA00-15=1
StatusA16-31=1
StatusB00-15=1
StatusB16-31=1
StatusC00-15=1
StatusC16-31=1
StatusD00-15=1
StatusD16-31=1
[TDC1]
Type=V1190A
BaseAddress=0x11110000
Name=Tdc1
StatusA00-15=1
StatusA16-31=1
StatusB00-15=1
StatusB16-31=1
StatusC00-15=1
StatusC16-31=1
StatusD00-15=1
StatusD16-31=1
[TDC2]
Type=V1190A
BaseAddress=0x22220000
Name=Tdc2
StatusA00-15=1
StatusA16-31=1
StatusB00-15=1
StatusB16-31=1
StatusC00-15=1
StatusC16-31=1
StatusD00-15=1
StatusD16-31=1
[TDC3]
Type=V1190A
BaseAddress=0x44440000
Name=Tdc3
StatusA00-15=1
StatusA16-31=1
StatusB00-15=1
StatusB16-31=1
StatusC00-15=1
StatusC16-31=1
StatusD00-15=1
StatusD16-31=1
[TDCSettings]
TriggerExtraSearchMargin=0
TriggerRejectMargin=0
TriggerTimeSubtraction=0b1
TdcDetectionMode=0b01
TdcResolution=0b10
TdcDeadTime=0b00
TdcHeadTrailer=0b1
TdcEventSize=0b1001
TdcTestMode=0b0
BLTMode=1
```

*Source Code A.7: INI configuration file template for 4 TDCs. In section [General], the number of TDCs is explicitated and information about the ongoing run is given. Then, there are sections for each and every VME modules. There buffer addresses are given and for the TDCs, the list of channels to enable is given. Finally, in section [TDCSettings], a part of the TDC settings are given.*

1138     In order to retrieve the information of the configuration file, the object `IniFile` has been developed  
 1139     to provide an INI parser, presented in Source Code A.8. It contains private methods returning a  
 1140     boolean to check the type of line written in the file, whether a comment, a group header or a key line  
 1141     (`IniFile::CheckIfComment()`, `IniFile::CheckIfGroup()` and `IniFile::CheckIfToken()`). The  
 1142     key may sometimes be referred to as *token* in the source code. Moreover, the private element  
 1143     `FileData` is a map of `const string` to `string` that allows to store the data contained inside the  
 1144     configuration file via the public method `IniFile::GetFileData()` following the formatting (see  
 1145     method `IniFile::Read()`):

```
1146
  1147     string group, token, value;
  // Get the field values for the 3 strings.
  // Then concatenate group and token together as a single string
  // with a dot separation.
  token = group + "." + token;
  FileData[token] = value;
```

1148     More methods have been written to translate the different keys into the right variable format  
 1149     when used by the DAQ. For example, to get a `float` value out of the configuration file data, knowing  
 1150     the group and the key needed, the method `IniFile::floatType()` can be used. It takes 3 arguments  
 1151     being the group name and key name (both `string`), and a default `float` value used as exception in  
 1152     the case the expected combination of group and key cannot be found in the configuration file. This  
 1153     default value is then used and the DAQ continues on working after sending an alert in the log file for  
 1154     further debugging.

```

1155 typedef map< const string, string > IniFileData;
1156
class IniFile{
    private:
        bool          CheckIfComment (string line);
        bool          CheckIfGroup(string line, string& group);
        bool          CheckIfToken(string line, string& key, string& value);
        string         FileName;
        IniFileData   FileData;
        int           Error;

    public:
        IniFile();
        IniFile(string filename);
        virtual      ~IniFile();

        // Basic file operations
        void          SetFileName(string filename);
        int           Read();
        int           Write();
        IniFileData GetFileData();

        // Data readout methods
        Data32         addressType (string groupname, string keyname, Data32
→     defaultvalue);
        long          intType     (string groupname, string keyname, long
→     defaultvalue);
        long long    longType    (string groupname, string keyname, long long
→     defaultvalue );
        string         stringType  (string groupname, string keyname, string
→     defaultvalue );
        float         floatType   (string groupname, string keyname, float
→     defaultvalue );

        // Error methods
        string         GetErrorMsg();
};


```

1157       *Source Code A.8: Description of C++ object `IniFile` used as a parser for INI file format.*

### 1158     A.5.3 WebDCS/DAQ intercommunication

1159     When shifters send instructions to the DAQ via the configuration file, it is the webDCS itself that  
 1160     gives the start command to the DAQ and then the 2 softwares use inter-process communication  
 1161     through file to synchronise themselves. This communication file is represented by the variable **const**  
 1162     string \_\_runstatuspath.

1163     On one side, the webDCS sends commands or status that are readout by the DAQ:

- 1164       • INIT, status sent when launching a scan and read via function `CtrlRunStatus(...)`,
- 1165       • START, command to start data taking and read via function `CheckSTART()`,
- 1166       • STOP, command to stop data taking at the end of the scan and read via function `CheckSTOP()`,  
 1167        and
- 1168       • KILL, command to kill data taking sent by user and read via function `CheckKILL()`

1169 and on the other, the DAQ sends status that are controled by the webDCS:

- 1170     ● `DAQ_RDY`, sent with `SendDAQReady()` to signify that the DAQ is ready to receive commands  
1171       from the webDCS,
- 1172     ● `RUNNING`, sent with `SendDAQRunning()` to signify that the DAQ is taking data,
- 1173     ● `DAQ_ERR`, sent with `SendDAQError()` to signify that the DAQ didn't receive the expected com-  
1174       mand from the webDCS or that the launch command didn't have the right number of argu-  
1175       ments,
- 1176     ● `RD_ERR`, sent when the DAQ wasn't able to read the communication file, and
- 1177     ● `WR_ERR`, sent when the DAQ wasn't able to write into the communication file.

#### 1178     **A.5.4 Example of inter-process communication cycle**

1179 Under normal conditions, the webDCS and the DAQ processes exchange commands and status via  
1180 the file hosted at the address `__runstatuspath`, as explained in subsection A.5.3. An example of  
1181 cycle is given in Table A.1. In this example, the steps 3 to 5 are repeated as long as the webDCS tells  
1182 the DAQ to take data. A data taking cycle is the equivalent as what is called a *Scan* in GIFT++ jargon,  
1183 referring to a set a runs with several HV steps. Each repetition of steps 3 to 5 is then equivalent to a  
1184 single *Run*.

1185

1186     At any moment during the data taking, for any reason, the shifter can decide that the data taking  
1187 needs to be stopped before it reached the end of the scheduled cycle. Thus at any moment on the  
1188 cycle, the content of the inter-process communication file will be changed to `KILL` and the DAQ will  
1189 shut down right away. The DAQ checks for `KILL` signals every 5s after the TDCs configuration is  
1190 over. So far, the function `CheckKILL()` has been used only inside of the data taking loop of method  
1191 `DataReader::Run()` and thus, if the shifter decides to KILL the data taking during the TDC con-  
1192 figuration phase or the HV ramping in between 2 HV steps, the DAQ will not be stopped smoothly  
1193 and a *force kill* command will be sent to stop the DAQ process that is still awake on the computer.  
1194 Improvements can be brought on this part of the software to make sure that the DAQ can safely  
1195 shutdown at any moment.

1196

## 1197     **A.6 Software export**

1198 In section A.2 was discussed the fact that the DAQ as written in its last version is not a standalone  
1199 software. It is possible to make it a standalone program that could be adapted to any VME setup  
1200 using V1190A and V1718 modules by creating a GUI for the software or by printing the log mes-  
1201 sages that are normally printed in the webDCS through the log file, directly into the terminal. This  
1202 method was used by the DAQ up to version 3.0 moment where the webDCS was completed. Also, it  
1203 is possible to check branches of DAQ v2.X to have example of communication through a terminal.

1204

1205     DAQ v2.X is nonetheless limited in it's possibilities and requires a lot of offline manual interven-  
1206 tions from the users. Indeed, there is no communication of the software with the detectors' power  
1207 supply system that would allow for a user a predefine a list of voltages to operate the detectors at

step	actions of webDCS	status of DAQ	<code>__runstatuspath</code>
1	launch DAQ ramp voltages ramping over wait for currents stabilization	readout of IniFile configuration of TDCs	INIT
2		configuration done send DAQ ready wait for START signal	DAQ_RDY
3	waiting time over send START		START
4	wait for run to end monitor DAQ run status	data taking ongoing check for KILL signal	RUNNING
5		run over send DAQ_RDY wait for next DCS signal	DAQ_RDY
6	ramp voltages ramping over wait for currents stabilization		DAQ_RDY
3	waiting time over send START		START
4	wait for run to end monitor DAQ run status	update IniFile information data taking ongoing check for KILL signal	RUNNING
5		run over send DAQ_RDY wait for next DCS signal	DAQ_RDY
7	send command STOP	DAQ shuts down	STOP

Table A.1: Inter-process communication cycles in between the webDCS and the DAQ through file string signals.

1208 and loop over to take data without any further manual intervention. In v2.X, the data is taken for a  
1209 single detector setting and at the end of each run, the softwares asks the user if he intends on taking  
1210 more runs. If so, the software invites the user to set the operating voltages accordingly to what is  
1211 necessary and to manual update the configuration file in consequence. This working mode can be a  
1212 very first approach before an evolution and has been successfully used by colleagues from different  
1213 collaborations.

1214

1215 For a more robust operation, it is recommended to develop a GUI or a web application to inter-  
1216 face the DAQ. Moreover, to limit the amount of manual interventions, and thus the probability to  
1217 make mistakes, it is also recommended to add an extra feature into the DAQ by installing the HV  
1218 Wrapper library provided by CAEN of which an example of use in a similar DAQ software devel-  
1219 opped by a master student of UGent, and called TinyDAQ, is provided on UGent's github. Then, this  
1220 HV Wrapper will help you communicating with and give instructions to a CAEN HV powered crate  
1221 and can be added into the DAQ at the same level where the communication with the user was made  
1222 in DAQ v2.X. In case you are using another kind of power system for your detectors, it is stringly  
1223 adviced to use HV modules or crates that can be remotely controled via a using C++ libraries.

1224

# B

1225

1226

## Details on the offline analysis package

1227 The data collected in GIF++ thanks to the DAQ described in Appendix A is difficult to interpret by  
1228 a human user that doesn't have a clear idea of the raw data architecture of the ROOT data files. In  
1229 order to render the data human readable, a C++ offline analysis tool was designed to provide users  
1230 with detector by detector histograms that give a clear overview of the parameters monitored during  
1231 the data acquisition [14]. In this appendix, details about this software in the context of GIF++, as of  
1232 how the software was written and how it functions will be given.

### 1233 B.1 GIF++ Offline Analysis file tree

1234 GIF++ Offline Analysis source code is fully available on github at [https://github.com/aafagot/GIF\\_OfflineAnalysis](https://github.com/aafagot/GIF_OfflineAnalysis). The software requires ROOT as non-optionnal dependency  
1235 as it takes ROOT files in input and write an output ROOT file containing histograms. To compile the  
1236 GIF++ Offline Analysis project is compiled with cmake. To compile, first a build/ directory must  
1237 be created to compile from there:

```
1239 mkdir build
1240 cd build
1241 cmake ..
1242 make
1243 make install
```

1241 To clean the directory and create a new build directory, the bash script cleandir.sh can be used:

```
1242
1243 ./cleandir.sh
```

1244 The source code tree is provided below along with comments to give an overview of the files' con-  
1245 tent. The different objects created for this project (`Infrastructure`, `Trolley`, `RPC`, `Mapping`, `RPCHit`,  
1246 `RPCCluster` and `Inifile`) will be described in details in the following sections.

1247

```

GIF_OfflineAnalysis
├── bin
│   └── offlineanalysis ..... EXECUTABLE
├── build..... CMAKE COMPILATION DIRECTORY
└── ...
    ├── include..... LIST OF C++ HEADER FILES
    │   ├── Cluster.h..... DECLARATION OF OBJECT RPCCLUSTER
    │   ├── Current.h..... DECLARATION OF GETCURRENT ANALYSIS MACRO
    │   ├── GIFTrolley.h..... DECLARATION OF OBJECT TROLLEY
    │   ├── Infrastructure.h..... DECLARATION OF OBJECT INFRASTRUCTURE
    │   ├── IniFile.h..... DECLARATION OF OBJECT INI FILE FORINI PARSER
    │   ├── Mapping.h..... DECLARATION OF OBJECT MAPPING
    │   ├── MsgSvc.h..... DECLARATION OF OFFLINE LOG MESSAGES
    │   ├── OfflineAnalysis.h..... DECLARATION OF DATA ANALYSIS MACRO
    │   ├── RPCTracker.h..... DECLARATION OF OBJECT RPC
    │   ├── RPCHit.h..... DECLARATION OF OBJECT RPCHIT
    │   ├── types.h..... DEFINITION OF USEFUL VARIABLE TYPES
    │   └── utils.h..... DECLARATION OF USEFUL FUNCTIONS
    ├── obj..... BINARY FILES CREATED BY COMPILER
    └── ...
        ├── src..... LIST OF C++ SOURCE FILES
        │   ├── Cluster.cc..... DEFINITION OF OBJECT RPCCLUSTER
        │   ├── Current.cc..... DEFINITION OF GETCURRENT ANALYSIS MACRO
        │   ├── GIFTrolley.cc..... DEFINITION OF OBJECT TROLLEY
        │   ├── Infrastructure.cc..... DEFINITION OF OBJECT INFRASTRUCTURE
        │   ├── IniFile.cc..... DEFINITION OF OBJECT INI FILE FORINI PARSER
        │   ├── main.cc..... MAIN FILE
        │   ├── Mapping.cc..... DEFINITION OF OBJECT MAPPING
        │   ├── MsgSvc.cc..... DECLARATION OF OFFLINE LOG MESSAGES
        │   ├── OfflineAnalysis.cc..... DECLARATION OF DATA ANALYSIS MACRO
        │   ├── RPCTracker.cc..... DECLARATION OF OBJECT RPC
        │   ├── RPCHit.cc..... DECLARATION OF OBJECT RPCHIT
        │   └── utils.cc..... DEFINITION OF USEFUL FUNCTIONS
        ├── cleandir.sh..... BASH SCRIPT TO CLEAN BUILD DIRECTORY
        ├── CMakeLists.txt..... SET OF INSTRUCTIONS FOR CMAKE
        ├── config.h.in..... DEFINITION OF VERSION NUMBER
        └── README.md..... README FILE FOR GITHUB

```

1248

## B.2 Usage of the Offline Analysis

1249

In order to use the Offline Analysis tool, it is necessary to know the Scan number and the HV Step of the run that needs to be analysed. This information needs to be written in the following format:

1251

1252

```
Scan00XXXX_HVY
```

1253

1254

where XXXX is the scan ID and Y is the high voltage step (in case of a high voltage scan, data will be taken for several HV steps). This format corresponds to the base name of data files in the database

1255 of the GIF++ webDCS. Usually, the offline analysis tool is automatically called by the webDCS at  
 1256 the end of data taking or by a user from the webDCS panel if an update of the tool was brought.  
 1257 Nonetheless, an expert can locally launch the analysis for tests on the GIF++ computer, or a user can  
 1258 get the code on its local machine from github and download data from the webDCS for its own anal-  
 1259 ysis. To launch the code, the following command can be used from the `GIF_OfflineAnalysis` folder:

1260

```
1261 bin/offlineanalysis /path/to/Scan00XXXX_HVY
```

1262 where, `/path/to/Scan00XXXX_HVY` refers to the local data files. Then, the offline tool will by itself  
 1263 take care of finding all available ROOT data files present in the folder, as listed below:

1264

- `Scan00XXXX_HVY_DAQ.root` containing the TDC data as described in Appendix ?? (events, hit  
 1265 and timestamp lists), and
- `Scan00XXXX_HVY_CAEN.root` containing the CAEN mainframe data recorded by the monitor-  
 1266 ing tool webDCS during data taking (HVs and currents of every HV channels). This file is  
 1268 created independently of the DAQ.

## 1269 B.2.1 Output of the offline tool

### 1270 B.2.1.1 ROOT file

1271 The analysis gives in output ROOT datafiles that are saved into the data folder and called using the  
 1272 naming convention `Scan00XXXX_HVY_Offline.root`. Inside those, a list of `TH1` histograms can be  
 1273 found. Its size will vary as a function of the number of detectors in the setup as each set of histograms  
 1274 is produced detector by detector. For each partition of each chamber, can be found:

1275

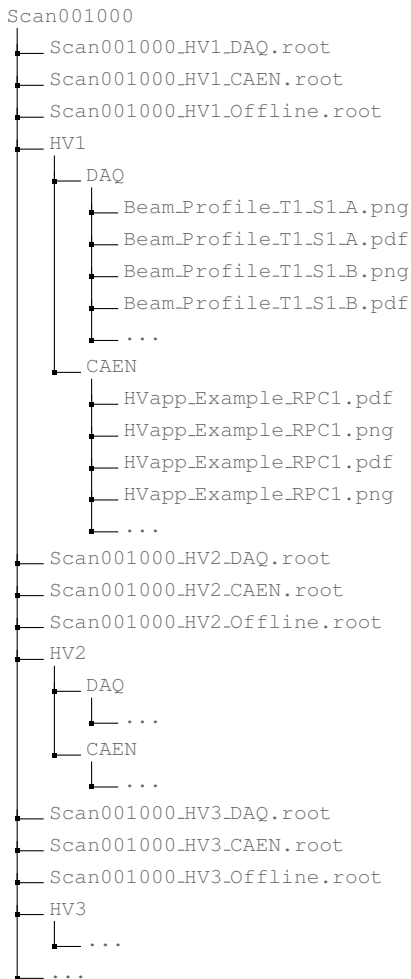
- `Time_Profile_Tt_Sc_p` shows the time profile of all recorded events (number of events per  
 1276 time bin),
- `Hit_Profile_Tt_Sc_p` shows the hit profile of all recorded events (number of events per chan-  
 1278 nel),
- `Hit_Multiplicity_Tt_Sc_p` shows the hit multiplicity (number of hits per event) of all recorded  
 1280 events (number of occurrences per multiplicity bin),
- `Strip_Mean_Noise_Tt_Sc_p` shows noise/gamma rate per unit area for each strip in a se-  
 1282 lected time range. After filters are applied on `Time_Profile_Tt_Sc_p`, the filtered version  
 1283 of `Hit_Profile_Tt_Sc_p` is normalised to the total integrated time and active detection area  
 1284 of a single channel,
- `Strip_Activity_Tt_Sc_p` shows noise/gamma activity for each strip (normalised version of  
 1286 previous histogram - strip activity = strip rate / average partition rate),
- `Strip_Homogeneity_Tt_Sc_p` shows the *homogeneity* of a given partition ( $\text{homogeneity} = \exp(-\text{strip rates standard deviation(strip rates in partition/average partition rate)})$ ),
- `mask_Strip_Mean_Noise_Tt_Sc_p` shows noise/gamma rate per unit area for each masked  
 1290 strip in a selected time range. Offline, the user can control the noise/gamma rate and decide to  
 1291 mask the strips that are judged to be noisy or dead. This is done via the *Masking Tool* provided  
 1292 by the webDCS,

- 1293     ● `mask_Strip_Activity_Tt_Sc_p` shows noise/gamma activity per unit area for each masked  
1294       strip with respect to the average rate of active strips,
- 1295     ● `NoiseCSize_H_Tt_Sc_p` shows noise/gamma cluster size, a cluster being constructed out of  
1296       adjacent strips giving a signal at the *same time* (hits within a time window of 25 ns),
- 1297     ● `NoiseCMult_H_Tt_Sc_p` shows noise/gamma cluster multiplicity (number of reconstructed  
1298       clusters per event),
- 1299     ● `Chip_Mean_Noise_Tt_Sc_p` shows the same information than `Strip_Mean_Noise_Tt_Scp` us-  
1300       ing a different binning (1 chip corresponds to 8 strips),
- 1301     ● `Chip_Activity_Tt_Sc_p` shows the same information than `Strip_Activity_Tt_Scp` using  
1302       chip binning,
- 1303     ● `Chip_Homogeneity_Tt_Sc_p` shows the homogeneity of a given partition using chip binning,
- 1304     ● `Beam_Profile_Tt_Sc_p` shows the estimated beam profile when taking efficiency scan. This  
1305       is obtained by filtering `Time_Profile_Tt_Sc_p` to only consider the muon peak where the  
1306       noise/gamma background has been subtracted. The resulting hit profile corresponds to the  
1307       beam profile on the detector channels,
- 1308     ● `L0_Efficiency_Tt_Sc_p` shows the level 0 efficiency that was estimated **without** muon track-  
1309       ing,
- 1310     ● `MuonCSize_H_Tt_Sc_p` shows the level 0 muon cluster size that was estimated **without** muon  
1311       tracking, and
- 1312     ● `MuonCMult_H_Tt_Sc_p` shows the level 0 muon cluster multiplicity that was estimated **without**  
1313       muon tracking.

1314     In the histogram labels,  $t$  stands for the trolley number (1 or 3),  $c$  for the chamber slot label in  
1315       trolley  $t$  and  $p$  for the partition label (A, B, C or D depending on the chamber layout) as explained  
1316       in Chapter 5.3.

1317     In the context of GIF++, an extra script called by the webDCS is called to extract the histograms  
1318       from the ROOT files. The histograms are then stored in PNG and PDF formats into the correspond-  
1319       ing folder (a single folder per HV step, so per ROOT file). the goal is to then display the histograms  
1320       on the Data Quality Monitoring (DQM) page of the webDCS in order for the users to control the  
1321       quality of the data taking at the end of data taking. An example of histogram organisation is given  
1322       below:

1324



**1325      Here can put some screens from the webDCS to show the DQM and the plots available to users.**

**1326**

### **1327      B.2.1.2 CSV files**

**1328** Moreover, up to 3 CSV files can be created depending on which ones of the 3 input files were in the  
**1329** data folder:

- 1330**     • `Offline-Corrupted.csv`, is used to keep track of the amount of data that was corrupted and  
**1331**       removed from old data format files that don't contain any data quality flag.
- 1332**     • `Offline-Current.csv`, contains the summary of the currents and voltages applied on each  
**1333**       RPC HV channel.
- 1334**     • `Offline-L0-EffC1.csv`, is used to write the efficiencies, cluster size and cluster multiplicity  
**1335**       of efficiency runs. Note that `L0` refers here to *Level 0* and means that the results of efficiency and  
**1336**       clusterization are a first approximation calculated without performing any muon tracking in

1337 between the different detectors. This offline tool provides the user with a preliminar calculation  
 1338 of the efficiency and of the muon event parameters. Another analysis software especially  
 1339 dedicated to muon tracking is called on selected data to retrieve the results of efficiency and  
 1340 muon clusterization using a tracking algorithm to discriminate noise or gamma from muons  
 1341 as muons are the only particles that pass through the full setup, leaving hits than can be used  
 1342 to reconstruct their tracks.

- 1343     ● `Offline-Rate.csv`, is used to write the noise or gamma rates measured in the detector readout  
 1344 partitions.

1345 Note that these 4 CSV files are created along with their *headers* (`Offline-[...]-Header.csv`  
 1346 containing the names of each data columns) and are automatically merged together when the offline  
 1347 analysis tool is called from the webDCS, contrary to the case where the tool is runned locally from  
 1348 the terminal as the merging bash script is then not called. Thus, the resulting files, used to make  
 1349 official plots, are:

- 1350     ● `Corrupted.csv`,  
 1351     ● `Current.csv`,  
 1352     ● `L0-EffCl.csv`.  
 1353     ● `Rate.csv`.

### 1354     **B.3 Analysis inputs and information handling**

1355 The usage of the Offline Analysis tool as well as its output have been presented in the previous section.  
 1356 It is now important to dig further and start looking at the source code and the inputs necessary  
 1357 for the tool to work. Indeed, other than the raw ROOT data files that are analysed, more information  
 1358 needs to be imported inside of the program to perform the analysis such as the description of the  
 1359 setup inside of GIFT++ at the time of data taking (number of trolleys, of RPCs, dimensions of the  
 1360 detectors, etc...) or the mapping that links the TDC channels to the coresponding RPC channels in  
 1361 order to translate the TDC information into human readable data. 2 files are used to transmit all this  
 1362 information:  
 1363

- 1364     ● `Dimensions.ini`, that provides the necessary setup and RPC information, and  
 1365     ● `ChannelsMapping.csv`, that gives the link between the TDC and RPC channels as well as the  
 1366 *mask* for each channel (masked or not?).

#### 1367     **B.3.1 Dimensions file and InFile parser**

1368 This input file, present in every data folder, allows the analysis tool to know of the number of active  
 1369 trolleys, the number of active RPCs in those trolleys, and the details about each RPCs such as  
 1370 the number of RPC gaps, the number of pseudo-rapidity partitions (for CMS-like prototypes), the  
 1371 number of strips per partion or the dimensions. To do so, there are 3 types of groups in the INI file  
 1372 architecture. A first general group, appearing only once at the head of the document, gives information  
 1373 about the number of active trolleys as well as their IDs, as presented in Source Code B.1. For

1374 each active trolley, a group similar to Source Code B.2 can be found containing information about  
 1375 the number of active detectors in the trolley and their IDs. Each trolley group as a `Tt` name format,  
 1376 where `t` is the trolley ID. Finally, for each detector stored in slots of an active trolley, there is a group  
 1377 providing information about their names and dimensions, as showed in Source Code B.3. Each slot  
 1378 group as a `TtSs` name format, where `s` is the slot ID of trolley `t` where the active RPC is hosted.

```
1379 [General]
1380 nTrolleys=2
1381 TrolleysID=13
```

1381 *Source Code B.1: Example of `[General]` group as might be found in `Dimensions.ini`. In Gif++, only 2 trolleys are available to hold RPCs and place them inside of the bunker for irradiation. The IDs of the trolleys are written in a single string as "13" and then read character by character by the program.*

```
1382 [T1]
1383 nSlots=4
      SlotsID=1234
```

1383 *Source Code B.2: Example of trolley group as might be found in `Dimensions.ini`. In this example, the file tells that there are 4 detectors placed in the holding slots of the trolley `T1` and that their IDs, written as a single string variable, are 1, 2, 3 and 4.*

```
1384 [T1S1]
Name=RE2-2-NPD-BARC-8
Partitions=3
Gaps=3
Gap1=BOT
Gap2=TN
Gap3=TW
AreaGap1=11694.25
AreaGap2=6432
AreaGap3=4582.82
Strips=32
ActiveArea-A=157.8
ActiveArea-B=121.69
ActiveArea-C=93.03
```

1385 *Source Code B.3: Example of slot group as might be found in `Dimensions.ini`. In this example, the file provides information about a detector named `RE2-2-NPD-BARC-8`, having 3 pseudo-rapidity readout partitions and stored in slot `S1` of trolley `T1`. This is a CMS RE2-2 type of detector. This information will then be used for example to compute the rate per unit area calculation.*

1386 This information is readout and stored in a C++ object called `IniFile`, that parses the information  
 1387 in the INI input file and stores it into a local buffer for later use. This INI parser is the exact same  
 1388 one that was previously developed for the Gif++ DAQ and described in Appendix A.5.2.

### 1389 **B.3.2 TDC to RPC link file and Mapping**

1390 The same way the INI dimension file information is stored using `map`, the channel mapping and mask  
 1391 information is stored and accessed through `map`. First of all, the mapping CSV file is organised into  
 1392 3 columns separated by tabulations (and not by commas, as expected for CSV files as it is easier using  
 1393 streams to read tab or space separated data using C++):

1394

1395      `RPC_channel`            `TDC_channel`            `mask`

1396      using as formatting for each field:

1397  
1398      `TSCCC`            `TCCC`            `M`

1399 `TSCCC` is a 5-digit integer where `T` is the trolley ID, `s` the slot ID in which the RPC is held insite  
1400        the trolley `T` and `ccc` is the RPC channel number, or *strip* number, that can take values up to  
1401        3-digits depending on the detector,

1402 `TCCC` is a 4 digit integer where `T` is the TDC ID, `ccc` is the TDC channel number that can take values  
1403        in between 0 and 127, and

1404 `M` is a 1-digit integer indicating if the channel should be considered (`M = 1`) or discarded (`M = 0`)  
1405        during analysis.

1406      This mapping and masking information is readout and stored thanks to the object `Mapping`, pre-  
1407      sented in Source Code B.4. Similarly to `IniFile` objects, this class has private methods. The first  
1408      one, `Mapping::CheckIfNewLine()` is used to find the newline character '`\n`' or return character  
1409      '`\r`' (depending on which kind of operating system interacted with the file). This is used for the  
1410      simple reason that the masking information has been introduced only during the year 2017 but the  
1411      channel mapping files exist since 2015 and the very beginning of data taking at GIF++. This means  
1412      that in the older data folders, before the upgrade, the channel mapping file only had 2 columns, the  
1413      RPC channel and the TDC channel. For compatibility reasons, this method helps controling the  
1414      character following the readout of the 2 first fields of a line. In case any end of line character is  
1415      found, no mask information is present in the file and the default `M = 1` is used. On the contrary, if  
1416      the next character was a tabulation or a space, the mask information is present.

1417      Once the 3 fields have been readout, the second private method `Mapping::CheckIfTDCCh()` is  
1418      used to control that the TDC channel is an existing TDC channel. Finally, the information is stored  
1419      into 3 different maps (`Link`, `ReverseLink` and `Mask`) thanks to the public method `Mapping::Read()`.  
1420 `Link` allows to get the RPC channel by knowing the TDC channel while `ReverseLink` does the op-  
1421      posite by returning the TDC channel by knowing the RPC channel. Finally, `Mask` returns the mask  
1422      associated to a given RPC channel.

```

1423 typedef map<Uint,Uint> MappingData;

1424 class Mapping {
1425     private:
1426         bool          CheckIfNewLine(char next);
1427         bool          CheckIfTDCCh(Uint channel);
1428         string        FileName;
1429         MappingData  Link;
1430         MappingData  ReverseLink;
1431         MappingData  Mask;
1432         int           Error;
1433
1434     public:
1435         Mapping();
1436         Mapping(string baseName);
1437         ~Mapping();
1438
1439         void SetFileName(const string filename);
1440         int  Read();
1441         Uint GetLink(Uint tdcchannel);
1442         Uint GetReverse(Uint rpcchannel);
1443         Uint GetMask(Uint rpcchannel);
1444     };

```

1425 *Source Code B.4: Description of C++ object Mapping used as a parser for the channel mapping and mask file.*

## 1426 B.4 Description of GIF++ setup within the Offline Analysis tool

1427 In the previous section, the tool input files have been discussed. The dimension file information is  
 1428 stored in a map hosted by the `IniFile` object. But this information is then used to create a series of  
 1429 new objects that helps defining the GIF++ infrastructure directly into the Offline Analysis. Indeed,  
 1430 from the `RPC`, to the more general `Infrastructure`, every element of the GIF++ infrastrucutre is  
 1431 recreated for each data analysis based on the information provided in input. All this information  
 1432 about the infrastructure will be used to assign each hit signal to a specific strip channel of a specific  
 1433 detector, and having a specific active area. This way, rate per unit area calculation is possible.  
 1434

### 1435 B.4.1 RPC objects

1436 `RPC` objects have been developped to represent physical active detectors in GIF++ at the moment  
 1437 of data taking. Thus, there are as many `RPC` objects created during the analysis than there were  
 1438 active `RPCs` tested during a run. Each `RPC` hosts the information present in the corresponding INI  
 1439 slot group, as shown in B.3, and organises it using a similar architecture. This can be seen from  
 1440 *Source Code B.5*.

1441 To make the object more compact, the lists of gap labels, of gap active areas and strip active  
 1442 areas are stored into `vector` dynamical containers. `RPC` objects are always contructed thanks to the  
 1443 dimension file information stored into the `IniFILE` and their ID, using the format `TtSs`. Using the  
 1444 `RPC` ID, the constructor calls the methods of `IniFILE` to initialise the `RPC`. The other constructors  
 1445 are not used but exist in case of need. Finally, some getters have been written to access the different  
 1446 private parameters storing the detector information.

```

1447 class RPC{
1448     private:
1449         string name;           //RPC name as in webDCS database
1450         Uint nGaps;          //Number of gaps in the RPC
1451         Uint nPartitions;    //Number of partitions in the RPC
1452         Uint nStrips;        //Number of strips per partition
1453         vector<string> gaps; //List of gap labels (BOT, TOP, etc...)
1454         vector<float> gapGeo;   //List of gap active areas
1455         vector<float> stripGeo; //List of strip active areas
1456
1457     public:
1458         RPC();
1459         RPC(string ID, IniFile* geofile);
1460         RPC(const RPC& other);
1461         ~RPC();
1462         RPC& operator=(const RPC& other);
1463
1464         string GetName();
1465         Uint GetNGaps();
1466         Uint GetNPartitions();
1467         Uint GetNStrips();
1468         string GetGap(Uint g);
1469         float GetGapGeo(Uint g);
1470         float GetStripGeo(Uint p);
1471     };

```

<sup>1449</sup> *Source Code B.5: Description of C++ objects RPC that describe each active detectors used during data taking.*

## <sup>1450</sup> B.4.2 Trolley objects

<sup>1451</sup> Trolley objects have been developped to represent physical active trolleys in GIFT++ at the moment  
<sup>1452</sup> of data taking. Thus, there are as many trolley objects created during the analysis than there were  
<sup>1453</sup> active trolleys hosting tested RPCs during a run. Each Trolley hosts the information present in the  
<sup>1454</sup> corresponding INI trolley group, as shown in B.2, and organises it using a similar architecture. In  
<sup>1455</sup> addition to the information hosted in the INI file, these object have a dynamical container of RPC  
<sup>1456</sup> objects, representing the active detectors the active trolley was hosting at the time of data taking.  
<sup>1457</sup> This can been seen from Source Code B.6.

<sup>1458</sup> Trolley objects are always contructed thanks to the dimension file information stored into the  
<sup>1459</sup> IniFILE and their ID, using the format Tt. Using the Trolley ID, the constructor calls the methods  
<sup>1460</sup> of IniFILE to initialise the Trolley. Retrieving the information of the RPC IDs via SlotsID, a new  
<sup>1461</sup> RPC is constructed and added to the container RPCs for each character in the ID string. The other  
<sup>1462</sup> constructors are not used but exist in case of need. Finally, some getters have been written to access  
<sup>1463</sup> the different private parameters storing the trolley and detectors information.

```

1464
class Trolley{
    private:
        Uint          nSlots; //Number of active RPCs in the considered trolley
        string        SlotsID; //Active RPC IDs written into a string
        vector<RPC*> RPCs;   //List of active RPCs

    public:
        //Constructors, destructor and operator =
        Trolley();
        Trolley(string ID, IniFile* geofile);
        Trolley(const Trolley& other);
        ~Trolley();
        Trolley& operator=(const Trolley& other);

        //Get GIFTrolley members
        Uint  GetNSlots();
        string GetSlotsID();
        Uint   GetSlotID(Uint s);

        //Manage RPC list
        RPC*  GetRPC(Uint r);
        void  DeleteRPC(Uint r);

        //Methods to get members of RPC objects stored in RPCs
        string GetName(Uint r);
        Uint   GetNGaps(Uint r);
        Uint   GetNPartitions(Uint r);
        Uint   GetNStrips(Uint r);
        string GetGap(Uint r, Uint g);
        float  GetGapGeo(Uint r, Uint g);
        float  GetStripGeo(Uint r, Uint p);
    };

```

*Source Code B.6: Description of C++ objects `Trolley` that describe each active trolley used during data taking.*

### 1467    B.4.3 Infrastructure object

1468 The `Infrastructure` object has been developped to represent the GIFT++ bunker area dedicated to  
 1469 CMS RPC experiments. With this very specific object, all the information about the CMS RPC  
 1470 setup within GIFT++ at the moment of data taking is stored. It hosts the information present in the  
 1471 corresponding INI general group, as shown in B.1, and organises it using a similar architecture. In  
 1472 addition to the information hosted in the INI file, this object have a dynamical container of `Trolley`  
 1473 objects, representing the active tolleys in GIFT++ area. This can be seen from Source Code B.7.

1474 The `Infrastructure` object is always contructed thanks to the dimension file information stored  
 1475 into the `IniFILE`. Retrieving the information of the trolley IDs via `TrolleysID`, a new `Trolley` is  
 1476 constructed and added to the container `Trolleys` for each character in the ID `string`. By extension,  
 1477 it is easy to understand that the process described in Section B.4.2 for the construction of RPCs  
 1478 takes place when a trolley is constructed. The other constructors are not used but exist in case of  
 1479 need. Finally, some getters have been written to access the different private parameters storing the  
 1480 infrastructure, tolleys and detectors information.

```

1481
class Infrastructure {
    private:
        Uint             nTrolleys;   //Number of active Trolleys in the run
        string          TrolleysID; //Active trolley IDs written into a string
        vector<Trolley*> Trolleys; //List of active Trolleys (struct)

    public:
        //Constructors and destructor
        Infrastructure();
        Infrastructure(IniFile* geofile);
        Infrastructure(const Infrastructure& other);
        ~Infrastructure();
        Infrastructure& operator=(const Infrastructure& other);

        //Get Infrastructure members
        Uint  GetNTrolleys();
        string GetTrolleysID();
        Uint  GetTrolleyID(Uint t);

1482
        //Manage Trolleys
        Trolley* GetTrolley(Uint t);
        void     DeleteTrolley(Uint t);

        //Methods to get members of GIFTrolley objects stored in Trolleys
        Uint  GetNSlots(Uint t);
        string GetSlotsID(Uint t);
        Uint  GetSlotID(Uint t, Uint s);
        RPC*  GetRPC(Uint t, Uint r);

        //Methods to get members of RPC objects stored in RPCs
        string GetName(Uint t, Uint r);
        Uint  GetNGaps(Uint t, Uint r);
        Uint  GetNPartitions(Uint t, Uint r);
        Uint  GetNStrips(Uint t, Uint r);
        string GetGap(Uint t, Uint r, Uint g);
        float  GetGapGeo(Uint t, Uint r, Uint g);
        float  GetStripGeo(Uint t, Uint r, Uint p);
    };

```

Source Code B.7: Description of C++ object *Infrastructure* that contains the full information about CMS RPC experiment in GIF++.

## 1484 B.5 Handeling of data

1485 As discussed in Appendix A.4.2, the raw data as a `TTree` architecture where every entry is related to  
 1486 a trigger signal provided by a muon or a random pulse, whether the goal of the data taking was to  
 1487 measure the performance of the detector or the noise/gamma background respectively. Each of these  
 1488 entries, referred also as events, contain a more or less full list of hits in the TDC channels to which  
 1489 the detectors are connected. To this list of hits corresponds a list of time stamps, marking the arrival  
 1490 of the hits within the TDC channel.

1491 The infrastructure of the CMS RPC experiment within GIF++ being defined, combining the  
 1492 information about the raw data with the information provided by both the mapping/mask file and the  
 1493 dimension file allows to build new physical objects that will help in computing efficiency or rates.

### 1494 B.5.1 RPC hits

1495 The raw data stored in the ROOT file as output of the GIFT++ DAQ, is readout by the analysis tool  
 1496 using the structure `RAWData` presented in Source Code B.9 that differs from the structure presented  
 1497 in Appendix A.4.2 as it is not meant to hold all of the data contained in the ROOT file. In this sense,  
 1498 this structure is in the case of the offline analysis tool not a dynamical object and will only be storing  
 1499 a single event contained in a single entry of the `TTree`.

```
1500
1501 class RPCHit {
1502     private:
1503         Uint Channel;      //RPC channel according to mapping (5 digits)
1504         Uint Trolley;      //0, 1 or 3 (1st digit of the RPC channel)
1505         Uint Station;      //Slot where is held the RPC in Trolley (2nd digit)
1506         Uint Strip;        //Physical RPC strip where the hit occurred (last 3
1507             digits)
1508         Uint Partition;    //Readout partition along eta segmentation
1509         float TimeStamp;   //Time stamp of the arrival in TDC
1510
1511     public:
1512         //Constructors, destructor & operator =
1513         RPCHit();
1514         RPCHit(Uint channel, float time, Infrastructure* Infra);
1515         RPCHit(const RPCHit& other);
1516         ~RPCHit();
1517         RPCHit& operator=(const RPCHit& other);
1518
1519         //Get RPCHit members
1520         Uint GetChannel();
1521         Uint GetTrolley();
1522         Uint GetStation();
1523         Uint GetStrip();
1524         Uint GetPartition();
1525         float GetTime();
1526     };
1527
1528     typedef vector<RPCHit> HitList;
1529     typedef struct GIFHitList { HitList rpc[NTROLLEYS][NSLOTS][NPARTITIONS]; } →
1530         GIFHitList;
1531
1532     bool SortHitbyStrip(RPCHit h1, RPCHit h2);
1533     bool SortHitbyTime(RPCHit h1, RPCHit h2);

```

1502 *Source Code B.8: Description of C++ object RPCHit.*

```
1503
1504     struct RAWData{
1505         int iEvent;          //Event i
1506         int TDCNHits;       //Number of hits in event i
1507         int QFlag;           //Quality flag list (1 flag digit per TDC)
1508         vector<Uint> *TDCCh; //List of channels giving hits per event
1509         vector<float> *TDCTS; //List of the corresponding time stamps
1510     };

```

1504 *Source Code B.9: Description of C++ structure RAWData.*

1505 Each member of the structure is then linked to the corresponding branch of the ROOT data tree,  
 1506 as shown in the example of Source Code B.10, and using the method `GetEntry(int i)` of the ROOT  
 1507 class `TTree` will update the state of the members of `RAWData`.

```

1508 TTree* dataTree = (TTree*)dataFile.Get("RAWData");
1509 RAWData data;
1510
1511 dataTree->SetBranchAddress("EventNumber", &data.iEvent);
1512 dataTree->SetBranchAddress("number_of_hits", &data.TDCNHits);
1513 dataTree->SetBranchAddress("Quality_flag", &data.QFlag);
1514 dataTree->SetBranchAddress("TDC_channel", &data.TDCCh);
1515 dataTree->SetBranchAddress("TDC_TimeStamp", &data.TDCTS);

```

1510         *Source Code B.10: Example of link in between RAWData and TTree.*

1511         The data is then analysed entry by entry and to each element of the TDC channel list, a `RPCHit` is  
1512         constructed by linking each TDC channel to the corresponding RPC channel thanks to the `Mapping`  
1513         object. The information carried by the RPC channel format allows to easily retrieve the trolley and  
1514         slot from which the hit was recorded (see section B.3.2). Using these 2 values, the readout partition  
1515         can be found by knowing the strip channel and comparing it with the number of partitions and strips  
1516         per partition stored into the `Infrastructure` object.

1517         Thus `RPCHit` objects are then stored into 3D dynamical list called `GIFHitList` (Source Code B.9)  
1518         where the 3 dimensions refer to the 3 layers of the readout in `GIF++` : in the bunker there are *trolleys*  
1519         ( $\tau$ ) holding detectors in *slots* ( $s$ ) and each detector readout is divided into 1 or more pseudo-rapidity  
1520         *partitions* ( $p$ ). Using these 3 information allows to assign an address to each readout partition and  
1521         this address will point to a specific hit list.

1522

## 1523         B.5.2 Clusters of hits

1524         All the hits contained in the ROOT file have been sorted into the different hit lists through the  
1525         `GIFHitList`. At this point, it is possible to start looking for clusters. A cluster is a group of adjacent  
1526         strips getting hits within a time window of 25 ns. These strips are then assumed to be part of the same  
1527         physical avalanche signal generated by a muon passing through the chamber or by the interaction of  
1528         a gamma stopping into the electrodes of the RPCs.

1529         To keep the cluster information, `RPCCluster` objects have been defined as shown in Source  
1530         Code B.11. Using the information of each individual `RPCHit` taken out of the hit list, it stores  
1531         the cluster size (number of adjacent strips composing the cluster), the first and last hit, the center for  
1532         spatial reconstruction and finally the start and stop time stamps as well as te time spread in between  
1533         the first and last hit.

```
1534
class RPCCluster{
    private:
        Uint ClusterSize; //Size of cluster #ID
        Uint FirstStrip; //First strip of cluster #ID
        Uint LastStrip; //Last strip of cluster #ID
        float Center; //Center of cluster #ID ((first+last)/2)
        float StartStamp; //Time stamp of the earliest hit of cluster #ID
        float StopStamp; //Time stamp of the latest hit of cluster #ID
        float TimeSpread; //Time difference between earliest and latest hits
                           //of cluster #ID

    public:
        //Constructors, destructor & operator =
        RPCCluster();
        RPCCluster(HitList List, Uint cID, Uint cSize, Uint first, Uint firstID);
        RPCCluster(const RPCCluster& other);
        ~RPCCluster();
        RPCCluster& operator=(const RPCCluster& other);

        //Get Cluster members
        Uint GetID();
        Uint GetSize();
        Uint GetFirstStrip();
        Uint GetLastStrip();
        float GetCenter();
        float GetStart();
        float GetStop();
        float GetSpread();
};

typedef vector<RPCCluster> ClusterList;

//Other functions to build cluster lists out of hit lists
void BuildClusters(HitList &cluster, ClusterList &clusterList);
void Clusterization(HitList &hits, TH1 *hcSize, TH1 *hcMult);
```

Source Code B.11: Description of C++ object cluster.

To investigate the hit list of a given detector partition, the function `Clusterization()` defined in `include/Cluster.h` needs the hits in the list to be time sorted. This is achieved by calling function `sort()` of library `<algorithm>` using the comparator `SortHitbyTime(RPCHit h1, RPCHit h2)` defined in `include/RPCHit.h` that returns `true` if the time stamp of hit `h1` is lower than that of `h2`. A first isolation of strips is made only based on time information. All the hits within the 25 ns window are taken separately from the rest. Then, this sub-list of hits is sorted this time by ascending strip number, using this time the comparator `SortHitbyStrip(RPCHit h1, RPCHit h2)`. Finally, the groups of adjacent strips are used to construct `RPCCluster` objects that are then stored in a temporary list of clusters that is at the end of the process used to know how many clusters were reconstructed and to fill their sizes into an histogram that will allows to know the mean size of muon or gamma clusters.

1549 B.6 DAQ data Analysis

All the ingredients to analyse GIF++ data have been defined. This section will focus on the different part of the analysis performed on the data, from determining the type of data the tool is dealing with

1552 to calculating the rate in each detector or reconstructing muon or gamma clusters.

### 1553 B.6.1 Determination of the run type

1554 In GIF++, both the performance of the detectors in detecting muons in an irradiated environment and  
 1555 the gamma background can be independantly measured. These corresponds to different run types  
 1556 and thus, to different TDC settings giving different data to look at.

1557

1558 In the case of performance measurements, the trigger for data taking is provided by the coïncidence  
 1559 of several scintillators when muons from the beam passing through the area are detected. Data  
 1560 is collected in a 600 ns wide window around the arrival of muons in the RPCs. The expected time  
 1561 distribution of hits is shown in Figure B.1a. The muon peak is clearly visible in the center of the  
 1562 distribution and is to be extracted from the gamma background that composes the flat part of the  
 1563 distribution.

1564 On the other hand, gamma background or noise measurements are focussed on the non muon  
 1565 related physics and the trigger needs to be independant from the muons to give a good measurement  
 1566 of the gamma/noise distribution as seen by the detectors. The trigger is then provided by a pulse  
 1567 generator at a frequency of 300 Hz whose pulse is not likely to be on time with a muon. In order  
 1568 to increase the integrated time without increasing the acquisition time too much, the width of the  
 1569 acquisition windows are increased to 10  $\mu$ s. The time distribution of the hits is expected to be flat, as  
 1570 shown by Figure B.1b.

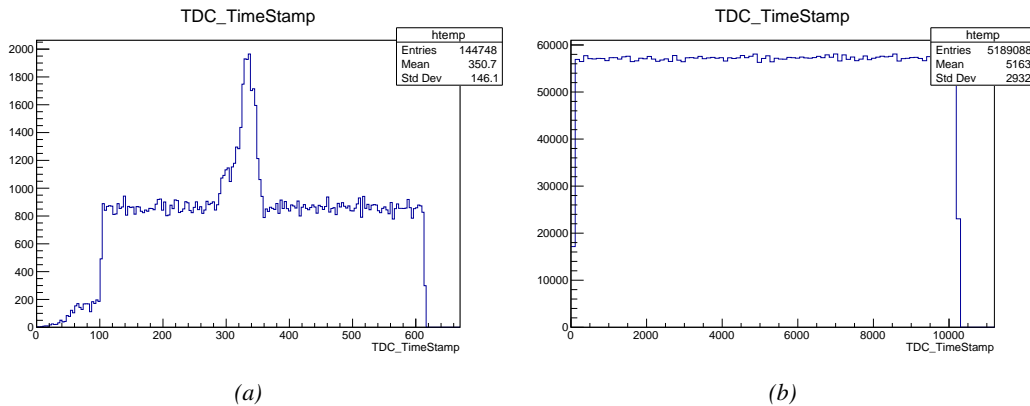


Figure B.1: Example of expected hit time distributions in the cases of efficiency (Figure B.1a) and noise/gamma rate per unit area (Figure B.1b) measurements as extracted from the raw ROOT files. The unit along the x-axis corresponds to ns. The fact that "the" muon peak is not well defined in Figure B.1a is due to the contribution of all the RPCs being tested at the same time that don't necessarily have the same signal arrival time. Each individual peak can have an offset with the ones of other detectors. The inconsistency in the first 100 ns of both time distributions is an artefact of the TDCs and are systematically rejected during the analysis.

1571 The ROOT files include a TTree called RunParameters containing, among other things, the in-  
 1572 formation related to the type of run. The run type can then be accessed as described by Sourcere  
 1573 Code B.12 and the function IsEfficiencyRun() is then used to determine if the run file is an effi-  
 1574 ciency run or, on the contrary, another type of run (noise or gamma measurement).

```

1575     TTree* RunParameters = (TTree*)dataFile.Get("RunParameters");
1576     TString* RunType = new TString();
1577     RunParameters->SetBranchAddress("RunType", &RunType);
1578     RunParameters->GetEntry(0);

```

1577       *Source Code B.12: Access to the run type contained in TTree\* RunParameters.*

1578       Finally, the data files will have a slightly different content whether it was collected before or after  
1579       October 2017 and the upgrade of the DAQ software that brought a new information into the ROOT  
1580       output. This is discussed in Appendix A.4.3 and implies that the analysis will differ a little depending  
1581       on the data format. Indeed, as no information on the data quality is stored, in older data files, the cor-  
1582       rections for missing events has to be done at the end of the analysis. The information about the type  
1583       of data format is stored in the variable **bool** `isNewFormat` by checking the list of branches contained  
1584       in the data tree via the methods `TTree::GetListOfBranches()` and `TCollection::Contains()`.

## 1585     **B.6.2 Beam time window calculation for efficiency runs**

1586       Knowing the run type is important first of all to know the width of the acquisition window to be used  
1587       for the rate calculation and finally to be able to seek for muons. Indeed, the peak that appears in the  
1588       time distribution for each detectors is then fitted to extract the most probable time window in which  
1589       the tool should look for muon hits. The data outside of this time window is then used to evaluate the  
1590       noise or gamma background the detector was subjected to during the data taking. Computing the  
1591       position of the peak is done calling the function `SetBeamWindow()` defined in file `src/RPCHit.cc` that  
1592       loops a first time on the data. The data is first sorted in a 3D array of 1D histograms (`GIFH1Array`, see  
1593       `include/types.h`). Then the location of the highest bin is determined using `TH1::GetMaximumBin()`  
1594       and is used to define a window in which a gaussian fit will be applied to compute the peak width.  
1595       This window is a 80 ns defined by Formula B.1 around the central bin.

$$t_{center}(ns) = bin \times width_{bin}(ns) \quad (\text{B.1a})$$

$$[t_{low}; t_{high}] = [t_{center} - 40; t_{center} + 40] \quad (\text{B.1b})$$

1596       Before the fit is performed, the average number of noise/gamma hits per bin is evaluated using  
1597       the data outside of the fit window. Excluding the first 100 ns, the average number of hits per bin  
1598       due to the noise or gamma is defined by Formula B.2 after extracting the amount of hits in the time  
1599       windows  $[100; t_{low}]$  and  $[t_{high}; 600]$  thanks to the method `TH1::Integral()`. This average number  
1600       of hits is then subtracted to every bin of the 1D histogram, in order to *clean* it from the noise or  
1601       gamma contribution as much as possible to improve the fit quality. Bins where  $\langle n_{hits} \rangle$  is greater  
1602       than the actual bin content are set to 0.

$$\Delta t_{noise}(ns) = 600 \overbrace{-t_{high} + t_{low}}^{-80ns} - 100 = 420ns \quad (\text{B.2a})$$

$$\langle n_{hits} \rangle = width_{bin}(ns) \times \frac{\sum_{t=100}^{t_{low}} + \sum_{t=t_{high}}^{600}}{\Delta t_{noise}(ns)} \quad (\text{B.2b})$$

1603       Finally, the fit parameters are extracted and saved for each detector in 3D arrays of **float**  
1604       (`muonPeak`, see `include/types.h`), a first one for the mean arrival time of the muons, `PeakTime`,

1605 and a second one for the width of the peak, `PeakWidth`. The width is defined as  $6\sigma$  of the gaussian  
 1606 fit. The same settings are applied to every partitions of the same detector. To determine which one  
 1607 of the detector's partitions is directly illuminated by the beam, the peak height of each partition is  
 1608 compared and the highest one is then used to define the peak settings.

### 1609 **B.6.3 Data loop and histogram filling**

1610 3D arrays of histogram are created to store the data and display it on the DQM of GIF++ webDCS  
 1611 for the use of shifters. These histograms, presented in section B.2.1.1, are filled while looping on  
 1612 the data. Before starting the analysis loop, it is necessary to control the entry quality for the new  
 1613 file formats featuring `QFlag`. If the `QFlag` value for this entry shows that 1 TDC or more have a  
 1614 `CORRUPTED` flag, then this event is discarded. The loss of statistics is low enough to be neglected.  
 1615 `QFlag` is controled using the function `IsCorruptedEvent()` defined in `src/utils.cc`. As explained  
 1616 in Appendix A.4.3, each digit of this integer represent a TDC flag that can be 1 or 2. Each 2 is  
 1617 the sign of a `CORRUPTED` state. Then, the data is accessed entry by entry in the ROOT `TTree` using  
 1618 `RAWData` and each hit in the hit list is assigned to a detector channel and saved in the corresponding  
 1619 histograms. In the first part of the analysis, in which the loop over the ROOT file's content is  
 1620 performed, the different steps are:

1621 **1- RPC channel assignment and control:** a check is done on the RPC channel extracted thanks  
 1622 to the mapping via the method `Mapping::GetLink()`. If the channel is not initialised and is 0, or if  
 1623 the TDC channel was greater than 5127, the hit is discarded. This means there was a problem in the  
 1624 mapping. Often a mapping problem leads to the crash of the offline tool.

1625 **2- Creation of a `RPCHit` object:** to easily get the trolley, slot and partition in which the hit has  
 1626 been assigned, this object is particularly helpful.

1627 **3- General histograms are filled:** the hit is filled into the time distribution and the general hit  
 1628 distribution histograms, and if the arrival time is within the first 100 ns, it is discarded and nothing  
 1629 else happens and the loop proceeds with the next hit in the list.

1630 **4- Multiplicity counter:** the hit multiplicity counter of the corresponding detectors incremented.

1631 **5-a- Efficiency runs - Is the hit within the peak window? :** if the peak is contained in the peak  
 1632 window previously defined in section B.6.2, the hit is filled into the beam hit profile histogram of  
 1633 the corresponding chamber, added into the list of muon hits and increments the counter of *in time*  
 1634 hits. The term *in time* here refers to the hits that are likely to be muons by arriving in the expected  
 1635 time window. If the hit is outside of the peak window, it is filled into the noise profile histogram  
 1636 of the corresponding detector, added into the list of noise/gamma hits and increments the counter of  
 1637 noise/gamma hits.

1638 **5-b- Noise/gamma rate runs - Noise histograms are filled:** the hit is filled into the noise profile  
 1639 histogram of the corresponding detector, added into the list of noise/gamma hits and increments the  
 1640 counter of noise/gamma hits.

1641 After the loop on the hit list of the entry is over, the next step is to clusterize the 3D lists filled  
 1642 in the previous steps. A 3D loop is then started over the active trolley, slot and RPC partitions to

1643 access these objects. Each `NoiseHitList` and `MuonHitList`, in case of efficiency run, are clusterized  
 1644 as described in section B.5.2. There corresponding cluster size and multiplicity histograms are filled  
 1645 at the end of the clustering process. Then, the efficiency histogram is filled in case of efficiency run.  
 1646 The selection is simply made by checking whether the RPC detected signals in the peak window  
 1647 during this event. Nevertheless, it is useful to highlight that at this level, it is not possible yet to  
 1648 discriminate in between a muon hit and noise or gamma hit. Thus, `MuonCSize_H`, `MuonCMult_H`  
 1649 and `Efficiency0_H` are subjected to noise and gamma contamination. This contamination will be  
 1650 estimated and corrected at the moment the results will be written into output CSV files. Finally, the  
 1651 loop ends on the filling of the general hit multiplicity histogram.

#### 1652 B.6.4 Computation of the final results

1653 As mentioned in section B.2.1, the analysis of DAQ data provides the user with 3 CSV files and  
 1654 a ROOT file associated to each and every ROOT data file. The fourth CSV file is provided by the  
 1655 extraction of the CEAN main frame data monitored during data taking and will be discussed later.  
 1656 After looping on the data in the previous part of the analysis macro, the output files are created and a  
 1657 3D loop on each RPC readout partitions is started to extract the histograms parameters and compute  
 1658 the final results.

1659

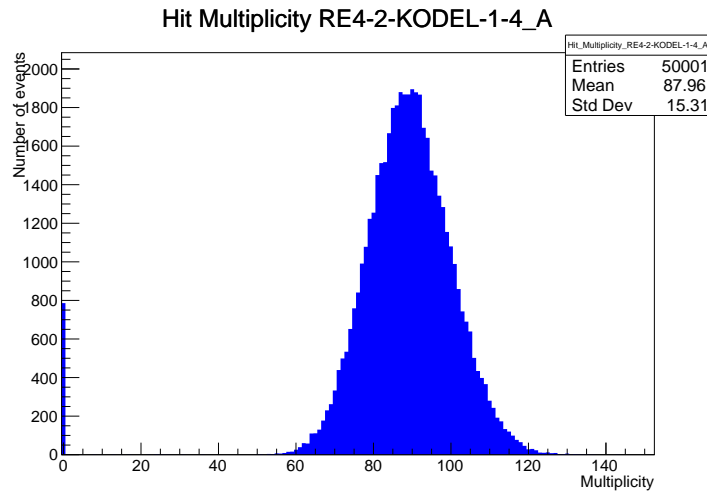
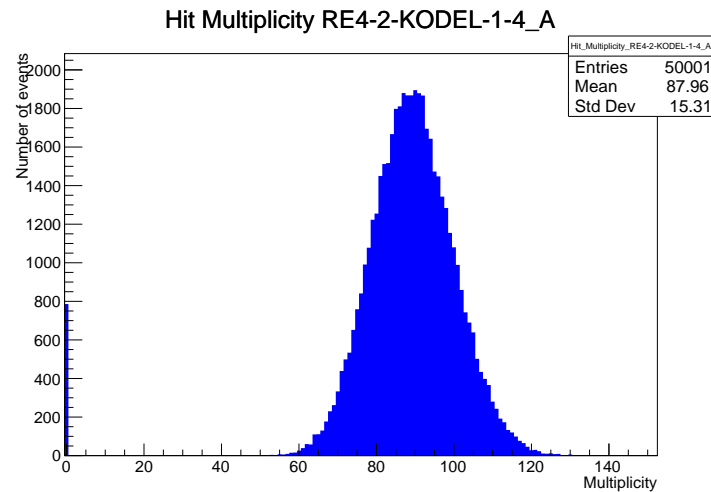


Figure B.2: The effect of the quality flag is explained by presenting the reconstructed hit multiplicity of a data file without `Quality_flag`. The artificial high content of bin 0 is the effect of corrupted data.

1660 **Corrupted data estimation :** In case of old data format files, not containing any quality flag, it is  
 1661 need to estimate the amount of corrupted data via a fit as the corrupted data will always fill events  
 1662 with a fake "0 multiplicity". Indeed, as no hits were stored in the DAQ ROOT files, these events  
 1663 artificially contribute to fill the bin corresponding to a null multiplicity, as shown in Figure B.2.



*Figure B.3: The effect of the quality flag is explained by presenting the reconstructed hit multiplicity of a data file without Quality\_flag. The artificial high content of bin 0 is the effect of corrupted data.*

# C

1664

1665

## Structure of the hybrid simulation software

1666

### C.1 Introduction

1667

insert text here...

